The interaction of multiple bodies and water waves

with the application to the motion of ice floes

A thesis presented in partial fulfillment of the requirements for the degree of

Master of Science
in
Mathematics

at Massey University, Albany,
New Zealand

Malte Andreas Peter

2002

Abstract

To understand the propagation of water waves through arrays of floating or (fully or partially) submerged bodies it is necessary to know how these bodies interact with each other under the influence of ambient waves. However, the conventional full diffraction calculation of the scattered wavefields of many interacting bodies requires a considerable computational effort.

In this thesis, a method is developed which makes it possible to quickly calculate the wave scattering of many interacting floating or (fully or partially) submerged, vertically non-overlapping bodies of arbitrary geometry in water of infinite depth. It extends Kagemoto and Yue's analysis for axisymmetric bodies in finite depth.

The idea of this method is to expand the water velocity potential into its cylindrical eigenfunctions such that the scattered potentials of the bodies are defined by a set of coefficients only. Representing the scattered wavefield of each body as an incident wave upon all other bodies, a linear system of equations for the coefficients of the scattered wavefields is derived.

Diffraction transfer matrices which relate the coefficients of the incoming wavefield upon a single body to those of its scattered wavefield play an important role in the process. The calculation of the diffraction transfer matrices for bodies of arbitrary shape requires the representation of the infinite depth free surface Green's function in the eigenfunctions of an outgoing wave. This eigenfunction expansion will be derived from the equivalent finite depth Green's function.

An important application of this interaction method is the propagation of ocean waves through fields of ice floes which can be modelled as floating flexible thin plates. Meylan's method of solution is used to calculate the motion of a single ice floe from which the solutions for multiple interacting ice floes are computed.

While the interaction theory will be derived for general floating or submerged bodies, particular examples are always given for the case of ice floes. Results are presented for ice floes of different geometries and in different arrangements and convergence tests comparing the finite and the infinite depth method are conducted with two square interacting ice floes where full diffraction calculations serve as references.

Acknowledgements

I would like to thank Dr Michael Meylan for the great support he has shown me during the completion of this thesis. He has been an excellent supervisor and I have learnt very much from his comments and suggestions.

I would also like to thank the German National Scholarship Foundation for financially supporting my research at Massey University.

Contents

List of Figures

Chapter 1

Introduction

The scattering of water waves by floating or submerged, rigid or flexible bodies has always been of great interest. Although the full non-linear problem is quite complex, if the amplitudes of the waves are much smaller than their wavelengths, the problem can be linearised and viscous effects can be neglected as long as the wavelengths are smaller or of similar size as the typical diameter of the body. These restrictions apply to many applications such as the hulls of ships or single legs supporting structures above the water surface.

While analytic solutions have been found for simplified problems (especially for simple geometries or in two dimensions) the arbitrary three-dimensional linear diffraction problem can only be solved by numerical methods involving the discretisation of the body's surface.

Practical applications such as offshore platforms with many legs, however, require the calculation of the scattering of incident water waves by many interacting single bodies, as does the scattering of ocean waves by fields of ice floes in the Marginal Ice Zone which is very important to the progress of climate research.

If more than one body is present, all bodies will scatter the incoming waves. Therefore, the scattered wave of one body will be incident upon all other ones and, given that they are not too far apart, notably change the total incident wave upon these other bodies. Thus, it is necessary to perform a complete diffraction calculation for all bodies (as opposed to single diffraction problems) which involves the discretisation of all the bodies' surfaces.

Basic numerical methods of solution for the full diffraction problem can be developed quite straightforwardly from the solution of the scattering of a single body and have been available since the late 1970s. However, the numerical expense of such computations quickly becomes excessive with an increasing number of bodies.

Since in most applications the single bodies share the same properties (e.g. the legs of an offshore platform), it was proposed to reduce the full diffraction problem to many single scattering problems and account for the interaction separately. The major advantage of this division was a much smaller resulting system of equations for the interaction problem than for the full diffraction problem and single diffraction calculations only needed to be performed once for equivalent bodies (and could be saved for later use).

While a few earlier works presented approximative solutions based on this idea, Kagemoto & Yue (1986) found an exact algebraic method (within the context of the linearised theory) for vertically non-overlapping bodies in water of finite depth. The interaction of the bodies was accounted for by taking the scattered wave of a body to be the incident wave upon all other bodies (in addition to the ambient incident wave). Doing this for all bodies simultaneously and representing the scattered and incident water velocity potentials of each body in their cylindrical eigenfunction expansions (suitably truncated), Kagemoto & Yue were able to solve for the coefficients of the scattered wavefields (in this expansion) of all bodies. The difficulty with this method, however, is that the solutions of the single diffraction problems have to be available in the cylindrical eigenfunction expansion of an outgoing wave. Kagemoto & Yue therefore only solved for axisymmetric bodies because the single diffraction solution for cylinders was available in the required representation.

Intending to apply Kagemoto & Yue's interaction method to bodies of arbitrary shape, Goo & Yoshida (1990) suggested a general way to solve the single diffraction problem such that the solution was automatically given in the required representation. They transformed the boundary value problem to an integral equation over the immersed surface of the body with the help of a free surface Green's function. Utilising a representation of the finite depth free surface Green's function which was given in the eigenfunction expansion of cylindrical outgoing waves centred at an arbitrary point of the water surface (above the body's mean centre position in this case) they allowed arbitrary geometries of the bodies. This Green's function was first used by Black (1975) and was further investigated by Fenton (1978) who both considered single vertical axisymmetric bodies. It is based on the cylindrical eigenfunction expansion of the finite depth free surface Green's function where the origin of the coordinate system is at the water surface above the source point which was given by John (1950). Goo & Yoshida therefore extended Kagemoto & Yue's finite depth interaction method to bodies of arbitrary shape. Investigating multiple arrays of cylinders, Chakrabarti (2000) used Goo & Yoshida's results to decrease the dimension of the system of equations accounting for the interaction. He divided arrays of cylinders into identical modules, each of which contained many bodies, and computed the diffraction solution of each module before combining the modules to the full array.

This work applies the ideas of Kagemoto & Yue's finite depth interaction theory to water of infinite depth. In particular, this involves the representation of the incident and scattered potentials in the cylindrical eigenfunction expansions corresponding to water of infinite depth. To also allow arbitrary geometries, the Green's function used by Goo & Yoshida is derived explicitly from John's representation (similarly to the derivation of Fenton) and, using the same technique, an analogous Green's function for water of infinite depth is derived. However, this requires the derivation of the cylindrical eigenfunction expansion of the infinite depth free surface Green's function where the origin of the co-ordinate system is centred at the water surface above the source point, the analogous representation to John's finite depth Green's function. Additionally, this eigenfunction representation of the infinite depth Green's function will be examined in detail and compared to existing representations from a numerical point of view.

A very interesting and important application of this interaction theory is the wave scattering by multiple ice floes. As mentioned above, the scattering of ocean waves by fields of ice floes or in the Marginal Ice Zone is of great importance to climate research. Ocean waves, generated in the open water and passing through this interfacial region, play a major role in the interaction between open and ice covered seas.

A method of solving for the wave response of an ice floe of arbitrary geometry in water of infinite depth was suggested by Meylan (2002). The ice floe was modelled as a floating, flexible thin plate and its motion was expanded into the plate's modes of vibration. Converting the problem for the water in an integral equation and substituting the modes into it, a system of equations for the coefficients in the basis of these modes was obtained.

Using Meylan's result, the motion and scattering of many interacting ice floes is calculated and presented in this work. For two square interacting ice floes the convergence of the method obtained from the developed interaction theory is compared to the result of the full diffraction calculation. The solutions of more than two interacting ice floes and of other shapes in different arrangements are presented as well.

To illustrate the advantages of the infinite depth method over the finite depth method in deep water, their convergence is compared for two square interacting ice floes in deep water. It will be shown that the Green's function used by Goo & Yoshida can only be used up to a certain water depth due to a numerical problem and a solution for this problem is suggested. Both theories, for finitely and infinitely deep water, are developed simultaneously to point out their differences and similarities.

Chapter 2

Mathematical formulation and solution for a single ice floe

The mathematical description of the interaction of water waves and floating or (fully or partially) submerged bodies requires the consideration of one model for the water and one for the body. Due to their interaction, the models will be coupled.

At first, the model for the water will be developed in a general way. Where necessary, boundary conditions will be specified assuming a floating body at the water surface. The extension to the case of many bodies is trivial. Then, following Meylan (2002), a model for one ice floe will be derived and coupled with the one for the water. It will be shown how the general boundary value problem can be converted to an integral equation.

In the second part of the chapter, Meylan's method of solution will be developed by expanding the plate's motion into its modes of vibration. The modes will be substituted into the integral equation and a system of equations for the coefficients of the surface displacement in the expansion of these modes is obtained.

2.1 The models

A body is located in deep water of infinite expansion within the plane. The vertical dimension shall be labelled with z, the horizontal ones with x and y. The inner volume occupied by the body is labelled with $\Delta \subset \mathbb{R}^3$ and its immersed surface with Γ. The inner volume occupied by the water, assuming there is no movement, is labelled with D. Assuming the water surface at $z = 0$, D is defined as

$$D := \left\{ \mathbf{y} \in \mathbb{R}^3 \backslash \bar{\Delta} \,\middle|\, z < 0 \right\}$$

and the free water surface is labelled with S. As a simplification, $\mathbf{y} = (x, y, z)$ always denotes a point of the water. In the case of a floating body of constant but small thickness h (e.g. an ice floe), $\Delta \subset \mathbb{R}^2 \times \{0\}$ denotes the inner (bottom) surface of the body. Usually no distinction between the two- and three-dimensional case is necessary but in cases which only apply to the two-dimensional floating body, this will be specially marked by a tilde, $\tilde{\Delta}$. $T \subset \mathbb{R}$ is a closed interval for the considered time t. As a simplification, the vector $\mathbf{x} := (x, y, 0)$ always denotes a point of the undisturbed water surface.

2.1.1 The water

The equation of motion for the water has to be considered. Since only waves with small amplitudes and wavelengths smaller or of similar size as the bodies are investigated, the linearised and inviscid theory applies to the problem.

Under the assumption of irrotational motion the velocity vector field of the water can be written as the gradient field of a scalar velocity potential $\Phi\colon D \times T \to \mathbb{R}$. Due to the incompressibility of the water, the divergence of its velocity vector field must be zero everywhere in order to satisfy the conservation of mass constraint. Therefore the potential Φ has to be a harmonic function (with respect to the spatial coordinates),

$$\nabla^2 \Phi = 0, \quad (\mathbf{y}, t) \in D \times T.$$

As the water is assumed infinitely deep, the condition

$$\sup_{\mathbf{y} \in D} |\Phi(\mathbf{y}, t)| \leq \text{const} < \infty, \quad t \in T \tag{2.1}$$

must hold to ensure that the potential remains bounded. Although this condition does not have a direct hydrodynamic meaning, it is essential in the following. Also, it implies the natural boundary condition

$$\frac{\partial \Phi}{\partial z} \to 0 \text{ as } z \to -\infty, \quad (x, y, t) \in \mathbb{R}^2 \times T.$$

At the water surface, the area where the body is located (if the body is not completely submerged) and the free surface area must be distinguished. At the free water surface, no water particle can leave the free surface which is ensured by the (linearised) kinematic condition,

$$\frac{\partial \Phi}{\partial z} = \frac{\partial W}{\partial t}, \quad (\mathbf{x}, t) \in S \times T,$$

where $W\colon S \times T \to \mathbb{R}$ denotes the water surface displacement from the undisturbed position. In the case of a shallow draft $\tilde{\Delta}$ which is assumed to be in contact with the

water at all times, W is continued onto $\tilde{\Delta}$. The kinematic condition is then applied at the complete water surface and further ensures that no water particle leaves the water surface into the shallow draft.

A perturbation analysis shows that it is consistent with the linearised theory to apply the free-surface boundary conditions at $z = 0$ (Stoker, 1958).

In order to link the surface displacement and the velocity potential of the water, the linearised Bernoulli equation at the water surface is considered,

$$p = -\rho \frac{\partial \Phi}{\partial t} - \rho g W, \quad (\mathbf{x}, t) \in S \times T, \tag{2.2}$$

where ρ is the density of the water, g denotes the acceleration due to gravity and $p\colon D \times T \to \mathbb{R}$ is the pressure in the water relative to the atmospheric pressure. Assuming p to be constant along the water surface, and therefore zero, yields the dynamic boundary condition,

$$\frac{\partial \Phi}{\partial t} + gW = 0, \quad (\mathbf{x}, t) \in S \times T.$$

The two boundary conditions may be combined at the free surface. Differentiation with respect to time and utilisation of the kinematic boundary condition leads to the single free surface boundary condition

$$\frac{\partial \Phi}{\partial z} = -\frac{1}{g} \frac{\partial^2 \Phi}{\partial t^2}, \quad (\mathbf{x}, t) \in S \times T.$$

For a general floating or submerged body further boundary conditions apply at that body's surface. The normal component of the velocity of the body at any point of its immersed surface must equal the normal derivative of the water velocity potential at that point.

Only single wave frequencies will be considered since more complex waves can be obtained by addition of multiple single frequency solutions. Therefore, the displacement can be expressed as the real part of a complex quantity whose time dependence is $\mathrm{e}^{-\mathrm{i}\omega t}$ where ω is the radian frequency. Due to the linearity of the equations of motion, the displacement and the potential must have the same single frequency dependence,

$$W(\mathbf{x}, t) = \mathrm{Re}\left\{w(\mathbf{x})\mathrm{e}^{-\mathrm{i}\omega t}\right\} \quad \text{and} \quad \Phi(\mathbf{y}, t) = \mathrm{Re}\left\{\phi(\mathbf{y})\mathrm{e}^{-\mathrm{i}\omega t}\right\}, \tag{2.3}$$

which reduces the boundary condition at the water surface to

$$\frac{\partial \phi}{\partial z} = \alpha \phi, \qquad \mathbf{x} \in S,$$

where $\alpha := \omega^2/g$ and, additionally,

$$\frac{\partial \phi}{\partial z} = -\mathrm{i}\,\omega\, w, \qquad \mathbf{x} \in \tilde{\Delta},$$

in the case of a shallow draft.

This boundary value problem is subject to an incident wave which can be described by a condition which implies that at large distances the potential consists of a radial outgoing wave (the wave generated by the body) and the incident wave. Denoting the wavelength of a wave with λ and defining the wavenumber k as the number of wavelengths in a distance 2π, $k := 2\pi/\lambda$, this is imposed through the boundary condition

$$\lim_{r\to\infty} \sqrt{r}\left(\frac{\partial}{\partial r} - \mathrm{i}k\right)(\phi - \phi^{\mathrm{In}}) = 0,$$

where $r = \sqrt{(x^2+y^2)}$. It is sometimes called Sommerfeld radiation condition. The ambient incident potential ϕ^{In} can be expressed as

$$\phi^{\mathrm{In}}(x,y,z) = A\,\mathrm{e}^{\mathrm{i}k(x\cos\chi + y\sin\chi)+kz}, \tag{2.4}$$

where A is the wave amplitude and χ is the angle between the x-axis and the direction in which the waves are propagating. The required relations between the radian frequency and the wavenumber will be discussed in chapter 3.

It shall be noted that for water of constant finite depth d, the (inner) volume occupied by the water reduces to

$$D_d := \{\mathbf{y} \in \mathbb{R}^3\backslash\tilde{\Delta} \mid z \in]-d, 0[\}.$$

The depth condition (2.1) is replaced by an analogous boundary condition, namely the bed condition,

$$\frac{\partial\phi}{\partial z} = 0, \quad (x,y,z) \in \mathbb{R}^2 \times \{-d\}, \tag{2.5}$$

and the ambient incident potential is of the form

$$\phi^{\mathrm{In}}(x,y,z) = A\,\frac{\cosh(k(z+d))}{\cosh kd}\,\mathrm{e}^{\mathrm{i}k(x\cos\chi + y\sin\chi)}. \tag{2.6}$$

With these replacements, the above problem applies to water of constant finite depth.

2.1.2 The ice floe

The problem for the body will now be specified for the case of an ice floe. Assuming that the ice floe is in contact with the water at all times, its displacement is just W restricted to $\tilde{\Delta} \times T$. The motion of this thin flexible plate can then be described by the linear plate equation,

$$D\,\nabla^4 W + \rho_\Delta\, h\,\frac{\partial^2 W}{\partial t^2} = p, \quad (\mathbf{x},t) \in \tilde{\Delta} \times T, \tag{2.7}$$

with density ρ_Δ, thickness h and modulus of rigidity D. This is an accurate model due to the small displacements and the small value of h.

Free edge boundary conditions apply, namely

$$\frac{\partial^2 W}{\partial n^2} + \nu \frac{\partial^2 W}{\partial s^2} = 0 \quad \text{and} \quad \frac{\partial^3 W}{\partial n^3} + (2-\nu)\frac{\partial^3 W}{\partial n \partial s^2} = 0, \quad (\mathbf{x}, t) \in \partial\tilde{\Delta} \times T, \tag{2.8}$$

where n and s denote the normal and tangential directions on $\partial\tilde{\Delta}$ (where they exist), respectively, and ν is Poisson's ratio. An equation for the pressure, p, is given by the linearised Bernoulli equation (2.2) at the water surface. Substituting it into the plate equation (2.7) and making use of the restriction to time-harmonic motion (2.3) yields

$$D\,\nabla^4 w - \omega^2 \rho_\Delta h\, w = \mathrm{i}\omega\rho\phi - \rho g\, w, \quad \mathbf{x} \in \tilde{\Delta}. \tag{2.9}$$

2.1.3 Non-dimensionalisation

Non-dimensional variables (denoted with an overbar) are introduced,

$$(\bar{x}, \bar{y}, \bar{z}) := \frac{1}{a}(x, y, z), \quad \bar{w} := \frac{w}{a}, \quad \bar{k} := ak, \quad \bar{\alpha} := a\alpha, \quad \bar{\omega} := \omega\sqrt{\frac{a}{g}} \quad \text{and} \quad \bar{\phi} := \frac{\phi}{a\sqrt{ag}},$$

where $4a^2$ is the surface area of the ice floe. Dropping the overbars again, the complete non-dimensionalised boundary value problem for the scattered water velocity potential in infinite depth becomes

$$\nabla^2\phi = 0, \qquad \mathbf{y} \in D, \tag{2.10a}$$

$$\sup_{\mathbf{y}\in D} |\phi| < \infty, \tag{2.10b}$$

$$\frac{\partial\phi}{\partial n_{\mathbf{y}}} = f, \qquad \mathbf{y} \in \Gamma, \tag{2.10c}$$

$$\frac{\partial\phi}{\partial z} = \alpha\phi, \qquad \mathbf{x} \in S, \tag{2.10d}$$

where $f\colon \Gamma \to \mathbb{C}$ represents the forcing from the body, e.g. $f = -\partial\phi^{\mathrm{In}}/\partial n_{\mathbf{y}}$ in the case of a rigid body. The radiation condition remains,

$$\lim_{r\to\infty} \sqrt{r}\left(\frac{\partial}{\partial r} - \mathrm{i}k\right)(\phi - \phi^{\mathrm{In}}) = 0. \tag{2.10e}$$

In the case of an ice floe the kinematic boundary condition at the position of the ice floe,

$$\frac{\partial\phi}{\partial z} = -\mathrm{i}\sqrt{\alpha}w, \qquad \mathbf{x} \in \tilde{\Delta}, \tag{2.11}$$

replaces condition (2.10c).

In non-dimensional variables, the equation for the ice floe (2.9) reduces to

$$\beta\nabla^4 w - \alpha\gamma w = \mathrm{i}\sqrt{\alpha}\phi - w, \quad \mathbf{x} \in \tilde{\Delta} \tag{2.12}$$

with

$$\beta := \frac{D}{g\rho a^4} \quad \text{and} \quad \gamma := \frac{\rho_\Delta h}{\rho a}.$$

The constants β and γ represent the stiffness and the mass of the plate respectively. For convenience, non-dimensional variables will always be assumed in the sequel.

2.1.4 Transformation into an integral equation

Problem (2.10) for the water can be expressed as an integral equation over the immersed surface of the body. Let $\mathbb{R}^3_-$ denote the lower three-dimensional half-space and G: $\mathbb{R}^3_- \times \mathbb{R}^3_- \to \bar{\mathbb{C}}$ be the free surface Green's function satisfying the boundary value problem

$$\begin{aligned} \nabla^2_{\mathbf{y}} G(\mathbf{y};\zeta) &= \delta(\mathbf{y}-\zeta), && \mathbf{y},\zeta \in \mathbb{R}^3_-, \\ \sup_{\mathbf{y}\in\mathbb{R}^3_-} \left| G(\mathbf{y};\zeta) - \frac{1}{4\pi\|\mathbf{y}\|} \right| &< \infty, && \zeta \in \mathbb{R}^3_-, \\ \frac{\partial G}{\partial z} &= \alpha G, && \mathbf{x} \in S,\ \zeta \in \mathbb{R}^3_-, \end{aligned}$$

with the radiation condition

$$\lim_{r\to\infty} \sqrt{r}\left(\frac{\partial}{\partial r} - \mathrm{i}\alpha\right) G(\mathbf{y};\zeta) = 0, \quad z < 0,\ \zeta \in \mathbb{R}^3_-.$$

The scattered potential, denoted with ϕ^{S} for clarity, can then either be expressed as

$$\phi^{\mathrm{S}}(\mathbf{y}) = \int_\Gamma G(\mathbf{y},\zeta)\,\varsigma(\zeta)\,\mathrm{d}\sigma_\zeta, \tag{2.13}$$

where the source strength distribution function $\varsigma : \Gamma \to \mathbb{C}$ is given as the solution of the integral equation

$$\frac{1}{2}\varsigma(\mathbf{y}) - \int_\Gamma \frac{\partial G}{\partial n_{\mathbf{y}}}(\mathbf{y},\zeta)\,\varsigma(\zeta)\,\mathrm{d}\sigma_\zeta = -f(\mathbf{y}), \quad \mathbf{y} \in \Gamma, \tag{2.14}$$

as described by Wehausen & Laitone (1960). Or it can be represented by the use of Green's theorem,

$$\phi^{\mathrm{S}}(\mathbf{y}) = \int_\Gamma \phi^{\mathrm{S}}(\zeta)\frac{\partial G}{\partial n_\zeta}(\mathbf{y};\zeta) - G(\mathbf{y};\zeta)\frac{\partial \phi^{\mathrm{S}}}{\partial n_\zeta}(\zeta)\,\mathrm{d}\sigma_\zeta, \tag{2.15}$$

where the potential at the immersed surface of the body is given as the solution of the integral equation

$$\frac{1}{2}\phi^{\mathrm{S}}(\mathbf{y}) = \int_\Gamma \phi^{\mathrm{S}}(\zeta)\frac{\partial G}{\partial n_\zeta}(\mathbf{y};\zeta) - G(\mathbf{y};\zeta)\frac{\partial \phi^{\mathrm{S}}}{\partial n_\zeta}(\zeta)\,\mathrm{d}\sigma_\zeta, \quad \mathbf{y} \in \Gamma, \tag{2.16}$$

as illustrated by Linton & McIver (2001).

For water of finite depth, the same representation as in equations (2.13) and (2.15) can be obtained. The Green's function must then satisfy the bed condition instead of the depth condition and the lower half-space has to be replaced by $\mathbb{R}^2\times]-d,0[$.

2.2 Solving the problem with one ice floe

The following method can be used to solve for the surface displacement and the potential at the position of the ice floe (as suggested by Meylan, 2002). The boundary conditions at the water surface are applied to the representation of the potential given by equation (2.15) which then contains the surface displacement of the ice floe. From this, an integral equation for the potential is obtained by limiting the representation of the potential to the ice floe. The surface displacement of the ice floe is expanded into its modes of vibration by calculating the eigenfunctions and eigenvalues of the biharmonic operator. The integral equation for the potential is then solved for every eigenfunction which gives a corresponding potential to each eigenfunction. The expansion in the eigenfunctions simplifies the biharmonic equation and, by using the orthogonality of the eigenfunctions, a system of equations for the unknown coefficients of the eigenfunction expansion is obtained.

2.2.1 Simplification of the integral equation

In the case of a shallow draft, the immersed water surface of the body is given by $\tilde{\Delta}$. The kinematic boundary condition valid at the position of the shallow draft, equation (2.11), can therefore be applied to the representation of the potential given by equation (2.15). Furthermore, the Green's function is symmetric so it satisfies the free surface condition with respect to both variables which leaves

$$\phi^{\mathrm{S}}(\mathbf{y}) = \int_{\tilde{\Delta}} G(\mathbf{y};\zeta)\big(\alpha\phi^{\mathrm{S}}(\zeta) + \mathrm{i}\sqrt{\alpha}w(\zeta)\big)\,\mathrm{d}\sigma_\zeta. \tag{2.17}$$

Due to the linearity of the problem the incident potential can just be added to the equation to obtain the total water velocity potential, $\phi = \phi^{\mathrm{In}}+\phi^{\mathrm{S}}$. The total water velocity potential can also be written under the integral since the ambient incident potential satisfies the free surface condition (2.10d). Limiting the result to the water surface yields the integral equation

$$\phi(\mathbf{x}) = \phi^{\mathrm{In}}(\mathbf{x}) + \int_{\tilde{\Delta}} G(\mathbf{x};\xi)\big(\alpha\phi(\xi) + \mathrm{i}\sqrt{\alpha}w(\xi)\big)\,\mathrm{d}\sigma_\xi, \quad \mathbf{x}\in\tilde{\Delta}, \tag{2.18}$$

(Meylan, 2002). The appropriate Green's function is given by Havelock (1955),

$$G(\mathbf{x};\xi) = \frac{\mathrm{i}\alpha}{2} H_0^{(1)}(\alpha\|\mathbf{x}-\xi\|) + \frac{1}{2\pi\|\mathbf{x}-\xi\|} - \frac{1}{\pi^2}\int_0^\infty \frac{\alpha^2}{\eta^2+\alpha^2} K_0(\eta\|\mathbf{x}-\xi\|)\,\mathrm{d}\eta, \tag{2.19}$$

where $H_0^{(1)}$ is the Hankel function of the first kind and K_0 is the modified Bessel function of the second kind, both of order zero as defined in Abramowitz & Stegun (1964). Another equivalent representation is due to Havelock (1955) and Kim (1965),

$$G(\mathbf{x};\xi) = \frac{1}{2\pi\|\mathbf{x}-\xi\|} - \frac{\alpha}{4}\big(\mathbf{H}_0(\alpha\|\mathbf{x}-\xi\|) + Y_0(\alpha\|\mathbf{x}-\xi\|) - 2\mathrm{i}J_0(\alpha\|\mathbf{x}-\xi\|)\big), \tag{2.20}$$

where J_0 and Y_0 are Bessel functions of first and second kind of order zero respectively, and $\mathbf{H}_0$ is the Struve function of order zero. This result is due to the definition of the Hankel function of the first kind, $H_\nu^{(1)}(x) = J_\nu(x) + \mathrm{i}Y_\nu(x)$, and the fact that

$$\int_0^\infty \frac{\alpha^2}{\eta^2+\alpha^2} K_0(\eta x)\,\mathrm{d}\eta = \frac{\alpha\pi^2}{4}\big(\mathbf{H}_0(\alpha x) - Y_0(\alpha x)\big)$$

(Abramowitz & Stegun, 1964). Representation (2.20) will be used for the single diffraction calculations of the ice floes since it is numerically more favourable.

For general floating or submerged bodies the full three-dimensional free surface Green's function is required. The representations of this Green's function will be thoroughly discussed in chapter 4.

2.2.2 Solving the plate equation

Since the operator ∇^4, subject to the free edge boundary conditions, is linear and self-adjoint, it possesses a set of orthogonal eigenfunctions w^j and positive real eigenvalues λ_j which satisfy

$$\nabla^4 w^j = \lambda_j w^j, \quad j \in \mathbb{N}_{>0}.$$

The modes are assumed orthonormal and represent a basis for the possible motions. The eigenvalues λ_j are numbered with increasing value, i.e. $\lambda_j \geq \lambda_k$ for $j > k$.

Now, the displacement can be expanded into the eigenfunction basis,

$$w(\mathbf{x}) = \sum_{j=1}^{\infty} c_j w^j(\mathbf{x}), \quad \mathbf{x} \in \tilde{\Delta}. \tag{2.21}$$

Due to the linearity of equation (2.18), the potential can be expressed as

$$\phi(\mathbf{x}) = \phi^0(\mathbf{x}) + \sum_{j=1}^{\infty} c_j \phi^j(\mathbf{x}), \quad \mathbf{x} \in \tilde{\Delta}, \tag{2.22}$$

where ϕ^0 represents the potential due to the incoming wave assuming that the displacement of the ice floe is zero and the potentials ϕ^j represent the potential generated by the ice floe vibrating with the jth mode in the absence of any input wave force. Therefore, ϕ^0 and ϕ^j respectively satisfy the integral equations

$$\phi^0(\mathbf{x}) = \phi^{\mathrm{In}}(\mathbf{x}) + \int_{\tilde{\Delta}} \alpha G(\mathbf{x};\xi)\phi^0(\xi)\,\mathrm{d}\sigma_\xi, \quad \mathbf{x} \in \tilde{\Delta}, \tag{2.23a}$$

and

$$\phi^j(\mathbf{x}) = \int_{\Delta} G(\mathbf{x};\xi)\left(\alpha\phi^j(\mathbf{x}) + \mathrm{i}\sqrt{\alpha}w^j(\xi)\right)\,\mathrm{d}\sigma_\xi, \quad \mathbf{x} \in \tilde{\Delta}. \tag{2.23b}$$

Substituting equations (2.21) and (2.22) into the plate equation (2.12) yields

$$\beta\sum_{j=1}^{\infty}\lambda_j c_j w^j - \alpha\gamma\sum_{j=1}^{\infty} c_j w^j = \mathrm{i}\sqrt{\alpha}\Big(\phi^0 + \sum_{j=1}^{\infty} c_j\phi^j\Big) - \sum_{j=1}^{\infty} c_j w^j, \quad \mathbf{x} \in \tilde{\Delta}. \tag{2.24}$$

Keeping in mind the orthogonality of the eigenfunctions, multiplying by w^k and integrating over $\tilde{\Delta}$ leaves

$$\beta\lambda_k c_k + (1-\alpha\gamma)c_k = \int_{\tilde{\Delta}} \mathrm{i}\sqrt{\alpha}\Big(\phi^0(\mathbf{x}) + \sum_{j=1}^{\infty} c_j\phi^j(\mathbf{x})\Big)w^k(\mathbf{x})\,\mathrm{d}\sigma_{\mathbf{x}}, \quad k \in \mathbb{N}_{>0}, \tag{2.25}$$

which gives the required equations to determine the coefficients c_k. Since $c_k \to 0$ for $k \to \infty$, it is sufficient to consider the first N values (N chosen to the desired accuracy).

Figures 2.1 and 2.2 show the solutions for a single ice floe on water of infinite depth in two different situations (the implementation was developed by Michael H. Meylan). The properties of the ice floe, the stiffness β and the mass γ, are both chosen to be 0.02 and Poisson's ratio ν is 0.3333. The amplitude of the ambient wavefield, travelling in positive x-direction, is 1. Due to the normalisation, the ice floes occupy the area $]-1,1[\times]-1,1[$. Figure 2.1 shows the ice floe displacement if the wavelength of the ambient wavefield is $\lambda = 2$ (the length of the side of the ice floe) and figure 2.2 corresponds to a wavelength of $\lambda = 1$. Wavelengths greater than the side of the ice floe are not as interesting because the ice floe then just bends with the wave and does not notably scatter it (given the same stiffness and mass of the ice floe).

Since only the relation of the wavelength compared to the size of the ice floes and not the wavelength itself is important, the second plot can also be interpreted as being a larger ice floe under the same ambient wave as in the first plot. Then, however, the real stiffness and mass are not the same as in the first plot since the normalised parameters depend on the ice floe's size.

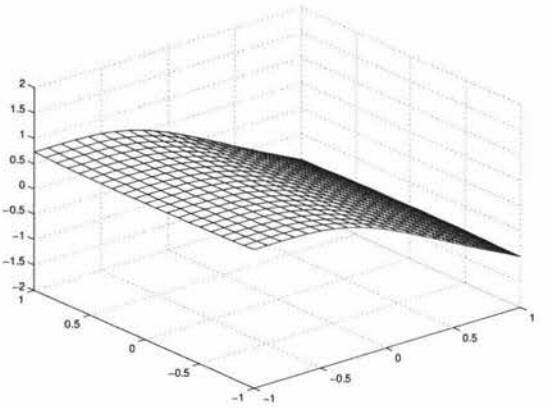

Figure 2.1: Displacement of the ice floe under incident wave of wavelength 2

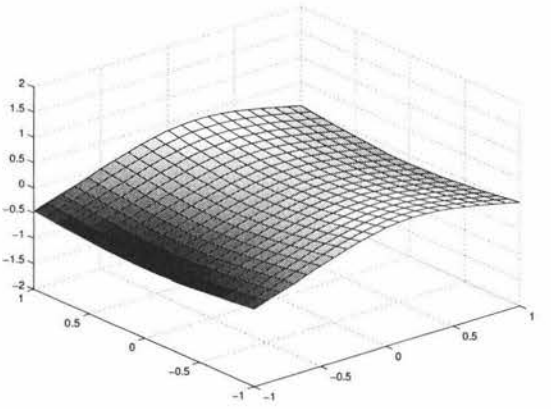

Figure 2.2: Displacement of the ice floe under incident wave of wavelength 1

All plots of ice floes appearing in this thesis are also available as animations over one period. These animations are stored on the attached CD-ROM (see appendix B for details).

Chapter 3

The cylindrical eigenfunction expansion of the water velocity potential

In this chapter a general solution for the water velocity potential will be developed. At first local cylindrical coordinates are introduced and Laplace's equation is solved in these coordinates by separation of variables assuming water of finite depth. This leads to the eigenfunction expansion of the water velocity potential in cylindrical waves. An equivalent solution will then be developed in water of infinite depth and it will be shown how this solution can also be obtained by taking the limit of the finite depth solution as the depth tends towards infinity.

3.1 Local cylindrical coordinates

For the body Δ a local cylindrical coordinate system is introduced by the transformation

$$\begin{aligned} \mathbb{R}^3 &\rightarrow [0,\infty[\times]-\pi,\pi] \times \mathbb{R}, \\ (x,y,z) &\mapsto (r,\theta,z), \\ x_o = x - O_x &= r\cos\theta, \\ y_o = y - O_y &= r\sin\theta, \\ z &= z, \end{aligned}$$

where r denotes the radius from the mean centre position $O = (O_x, O_y)$ of the body Δ and θ is the angle between r and the x-axis. Figure 3.1 illustrates the setting.

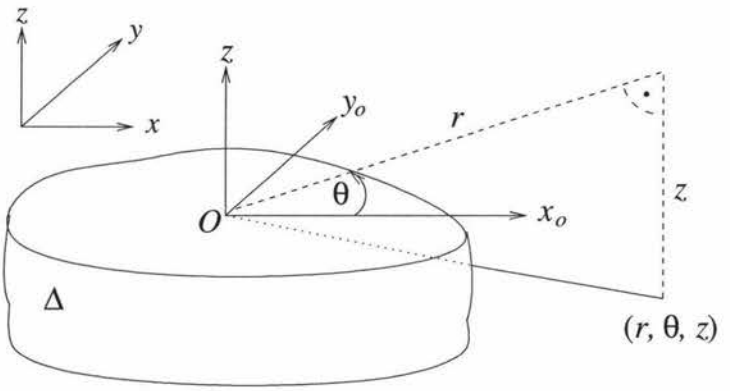

Figure 3.1: Coordinate systems of the body

3.2 Derivation of the eigenfunction expansion of the potential

In this section solutions for the water velocity potential shall be developed by separation of variables in the local cylindrical coordinates of the body in the two different settings of finitely and infinitely deep water.

In the local coordinates of the body, the problem for the potential $\phi(r, \theta, z)$ in the absence of the body transforms to

$$\frac{1}{r}\frac{\partial}{\partial r}\left(r\frac{\partial \phi}{\partial r}\right) + \frac{1}{r^2}\frac{\partial^2 \phi}{\partial \theta^2} + \frac{\partial^2 \phi}{\partial z^2} = 0, \qquad (r, \theta, z) \in \mathbb{R}_{>0} \times \,]-\pi, \pi] \times \mathbb{R}_{<0}, \tag{3.1a}$$

$$\frac{\partial \phi}{\partial z} - \alpha\phi = 0, \qquad (r, \theta, z) \in \mathbb{R}_{>0} \times \,]-\pi, \pi] \times \{0\}, \tag{3.1b}$$

as well as

$$\frac{\partial \phi}{\partial z} = 0, \qquad (r, \theta, z) \in \mathbb{R}_{>0} \times \,]-\pi, \pi] \times \{-d\}, \tag{3.1c}$$

in the case of constant finite depth d and

$$\sup\left\{\, |\phi| \;\middle|\; (r, \theta, z) \in \mathbb{R}_{>0} \times \,]-\pi, \pi] \times \mathbb{R}_{<0} \,\right\} < \infty \tag{3.1d}$$

in the case of infinite depth. The radiation condition

$$\lim_{r\to\infty} \sqrt{r}\left(\frac{\partial}{\partial r} - \mathrm{i}k\right)\phi = 0 \tag{3.1e}$$

with the wavenumber k as defined in the previous chapter also applies.

Since the coordinate system is located at the mean centre position of the body and only vertically non-overlapping bodies will be considered, the case $r = 0$ does not need to be taken into account.

3.2.1 The case of water of finite depth

The solution of problem (3.1) for the finite depth water velocity potential in local cylindrical coordinates is assumed separable,

$$\phi(r,\theta,z) =: Y(r,\theta)Z(z).$$

Substituting this into (3.1a) yields

$$\frac{1}{Y(r,\theta)}\left[\frac{1}{r}\frac{\partial}{\partial r}\left(r\frac{\partial Y}{\partial r}\right)+\frac{1}{r^2}\frac{\partial^2 Y}{\partial\theta^2}\right] = -\frac{1}{Z(z)}\frac{\mathrm{d}^2 Z}{\mathrm{d}z^2} = \eta^2. \tag{3.2}$$

The possible separation constants η will be determined by the free surface condition (3.1b) and the bed condition (3.1c).

In the setting of water of finite depth, the general solution of $Z(z)$ in equation (3.2) can be written as

$$Z(z) = F\cos\big(\eta(z+d)\big) + G\sin\big(\eta(z+d)\big), \quad \eta\in\mathbb{C}\backslash\{0\}, \tag{3.3}$$

since $\eta = 0$ is not an eigenvalue. To satisfy the bed condition (3.1c), G must be 0. $Z(z)$ satisfies the free surface condition (3.1b), provided the separation constants η are roots of the equation

$$-F\eta\sin\big(\eta(z+d)\big) - \alpha F\cos\big(\eta(z+d)\big) = 0 \ \text{ at } z=0,$$

or, equivalently, if they satisfy

$$\alpha + \eta\tan\eta d = 0. \tag{3.4}$$

Equation (3.4), also called dispersion relation, has an infinite number of real roots, denoted with k_m and $-k_m$ ($m\geq 1$), but the negative roots produce the same eigenfunctions as the positive ones and will therefore not be considered (Linton & McIver, 2001). It also has a pair of purely imaginary roots which will be denoted by k_0. Writing $k_0 = -\mathrm{i}k$, k is the (positive) root of the dispersion relation

$$\alpha = k\tanh kd, \tag{3.5}$$

again it suffices to consider only the positive root. The solutions can therefore be written as

$$Z_m(z) = F_m\cos\big(k_m(z+d)\big), \quad m\geq 0. \tag{3.6}$$

It follows that k is the previously introduced wavenumber and equation (3.5) gives the required relation to the radian frequency.

For the solution of

$$\frac{1}{r}\frac{\partial}{\partial r}\left(r\frac{\partial Y}{\partial r}\right)+\frac{1}{r^2}\frac{\partial^2 Y}{\partial\theta^2} = k_m^2 Y(r,\theta), \tag{3.7}$$

another separation will be used,

$$Y(r,\theta) =: R(r)\Theta(\theta).$$

Substituting this into equation (3.7) yields

$$\frac{r^2}{R(r)}\left[\frac{1}{r}\frac{\mathrm{d}}{\mathrm{d}r}\left(r\frac{\mathrm{d}R}{\mathrm{d}r}\right) - k_m^2 R(r)\right] = -\frac{1}{\Theta(\theta)}\frac{\mathrm{d}^2\Theta}{\mathrm{d}\theta^2} = \eta^2, \tag{3.8}$$

where the separation constant η must be an integer, say ν, in order for the potential to be continuous (Linton & McIver, 2001). $\Theta(\theta)$ can therefore be expressed as

$$\Theta(\theta) = C\,\mathrm{e}^{\mathrm{i}\nu\theta}, \quad \nu \in \mathbb{Z}.$$

Equation (3.8) also yields

$$r\frac{\mathrm{d}}{\mathrm{d}r}\left(r\frac{\mathrm{d}R}{\mathrm{d}r}\right) - (\nu^2 + k_m^2 r^2)R(r) = 0, \quad \nu \in \mathbb{Z}. \tag{3.9}$$

Substituting $\tilde{r} := k_m r$ and writing $\tilde{R}(\tilde{r}) := R(\tilde{r}/k_m) = R(r)$, this can be rewritten as

$$\tilde{r}^2\frac{\mathrm{d}^2\tilde{R}}{\mathrm{d}\tilde{r}^2} + \tilde{r}\frac{\mathrm{d}\tilde{R}}{\mathrm{d}\tilde{r}} - (\nu^2 + \tilde{r}^2)\,\tilde{R} = 0, \quad \nu \in \mathbb{Z},$$

which is the modified version of Bessel's equation. Substituting back, the general solution of equation (3.9) is given by

$$R(r) = D\,I_\nu(k_m r) + E\,K_\nu(k_m r), \quad m \in \mathbb{N},\ \nu \in \mathbb{Z},$$

where I_ν and K_ν are the modified Bessel functions of the first and second kind, respectively, of order ν.

The potential ϕ can thus be expressed in local cylindrical coordinates as

$$\phi(r,\theta,z) = \sum_{m=0}^{\infty} Z_m(z) \sum_{\nu=-\infty}^{\infty} [D_{m\nu}I_\nu(k_m r) + E_{m\nu}K_\nu(k_m r)]\,\mathrm{e}^{\mathrm{i}\nu\theta}, \tag{3.10}$$

where $Z_m(z)$ is given by equation (3.6). Substituting Z_m into equation (3.10) as well as noting that $k_0 = -\mathrm{i}k$ yields

$$\begin{aligned}\phi(r,\theta,z) = {} & F_0 \cos(-\mathrm{i}k(z+d)) \sum_{\nu=-\infty}^{\infty} [D_{0\nu}I_\nu(-\mathrm{i}kr) + E_{0\nu}K_\nu(-\mathrm{i}kr)]\,\mathrm{e}^{\mathrm{i}\nu\theta} \\ & + \sum_{m=1}^{\infty} F_m \cos(k_m(z+d)) \sum_{\nu=-\infty}^{\infty} [D_{m\nu}I_\nu(k_m r) + E_{m\nu}K_\nu(k_m r)]\,\mathrm{e}^{\mathrm{i}\nu\theta}.\end{aligned}$$

Noting that $\cos \mathrm{i}x = \cosh x$ is an even function and the relations $I_\nu(-\mathrm{i}x) = (-\mathrm{i})^\nu J_\nu(x)$ where J_ν is the Bessel function of the first kind of order ν and $K_\nu(-\mathrm{i}x) = \pi/2\ \mathrm{i}^{\nu+1}H_\nu^{(1)}(x)$

with $H_\nu^{(1)}$ denoting the Hankel function of the first kind of order ν (Abramowitz & Stegun, 1964), it follows that

$$\begin{aligned}\phi(r,\theta,z) = \cosh(k(z+d)) \sum_{\nu=-\infty}^{\infty} \left[D'_{0\nu} J_\nu(kr) + E'_{0\nu} H_\nu^{(1)}(kr)\right] \mathrm{e}^{\mathrm{i}\nu\theta} \\ + \sum_{m=1}^{\infty} F_m \cos(k_m(z+d)) \sum_{\nu=-\infty}^{\infty} \left[D'_{m\nu} I_\nu(k_m r) + E'_{m\nu} K_\nu(k_m r)\right] \mathrm{e}^{\mathrm{i}\nu\theta}.\end{aligned} \tag{3.11}$$

However, J_ν does not satisfy the radiation condition (3.1c) and neither does I_ν since it becomes unbounded for increasing real argument. These two solutions represent incoming waves which will also be required later.

Therefore, the solution of problem (3.1a), (3.1b), (3.1c) and (3.1e) requires $D'_{m\nu} = 0$ for all m, ν and (3.11) simplifies to the eigenfunction expansion of the water velocity potential into cylindrical outgoing waves with coefficients $A_{m\nu}$,

$$\begin{aligned}\phi(r,\theta,z) = \frac{\cosh(k(z+d))}{\cosh kd} \sum_{\nu=-\infty}^{\infty} A_{0\nu} H_\nu^{(1)}(kr) \mathrm{e}^{\mathrm{i}\nu\theta} \\ + \sum_{m=1}^{\infty} \frac{\cos(k_m(z+d))}{\cos k_m d} \sum_{\nu=-\infty}^{\infty} A_{m\nu} K_\nu(k_m r) \mathrm{e}^{\mathrm{i}\nu\theta}.\end{aligned} \tag{3.12}$$

The two terms describe the propagating and the decaying wavefields respectively.

3.2.2 The case of infinitely deep water

A solution will be developed for the same setting as before but under the assumption of water of infinite depth. As in the previous section, Laplace's equation must be solved in cylindrical coordinates satisfying the free surface and the radiation condition. However, instead of the bed condition, the water velocity potential is also required to satisfy the depth condition. Therefore, $Z(z)$ in equation (3.2) must be solved for satisfying the depth condition (3.1d). It will turn out that in the case of infinitely deep water an uncountable amount of separation constants η is valid.

As in equation (3.3), the general solution can be represented as

$$Z(z) = F\mathrm{e}^{\mathrm{i}\eta z} + G\mathrm{e}^{-\mathrm{i}\eta z}, \quad \eta \in \mathbb{C}\backslash\{0\}.$$

Assuming η has got a positive imaginary part, in order to satisfy the depth condition, F must be zero. $Z(z)$ then satisfies the free surface condition if η is a root of

$$-G\mathrm{i}\eta\mathrm{e}^{-\mathrm{i}\eta z} - \alpha G\mathrm{e}^{-\mathrm{i}\eta z} = 0 \text{ at } z = 0,$$

which yields the dispersion relation

$$\eta = -\mathrm{i}\alpha. \tag{3.13}$$

Therefore, η must even be purely imaginary. For $\operatorname{Im}\eta < 0$, equation (3.13) is also obtained, but with a minus sign in front of η. However, this yields the same solution. One solution can therefore be written as

$$Z(z) = G\mathrm{e}^{\alpha z}. \tag{3.14}$$

Now, η is assumed real. In this case, it is convenient to write the general solution in terms of cosine and sine,

$$Z(z) = F\cos(\eta z) + G\sin(\eta z), \quad \eta \in \mathbb{R}\backslash\{0\}. \tag{3.15}$$

This solution satisfies the depth condition automatically. Making use of the free surface condition, it follows that

$$(-\eta F - \alpha G)\sin(\eta z) + (\eta G - \alpha F)\cos(\eta z) = 0 \quad \text{at } z = 0,$$

which can be solved for G,

$$G = \frac{\alpha}{\eta} F.$$

Substituting this back into (3.15) gives

$$Z(z) = F\big(\cos(\eta z) + \frac{\alpha}{\eta}\sin(\eta z)\big), \quad \eta \in \mathbb{R}\backslash\{0\}.$$

Obviously, a negative value of η produces the same eigenfunction as the positive one. Therefore, only positive ones are considered, leading to the definition

$$\psi(z,\eta) := \cos(\eta z) + \frac{\alpha}{\eta}\sin(\eta z), \quad (z,\eta) \in \mathbb{R}_{\leq 0} \times \mathbb{R}_{>0}. \tag{3.16}$$

Equations (3.14) and (3.16) therefore give the vertical eigenfunctions in infinite depth.

For the radial and angular coordinate the same separation can be used as in the finite depth case so that the general solution of problem (3.1a), (3.1b) and (3.1d), in analogy to (3.10), can be written as

$$\begin{aligned}\phi(r,\theta,z) = \mathrm{e}^{\alpha z} \sum_{\nu=-\infty}^{\infty} &[E_\nu(-\mathrm{i}\alpha) I_\nu(-\mathrm{i}\alpha r) + F_\nu(-\mathrm{i}\alpha) K_\nu(-\mathrm{i}\alpha r)]\,\mathrm{e}^{\mathrm{i}\nu\theta} \\ &+ \int_0^\infty \psi(z,\eta) \sum_{\nu=-\infty}^{\infty} [E_\nu I_\nu(\eta r) + F_\nu(\eta) K_\nu(\eta r)]\,\mathrm{e}^{\mathrm{i}\nu\theta}\,\mathrm{d}\eta.\end{aligned}$$

Making use of the radiation condition, equation (3.1e), as well as the relations of the Bessel functions in the same way as in the finite depth case, this can be rewritten as the

eigenfunction expansion of the water velocity potential into cylindrical outgoing waves in water of infinite depth,

$$\phi(r,\theta,z) = \mathrm{e}^{\alpha z} \sum_{\nu=-\infty}^{\infty} A_\nu(\mathrm{i}\alpha) H_\nu^{(1)}(\alpha r)\mathrm{e}^{\mathrm{i}\nu\theta} + \int_0^\infty \psi(z,\eta) \sum_{\nu=-\infty}^{\infty} A_\nu(\eta) K_\nu(\eta r)\mathrm{e}^{\mathrm{i}\nu\theta}\,\mathrm{d}\eta. \quad (3.17)$$

3.2.3 Derivation of the infinite depth solution by taking the limit of the finite depth one

The result from the previous section can also be obtained by considering the eigenfunction expansion in the finite depth case and letting the depth d tend towards infinity. The representation of the potential ϕ in the local cylindrical coordinates of the body in water of depth d is recalled from equation (3.12),

$$\begin{aligned}\phi(r,\theta,z) = {} & \frac{\cosh(k(z+d))}{\cosh kd} \sum_{\nu=-\infty}^{\infty} A_{0\nu} H_\nu^{(1)}(kr)\mathrm{e}^{\mathrm{i}\nu\theta} \\ & + \sum_{m=1}^{\infty} \frac{\cos(k_m(z+d))}{\cos k_m d} \sum_{\nu=-\infty}^{\infty} A_{m\nu} K_\nu(k_m r)\mathrm{e}^{\mathrm{i}\nu\theta}.\end{aligned}$$

The factors k_m and k are roots of the dispersion relations (3.4) and (3.5) and depend on the depth.

At first, the propagating modes (the first term of equation (3.12)) shall be considered. The factor k is a solution of the dispersion relation (3.5). Since $\lim_{d\to\infty} \tanh d = 1$, k tends towards α as the depth becomes greater. It can be noted that this is already a good approximation for relatively small values of d (compare figure 3.2).

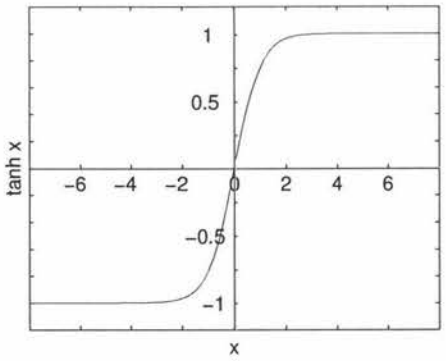

Figure 3.2: The graph of $\tanh x$

Regarding the following for the z-dependence term of the propagating modes,

$$\begin{aligned}\frac{\cosh(k(z+d))}{\cosh kd} &= \frac{\cosh kz\ \cosh kd + \sinh kz\ \sinh kd}{\cosh kd} \\ &= \cosh kz + \tanh kd\ \sinh kz,\end{aligned}$$

the limit $d \to \infty$ can be taken and the term for the propagating modes tends to

$$(\cosh \alpha z + \sinh \alpha z) \sum_{\nu=-\infty}^{\infty} A_{0\nu} H_\nu^{(1)}(\alpha r) \mathrm{e}^{\mathrm{i}\nu\theta} = \mathrm{e}^{\alpha z} \sum_{\nu=-\infty}^{\infty} A_{0\nu} H_\nu^{(1)}(\alpha r) \mathrm{e}^{\mathrm{i}\nu\theta},$$

which is exactly the same term as was obtained in the previous section, given in equation (3.17).

Now, the decaying modes will be considered. The factors k_m are the (positive) solutions of the dispersion relation (3.4). Rewriting the z-dependent term for the decaying modes,

$$\frac{\cos(k_m(z+d))}{\cos k_m d} = \frac{\cos k_m z\ \cos k_m d - \sin k_m z\ \sin k_m d}{\cos k_m d} = \cos k_m z - \tan k_m d \sin k_m z,$$

and making use of the dispersion relation in the following form,

$$-\frac{\alpha}{k_m} = \tan k_m d,$$

yields

$$\frac{\cos(k_m(z+d))}{\cos k_m d} = \cos k_m z + \frac{\alpha}{k_m} \sin k_m z. \tag{3.18}$$

Now, the dispersion relation (3.4) is considered for $\eta^* := \eta d$,

$$-\alpha d = \eta^* \tan \eta^*.$$

For large d, the roots of this equation tend towards $\eta^* = (m - \frac{1}{2})\pi$, $m \neq 0$ (compare figure 3.3), and, adopting the earlier notation, $k_m = \frac{\eta^*}{d}$ behaves like $(m - \frac{1}{2})\frac{\pi}{d}$ in the limit (only the positive roots are considered, so $m > 0$). These values for k_m are already good approximations for moderate depths.

The coefficients $A_{m\nu}$ depend on k_m and ν and can be written as $A_\nu(k_m)$. Substituting the asymptotics for k_m into the term for the decaying modes in equation (3.12), making use of the the rewritten term for the z-dependence from equation (3.18) and writing $h := \pi/d$ gives

$$h \sum_{m \in M}^{\infty} \left(\cos mhz + \frac{\alpha}{mh} \sin mhz \right) \sum_{\nu=-\infty}^{\infty} \frac{1}{h} A_\nu(mh) K_\nu(mhr) \mathrm{e}^{\mathrm{i}\nu\theta},$$

where M is the set of odd multiples of $1/2$, $M := \{m - 1/2 \,|\, m \in \mathbb{N}_{>0}\}$. Keeping in mind the behaviour of the coefficients in the limit due to the discrete points becoming a continuous line,

$$\lim_{h \to 0} \frac{1}{h} A_\nu(mh) = A_\nu(\eta), \quad m \in M,\ \eta \in \mathbb{R}_{>0},$$

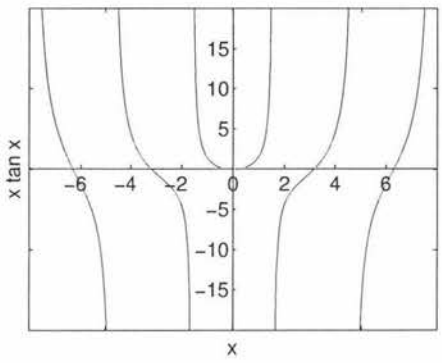

Figure 3.3: The graph of $x \tan x$

the limit as $h \to 0$ (which is equivalent to $d \to \infty$) of this Riemann sum is

$$\int_0^\infty \left(\cos \eta z + \frac{\alpha}{\eta} \sin \eta z\right) \sum_{\nu=-\infty}^{\infty} A_\nu(\eta) K_\nu(\eta r) \mathrm{e}^{\mathrm{i}\nu\theta} \, \mathrm{d}\eta.$$

This is exactly the same as the term for the decaying modes in the eigenfunction expansion derived in the previous section, given in equation (3.17).

Chapter 4

Different representations of the Green's functions

In this chapter different representations of the free surface Green's functions are developed. It was illustrated in chapter 2 how the scattered potential of a body can be represented with an appropriate Green's function. The interaction theory following in the next chapter requires this Green's function to be in the eigenfunction expansion introduced in the last chapter. It furthermore requires the representation of the potential due to the source point in the coordinates of the body and not, as it is standard, in the coordinates centred at the undisturbed water surface above the source point.

The finite depth case is considered first. After the equivalent representation of the infinite depth Green's function is found, numerical aspects are discussed which arise from the properties of the new representation of the Green's function.

At first however, Graf's addition theorem for Bessel functions is illustrated which will be required several times in the sequel.

4.1 Graf's addition theorem

In the following it will be necessary to be able to translate Bessel and Hankel functions to coordinate systems with different origins. This can be accomplished by using Graf's addition theorem for Bessel functions from Abramowitz & Stegun (1964). Adapted to the form in which it is required, it states

$$\mathscr{C}_\nu(w)\mathrm{e}^{\mathrm{i}\nu\beta} = \sum_{\mu=-\infty}^{\infty} \mathscr{C}_{\nu+\mu}(u)J_\mu(v)\mathrm{e}^{\mathrm{i}\mu\gamma} \quad \text{for } |v\mathrm{e}^{\pm\mathrm{i}\gamma}| < |u|, \tag{4.1}$$

where $\mathscr{C}_\nu$ denotes any linear combination of $H_\nu^{(1)}$, J_ν and Y_ν. The coefficients of the linear combination, however, may not depend on the order ν. The other variables are related by

$$w = \sqrt{u^2 + v^2 - 2uv\cos\gamma}, \quad u - v\cos\gamma = w\cos\beta \quad \text{and} \quad v\sin\gamma = w\sin\beta,$$

which is geometrically illustrated in figure 4.1 (for u,v real and positive and $0 < \gamma < \pi$).

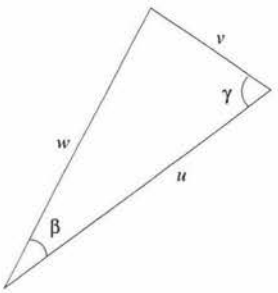

Figure 4.1: Triangle for Graf's addition theorem

It will now be shown how this can be applied to translate the Hankel function and the modified Bessel function of the second kind to coordinate systems with different origins. The particular case illustrated here will be used in the next chapter.

The coordinate systems of two different bodies Δ_j and Δ_l ($l, j \in \{1 \dots N\}$, $j \neq l$) are given by (r_j, θ_j, z) and (r_l, θ_l, z) respectively. Their geometrical relation in the (x, y)-plane is shown in figure 4.2.

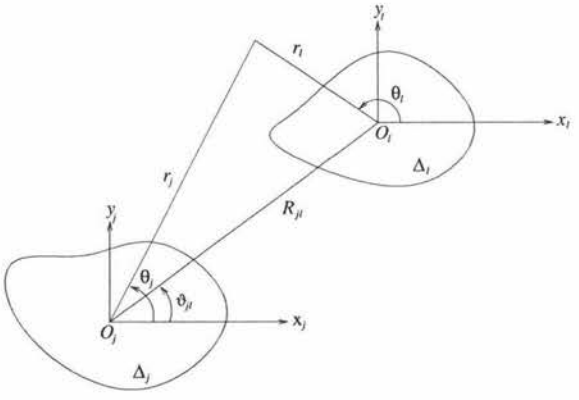

Figure 4.2: Relation between two bodies (plan view)

A comparison of figure 4.2 to the triangle for the addition theorem in figure 4.1 yields

$$H_\nu^{(1)}(kr_j)\mathrm{e}^{\mathrm{i}\nu(\theta_j - \vartheta_{jl})} = \sum_{\mu=-\infty}^{\infty} H_{\nu+\mu}^{(1)}(kR_{jl})\, J_\mu(kr_l)\mathrm{e}^{\mathrm{i}\mu(\pi - \theta_l + \vartheta_{jl})}, \quad j \neq l, \tag{4.2a}$$

for $r_l < R_{jl}$ from equation (4.1).

A similar relation is also required for $K_\nu(x)$ which is a linear combination of $J_\nu(\mathrm{i}x)$ and $Y_\nu(\mathrm{i}x)$,

$$K_\nu(x) = \frac{\pi}{2}\mathrm{i}^{\nu+1}(J_\nu(\mathrm{i}x) + Y_\nu(\mathrm{i}x)).$$

Although the coefficients depend on the order ν, the application of the relation $J_\mu(\mathrm{i}x) = \mathrm{i}^\mu I_\mu(x)$ between J_μ and I_μ (Abramowitz & Stegun, 1964) gives

$$K_\nu(k_m r_j)\mathrm{e}^{\mathrm{i}\nu(\theta_j - \vartheta_{jl})} = \sum_{\mu=-\infty}^{\infty} K_{\nu+\mu}(k_m R_{jl})\, I_\mu(k_m r_l)\mathrm{e}^{\mathrm{i}\mu(\pi-\theta_l+\vartheta_{jl})}, \quad j \neq l, \tag{4.2b}$$

as long as $r_l < R_{jl}$.

4.2 The eigenfunction expansion in finite depth

The interaction method requires the Green's function to be in the eigenfunction representation introduced in the last chapter. It is furthermore required that the coordinate system is not centred at the point above the source point but at an arbitrary point of the water surface. The application of Graf's addition theorem to the well-known eigenfunction representation of the Green's function allows this coordinate transformation while retaining the expansion in the modes.

In water of finite depth d the eigenfunction expansion of the velocity potential in cylindrical coordinates due to a single point source at $(0, 0, c)$, $c \leq 0$, with strength 1 is given by John (1950),

$$\begin{aligned} g(r, z; c) = {} & 2\pi\mathrm{i}\,\frac{\alpha^2 - k^2}{(\alpha^2 - k^2)d - \alpha}\cosh k(z+d)\cosh k(c+d)\, H_0^{(1)}(kr) \\ & + 4\sum_{m=1}^{\infty}\frac{k_m^2 + \alpha^2}{(k_m^2 + \alpha^2)d - \alpha}\cos k_m(z+d)\cos k_m(c+d)\, K_0(k_m r). \end{aligned} \tag{4.3}$$

Since this is the potential due to a single point, there is no angular dependence. It can be noted that this potential can be easily written in the eigenfunction representation introduced in the previous chapter by multiplying with the factor $\cosh kd/\cosh kd$.

Now, for points outside the body Δ, the velocity potential due to a point source at an arbitrary point $(s, \varphi, c) \in \Gamma$ shall be represented in terms of the local coordinates centred at the mean centre position O (compare figure 4.3).
Comparing figures 4.1 and 4.3, this can be accomplished by the application of Graf's

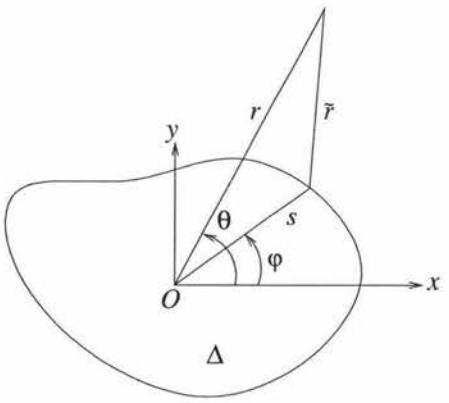

Figure 4.3: Setting with a single point source at (s, φ, c) (plan view)

addition theorem, equation (4.1), from the previous section in a slightly different way,

$$H_0^{(1)}(k\tilde{r}) = \sum_{\nu=-\infty}^{\infty} H_\nu^{(1)}(kr) J_\nu(ks) \mathrm{e}^{\mathrm{i}\nu(\theta-\varphi)}, \tag{4.4a}$$

$$K_0(k_m\tilde{r}) = \sum_{\nu=-\infty}^{\infty} K_\nu(k_m r) I_\nu(k_m s) \mathrm{e}^{\mathrm{i}\nu(\theta-\varphi)}, \tag{4.4b}$$

which is valid for $r > s$, thus for points outside the body. The potential due to the single point source can therefore be written in the local coordinates of the body Δ. Keeping in mind that the Green's function requires a source strength of $1/4\pi$, the Green's function is given by

$$\begin{aligned} &G(r, \theta, z; s, \varphi, c) \\ &\quad = \frac{\mathrm{i}}{2} \frac{\alpha^2 - k^2}{d(\alpha^2 - k^2) - \alpha} \cosh k(z+d) \cosh k(c+d) \sum_{\nu=-\infty}^{\infty} H_\nu^{(1)}(kr) J_\nu(ks) \mathrm{e}^{\mathrm{i}\nu(\theta-\varphi)} \\ &\qquad + \frac{1}{\pi} \sum_{m=1}^{\infty} \frac{k_m^2 + \alpha^2}{d(k_m^2 + \alpha^2) - \alpha} \cos k_m(z+d) \cos k_m(c+d) \sum_{\nu=-\infty}^{\infty} K_\nu(k_m r) I_\nu(k_m s) \mathrm{e}^{\mathrm{i}\nu(\theta-\varphi)}. \end{aligned} \tag{4.5}$$

It is given in the eigenfunction representation introduced in the last chapter except for the factor $\cosh kd / \cosh kd$. Due to the restriction of validity of Graf's addition theorem, this representation is valid for $r > s$ so certainly for points (r, θ, z) outside the escribed cylinder of the body. It can be noted that equation (4.5) states the same Green's function Goo & Yoshida (1990) and Chakrabarti (2000) used in their calculations.

Point sources of a shallow draft $\tilde{\Delta}$ imply $c = 0$ since its location is assumed at the water surface. If, furthermore, only the potential at the water surface needs to be evaluated as

in the calculation of ice floe motion, the required Green's function simplifies to

$$\begin{aligned} G(r,\theta;s,\varphi) = {} & \frac{\mathrm{i}}{2}\,\frac{\alpha^2-k^2}{d(\alpha^2-k^2)-\alpha}\,\cosh^2 kd \sum_{\nu=-\infty}^{\infty} H_\nu^{(1)}(kr)J_\nu(ks)\mathrm{e}^{\mathrm{i}\nu(\theta-\varphi)} \\ & + \frac{1}{\pi}\sum_{m=1}^{\infty}\frac{k_m^2+\alpha^2}{d(k_m^2+\alpha^2)-\alpha}\,\cos^2 k_m d \sum_{\nu=-\infty}^{\infty} K_\nu(k_m r)I_\nu(k_m s)\mathrm{e}^{\mathrm{i}\nu(\theta-\varphi)}, \quad r>s. \end{aligned} \tag{4.6}$$

4.3 The eigenfunction expansion in infinite depth

In water of infinite depth, the application of Graf's addition theorem also allows the eigenfunction expansion of the Green's function where the coordinate system is centred at an arbitrary point of the water surface. However, since the infinite depth single source potential is not given in eigenfunction representation, its eigenfunction expansion must first be derived. In the case where only the potential due to a shallow draft at the water surface is required, this can be accomplished easily from an existing representation. In the full three-dimensional case however, a more complex procedure is necessary which involves taking the limit of the finite depth single source potential in eigenfunction representation as the depth becomes infinite.

In infinitely deep water, the velocity potential due to a single point source at a point $(0,0,c)$, $c \le 0$, with strength 1 is given in cylindrical coordinates by Havelock (1955),

$$\begin{aligned} g(r,z;c) = {} & 2\pi\mathrm{i}\alpha\,\mathrm{e}^{\alpha(z+c)}\,H_0^{(1)}(\alpha r) + \frac{1}{R^0} + \frac{1}{R^1} \\ & - \frac{4}{\pi}\int_0^\infty \frac{\alpha}{\eta^2+\alpha^2}\big(\alpha\cos\eta(z+c) - \eta\sin\eta(z+c)\big)\,K_0(\eta r)\,\mathrm{d}\eta, \end{aligned} \tag{4.7}$$

where R^0 denotes the (three-dimensional) distance from the source point, $(R^0)^2 = x^2 + y^2 + (z-c)^2$, and R^1 the upward distance, $(R^1)^2 = x^2 + y^2 + (z+c)^2$. If the point source is located at the water surface and only the potential for $z = 0$ is considered, equation (4.7) simplifies to

$$g(r) = 2\pi\mathrm{i}\alpha\,H_0^{(1)}(\alpha r) + \frac{2}{r} - \frac{4}{\pi}\int_0^\infty \frac{\alpha^2}{\eta^2+\alpha^2}K_0(\eta r)\,\mathrm{d}\eta. \tag{4.8}$$

Using the fact that

$$\frac{1}{r} = \frac{1}{r}\,\frac{2}{\pi}\int_0^\infty K_0(s)ds \overset{s=\eta r}{=} \frac{2}{\pi}\int_0^\infty K_0(\eta r)\,\mathrm{d}\eta,$$

the second and the third term in equation (4.8) can be rewritten as

$$\frac{2}{r} - \frac{4}{\pi}\int_0^\infty \frac{\alpha^2}{\eta^2+\alpha^2} K_0(\eta r)\,\mathrm{d}\eta = \frac{4}{\pi}\int_0^\infty \Big(1 - \frac{\alpha^2}{\eta^2+\alpha^2}\Big) K_0(\eta r)\,\mathrm{d}\eta = \frac{4}{\pi}\int_0^\infty \frac{\eta^2}{\eta^2+\alpha^2} K_0(\eta r)\,\mathrm{d}\eta.$$

Now, the potential due to a single source point at the water surface can be easily converted into the eigenfunction representation from the last chapter,

$$g(r) = 2\pi \mathrm{i}\alpha\, H_0^{(1)}(\alpha r) + \frac{4}{\pi}\int_0^\infty \frac{\eta^2}{\eta^2+\alpha^2} K_0(\eta r)\,\mathrm{d}\eta. \tag{4.9}$$

In the case of a general floating or submerged body where the z-dependence is required or the point source is not located at the water surface, it is also possible to represent the potential in the eigenfunction expansion. This can be achieved by taking the limit of the finite depth single source potential in eigenfunction representation, equation (4.3), as d tends to infinity before applying Graf's addition theorem. Similar to the procedure in chapter 3 the propagating and the decaying modes will be considered separately.

At first the limit of the term representing the propagating modes,

$$2\pi \mathrm{i}\, \frac{\alpha^2 - k^2}{(\alpha^2 - k^2)d - \alpha} \cosh k(z+d) \cosh k(c+d)\, H_0^{(1)}(kr),$$

is taken. This can be accomplished by making use of the dispersion relation (3.5) and the relations of hyperbolic functions (Abramowitz & Stegun, 1964),

$$\tanh kd = \frac{\alpha}{k} \quad \Rightarrow \quad \cosh kd = \pm\frac{k}{\sqrt{k^2-\alpha^2}}.$$

Using this result,

$$\begin{aligned}\cosh k(z+d)\cosh k(c+d) &= (\cosh kd)^2 \frac{\cosh k(z+d)}{\cosh kd}\frac{\cosh k(c+d)}{\cosh kd} \\ &= \frac{k^2}{k^2-\alpha^2}\frac{\cosh k(z+d)}{\cosh kd}\frac{\cosh k(c+d)}{\cosh kd},\end{aligned}$$

and noting that

$$\frac{\alpha^2 - k^2}{(\alpha^2 - k^2)d - \alpha}\,\frac{k^2}{k^2-\alpha^2} = \frac{-k^2}{(\alpha^2 - k^2)d - \alpha},$$

the results from chapter 3 can be recalled,

$$k \longrightarrow \alpha \qquad \text{and} \qquad \frac{\cosh k(z+d)}{\cosh kd} \longrightarrow \mathrm{e}^{\alpha z} \qquad \text{as} \quad d \longrightarrow \infty,$$

to yield the limit of the term representing the propagating modes,

$$2\pi \mathrm{i}\alpha\, \mathrm{e}^{\alpha(z+c)}\, H_0^{(1)}(\alpha r).$$

Unsurprisingly, this is the same as the term for the propagating modes in equation (4.7) since it was already given in the eigenfunction expansion.

Now the term for the decaying modes,

$$4\sum_{m=1}^{\infty}\frac{k_m^2+\alpha^2}{(k_m^2+\alpha^2)d-\alpha}\cos k_m(z+d)\cos k_m(c+d)\,K_0(k_m r),$$

will be considered. The cosine terms are expanded,

$$\begin{aligned}\cos k_m(z+d)\cos k_m(c+d) &= \cos k_m z\cos k_m c\cos^2 k_m d+\sin k_m z\sin k_m c\sin^2 k_m d\\ &\quad-(\cos k_m z\sin k_m c+\cos k_m c\sin k_m z)\cos k_m d\sin k_m d,\end{aligned}$$

and the dispersion relation (3.4) is used: since

$$\tan k_m d=-\frac{\alpha}{k_m}$$

must hold, it follows from the relations of the angles and sides of a triangle that the sine and cosine are given by

$$\sin k_m d=\pm\frac{\alpha}{\sqrt{k_m^2+\alpha^2}}\quad\text{and}\quad\cos k_m d=\mp\frac{k_m}{\sqrt{k_m^2+\alpha^2}}.$$

Substituting this into the expansion of the cosine terms yields

$$\begin{aligned}&\cos k_m(z+d)\cos k_m(c+d)\\ &\quad=\cos k_m z\cos k_m c\frac{k_m^2}{k_m^2+\alpha^2}+\sin k_m z\sin k_m c\frac{\alpha^2}{k_m^2+\alpha^2}\\ &\qquad+(\cos k_m z\sin k_m c+\cos k_m c\sin k_m z)\frac{\alpha k_m}{k_m^2+\alpha^2}\\ &\quad=\frac{1}{2}\Big(\frac{k_m^2}{k_m^2+\alpha^2}\big(\cos k_m(z-c)+\cos k_m(z+c)\big)\\ &\qquad+\frac{\alpha^2}{k_m^2+\alpha^2}\big(\cos k_m(z-c)-\cos k_m(z+c)\big)+\frac{2\alpha k_m}{k_m^2+\alpha^2}\sin k_m(z+c)\Big)\\ &\quad=\frac{1}{2}\Big(\cos k_m(z-c)+\frac{k_m^2-\alpha^2}{k_m^2+\alpha^2}\cos k_m(z+c)+\frac{2\alpha k_m}{k_m^2+\alpha^2}\sin k_m(z+c)\Big).\end{aligned}$$

Using the result that k_m behaves like $(m-\frac{1}{2})\frac{\pi}{d}$ from chapter 3 as well as adopting the notation, $h=\pi/d$ and $M=\{m-1/2\,|\,m\in\mathbb{N}_{>0}\}$, the term for the decaying modes becomes

$$\begin{aligned}\frac{2}{\pi}h\sum_{m\in M}\frac{k_m^2+\alpha^2}{(k_m^2+\alpha^2)-\alpha/d}\Big(&\cos mh(z-c)+\frac{(mh)^2-\alpha^2}{(mh)^2+\alpha^2}\cos mh(z+c)\\ &+\frac{2\alpha mh}{(mh)^2+\alpha^2}\sin mh(z+c)\Big)K_0(mhr).\end{aligned}$$

The limit of this Riemann sum as h tends to zero (which is equivalent to d tending to infinity) is

$$\frac{2}{\pi}\int_0^\infty \Big(\cos\eta(z-c)+\frac{\eta^2-\alpha^2}{\eta^2+\alpha^2}\cos\eta(z+c)+\frac{2\alpha\eta}{\eta^2+\alpha^2}\sin\eta(z+c)\Big)K_0(\eta r)\,\mathrm{d}\eta.$$

The potential due to a single source point in water of infinite depth can therefore be written as

$$\begin{aligned} g(r,z;c) &= 2\pi\mathrm{i}\alpha\,\mathrm{e}^{\alpha(z+c)}H_0^{(1)}(\alpha r) \\ &\quad+\frac{2}{\pi}\int_0^\infty \Big(\cos\eta(z-c)\,\frac{\eta^2-\alpha^2}{\eta^2+\alpha^2}\,\cos\eta(z+c)+\frac{2\alpha\eta}{\eta^2+\alpha^2}\,\sin\eta(z+c)\Big)K_0(\eta r)\,\mathrm{d}\eta. \end{aligned} \tag{4.10}$$

In order to be used with the interaction theory, the Green's function has to be represented in the eigenfunction representation introduced in chapter 3. Therefore, the factors depending on z and c in the term for the decaying modes have to be written as a product of each other. This can be accomplished by the following calculation,

$$\begin{aligned} &\cos\eta(z-c)+\frac{\eta^2-\alpha^2}{\eta^2+\alpha^2}\cos\eta(z+c)+\frac{2\alpha\eta}{\eta^2+\alpha^2}\sin\eta(z+c) \\ &\quad=\cos\eta z\Big(\cos\eta c+\frac{\eta^2-\alpha^2}{\eta^2+\alpha^2}\cos\eta c+\frac{2\alpha\eta}{\eta^2+\alpha^2}\sin\eta c\Big) \\ &\qquad+\sin\eta z\Big(\sin\eta c-\frac{\eta^2-\alpha^2}{\eta^2+\alpha^2}\sin\eta c+\frac{2\alpha\eta}{\eta^2+\alpha^2}\cos\eta c\Big) \\ &\quad=\Big(\frac{2\eta^2}{\eta^2+\alpha^2}\cos\eta c+\frac{2\alpha\eta}{\eta^2+\alpha^2}\sin\eta c\Big)\Big(\cos\eta z+\frac{2\alpha^2\sin\eta c+2\alpha\eta\cos\eta c}{2\eta^2\cos\eta c+2\alpha\eta\sin\eta c}\sin\eta z\Big) \\ &\quad=2\Big(\frac{\eta^2}{\eta^2+\alpha^2}\cos\eta c+\frac{\alpha\eta}{\eta^2+\alpha^2}\sin\eta c\Big)\Big(\cos\eta z+\frac{\alpha}{\eta}\sin\eta z\Big). \end{aligned}$$

The three-dimensional single source potential in eigenfunction representation is therefore given by

$$\begin{aligned} g(r,z;c) &= 2\pi\mathrm{i}\alpha\,\mathrm{e}^{\alpha(z+c)}H_0^{(1)}(\alpha r) \\ &\quad+\frac{4}{\pi}\int_0^\infty \Big(\cos\eta z+\frac{\alpha}{\eta}\sin\eta z\Big)\frac{\eta^2}{\eta^2+\alpha^2}\Big(\cos\eta c+\frac{\alpha}{\eta}\sin\eta c\Big)K_0(\eta r)\,\mathrm{d}\eta. \end{aligned} \tag{4.11}$$

For $z=c=0$ this result is the same as the eigenfunction expansion of the single source potential at the water surface (4.9), which was derived directly. Equation (4.11) yields the eigenfunction expansion of the infinite depth free surface Green's function. The numerical expense of its computation will be compared to that of existing representations in the next section.

Now, as before, for points outside the body Δ, the velocity potential due to a point source at an arbitrary point $(s, \varphi, c) \in \Gamma$ shall be represented in terms of the local coordinates centred at the mean centre position O (compare figure 4.3). Again, this can be accomplished by the application of Graf's addition theorem, equation (4.1), to obtain

$$H_0^{(1)}(\alpha\tilde{r}) = \sum_{\nu=-\infty}^{\infty} H_\nu^{(1)}(\alpha r) J_\nu(\alpha s) \mathrm{e}^{\mathrm{i}\nu(\theta-\varphi)}, \tag{4.12a}$$

$$K_0(\eta\tilde{r}) = \sum_{\nu=-\infty}^{\infty} K_\nu(\eta r) I_\nu(\eta s) \mathrm{e}^{\mathrm{i}\nu(\theta-\varphi)}, \tag{4.12b}$$

which is valid for $r > s$, thus for points outside the body. Generally, the potential due to the single point source can therefore be written in the local coordinates of the body Δ. Keeping in mind that the Green's function requires a source strength of $1/4\pi$, the Green's function for the use in a fixed coordinate system is given by

$$\begin{aligned} G(r, \theta, z; s, \varphi, c) = {} & \frac{\mathrm{i}\alpha}{2} \mathrm{e}^{\alpha(z+c)} \sum_{\nu=-\infty}^{\infty} H_\nu^{(1)}(\alpha r) J_\nu(\alpha s) \mathrm{e}^{\mathrm{i}\nu(\theta-\varphi)} \\ & + \frac{1}{\pi^2} \int_0^\infty \Big(\cos\eta z + \frac{\alpha}{\eta} \sin\eta z \Big) \frac{\eta^2}{\eta^2 + \alpha^2} \Big(\cos\eta c + \frac{\alpha}{\eta} \sin\eta c \Big) \sum_{\nu=-\infty}^{\infty} K_\nu(\eta r) I_\nu(\eta s) \mathrm{e}^{\mathrm{i}\nu(\theta-\varphi)} \, \mathrm{d}\eta. \end{aligned} \tag{4.13}$$

Due to the restriction of validity of Graf's addition theorem, this representation is valid for $r > s$ thus certainly for points (r, θ, z) outside the escribed cylinder of the body.

In the case of a shallow draft $\tilde{\Delta}$, which is located at the water surface, c is zero. Furthermore, if only the potential at the water surface needs to be evaluated, the required Green's function simplifies to

$$\begin{aligned} G(r, \theta; s, \varphi) = {} & \frac{\mathrm{i}\alpha}{2} \sum_{\nu=-\infty}^{\infty} H_\nu^{(1)}(\alpha r) J_\nu(\alpha s) \mathrm{e}^{\mathrm{i}\nu(\theta-\varphi)} \\ & + \frac{1}{\pi^2} \int_0^\infty \frac{\eta^2}{\eta^2 + \alpha^2} \sum_{\nu=-\infty}^{\infty} K_\nu(\eta r) I_\nu(\eta s) \mathrm{e}^{\mathrm{i}\nu(\theta-\varphi)} \, \mathrm{d}\eta, \quad r > s. \end{aligned} \tag{4.14}$$

4.4 Numerical comparison to existing representations of the infinite depth Green's function

In this section the numerical properties of the different representations of the free surface Green's function in infinite depth will be compared to the eigenfunction expansion derived

in the previous section. At first, the most common and easily computable representations are introduced.

Let $\mathbf{y} = (x, y, z)$ and $\zeta = (a, b, c)$ represent points in the water (in absence of a body). One representation of the Green's function is easily obtained from equation (4.7),

$$G(\mathbf{y};\zeta) = \frac{\mathrm{i}\alpha}{2}\mathrm{e}^{\alpha(z+c)}\, H_0^{(1)}(\alpha r_\zeta) + \frac{1}{4\pi r^0} + \frac{1}{4\pi r^1} - \frac{1}{\pi^2}\int_0^\infty \frac{\alpha^2\cos\eta(z+c) - \eta\alpha\sin\eta(z+c)}{\eta^2+\alpha^2} K_0(\eta r_\zeta)\,\mathrm{d}\eta, \tag{4.15a}$$

where $r_\zeta^2 = (x-a)^2+(y-b)^2$ is the polar radius of the field point from the source point and r^0 and r^1 are defined anagolously to the previous section, $(r^0)^2 = (x-a)^2+(y-b)^2+(z-c)^2$ and $(r^1)^2 = (x-a)^2+(y-b)^2+(z+c)^2$. It was originally given by Havelock (1955) and will therefore be referred to as Havelock's representation of the Green's function. It can be noted that Havelock's representation can also be expressed in the closely related form

$$G(\mathbf{y};\zeta) = \frac{\mathrm{i}\alpha}{2}\, e^{\alpha(z+c)}\, H_0^{(1)}(\alpha r_\zeta) + \frac{1}{4\pi r^0} + \frac{1}{2\pi^2}\int_0^\infty \frac{(\eta^2-\alpha^2)\cos\eta(z+c) + 2\eta\alpha\sin\eta(z+c)}{\eta^2+\alpha^2} K_0(\eta r_\zeta)\,\mathrm{d}\eta \tag{4.15b}$$

(Linton & McIver, 2001). An equivalent representation is the three-dimensional version of equation (2.20), given by Kim (1965),

$$G(\mathbf{y};\zeta) = \frac{1}{4\pi r^0} + \frac{1}{4\pi r^1} - \frac{\alpha}{4}e^{\alpha(z+c)}\Big(\mathbf{H}_0(\alpha r_\zeta) + Y_0(\alpha r_\zeta) - 2\mathrm{i}J_0(\alpha r_\zeta) + \frac{2}{\pi}\int_{z+c}^0 \frac{\mathrm{e}^{-\alpha\eta}}{\sqrt{r_\zeta^2+\eta^2}}\,\mathrm{d}\eta\Big). \tag{4.15c}$$

This Green's function will be referred to as Kim's representation. The derivation from the last section yields a new representation of the free surface Green's function: its eigenfunction expansion into cylindrical outgoing waves. It can be easily obtained from equation (4.11),

$$G(\mathbf{y};\zeta) = \frac{\mathrm{i}\alpha}{2}\mathrm{e}^{\alpha(z+c)}H_0^{(1)}(\alpha r_\zeta) + \frac{1}{\pi^2}\int_0^\infty \Big(\cos\eta z + \frac{\alpha}{\eta}\sin\eta z\Big)\frac{\eta^2}{\eta^2+\alpha^2}\Big(\cos\eta c + \frac{\alpha}{\eta}\sin\eta c\Big)K_0(\eta r_\zeta)\,\mathrm{d}\eta. \tag{4.15d}$$

The numerically difficult parts of the Green's functions are compared. All functions appearing in the four different representations are quite standard except the Struve function

which occurs in Kim's representation of the Green's function, equation (4.15c). Although quick algorithms for its evaluation exist, the Struve function is not standard in many modern software packages which is a slight disadvantage of this representation. However, the calculation of the integrals,

$$\int_0^\infty \frac{\alpha^2 \cos\eta(z+c) - \eta\alpha \sin\eta(z+c)}{\eta^2+\alpha^2} K_0(\eta r_\zeta)\,\mathrm{d}\eta, \tag{4.16a}$$

$$\int_0^\infty \frac{(\eta^2-\alpha^2)\cos\eta(z+c) + 2\eta\alpha \sin\eta(z+c)}{\eta^2+\alpha^2} K_0(\eta r_\zeta)\,\mathrm{d}\eta, \tag{4.16b}$$

$$\int_{z+c}^0 \frac{\mathrm{e}^{-\alpha\eta}}{\sqrt{r_\zeta^2+\eta^2}}\,\mathrm{d}\eta, \tag{4.16c}$$

$$\int_0^\infty \Big(\cos\eta z + \frac{\alpha}{\eta}\sin\eta z\Big)\frac{\eta^2}{\eta^2+\alpha^2}\Big(\cos\eta c + \frac{\alpha}{\eta}\sin\eta c\Big) K_0(\eta r_\zeta)\,\mathrm{d}\eta, \tag{4.16d}$$

from equations (4.15), are the numerically most difficult tasks in the evaluation of the Green's functions.

The disadvantage of the first two terms from equations (4.16) is that the integrands are singular at zero. The numerical evaluation of the integrals is therefore rather expensive. Hearn (1977) showed that the evaluation of Kim's representation of the Green's function (the numerically difficult part given by equation (4.16c)) is in general much easier than that of Havelock's representation (the numerically difficult part given by equation (4.16a)) since it only involves the integration of a non-singular integrand. In the term from the eigenfunction representation of the Green's function, equation (4.16d), the integrand is non-singular over the integration interval as well. The only problem appears to be the infinite upper integration boundary. Due to the fast decay of the modified Bessel function of the second kind however, the integrand decays quickly for large argument and the integral only needs to be calculated over a small interval.

Figure 4.4 shows the integrands of the different terms in equations (4.16). In all plots, the remaining variables are chosen to be $\alpha = \pi$, $c = -1$, $z = -1$ and $r_\zeta = 1$. As can be seen, the lower two plots corresponding to Kim's representation and the eigenfunction expansion are numerically much easier to integrate. All integrands decay quickly so that the infinite integration intervals cause no difficulties.

Since Kim's representation is numerically much better than the first two, the eigenfunction expansion of the Green's function will be compared to this one more thoroughly. At first, a few qualitative remarks are made before quantitative results are presented.

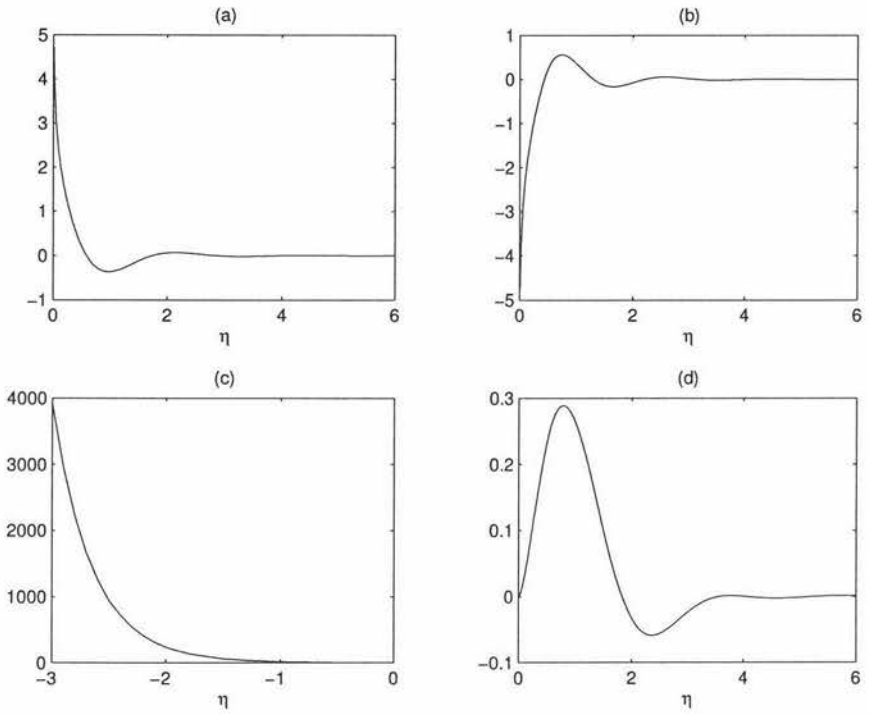

Figure 4.4: The graphs of the integrands in equations (4.16) for $\alpha = \pi$, $c = -1$, $z = -1$ and $r_\zeta = 1$

As can be seen from equations (4.16c) and (4.16d), interchanging the values of z and c does not make a difference in the calculation. If the absolute values of z and c become large, the integrand of the eigenfunction representation starts to oscillate more while the integration interval in Kim's representation becomes larger which results in the need to integrate a steeper function (since $z, c \leq 0$ always). An increase in the radial coordinate, r_ζ, smoothes the integrand in the eigenfunction representation since it accelerates the decay of the Bessel function but barely affects the integration in Kim's representation. A change in the wavenumber (since $\alpha = k$ for infinite depth) barely changes the integrand in the eigenfunction representation but dramatically alters the integrand in Kim's representation because it changes its steepness.

Table 4.1 compares the required function evaluations when integrating the integrands from Kim's representation in equation (4.16c) and the eigenfunction representation in equation (4.16d) with the adaptive Simpson quadrature provided by MATLAB. The integration in the eigenfunction representation has always been performed from zero until the point from which on the integrand is always less than 10^{-6} . In the cases illustrated in

Tolerance	Kim's repr.	eigenfunction repr.	Kim's repr.	eigenfunction repr.
	$\alpha = \pi,\ c = -1,\ z = -1,\ r = 1$		$\alpha = \pi,\ c = -1,\ z = -1/2,\ r = 1$	
10^{-2}	13	5	9	5
10^{-4}	37	25	25	21
10^{-6}	89	61	53	53
	$\alpha = \pi,\ c = -1,\ z = -1,\ r = 1/2$		$\alpha = \pi,\ c = -1,\ z = -1,\ r = 2$	
10^{-2}	13	17	13	5
10^{-4}	41	37	33	17
10^{-6}	93	117	89	41
	$\alpha = \pi/2,\ c = -1,\ z = -1,\ r = 1$		$\alpha = 2\pi,\ c = -1,\ z = -1,\ r = 1$	
10^{-2}	5	5	57	5
10^{-4}	17	21	133	17
10^{-6}	33	65	365	73

Table 4.1: Required function evaluations when numerically integrating the integrands from equations (4.16c) and (4.16d)

table 4.1 this upper boundary of the integration interval is between 6 and 26.

The results in table 4.1 show that the number of function evaluations required by Kim's representation is generally greater, often by a considerable amount, than the number required by the eigenfunction representation. In the only cases where Kim's representation performs better ($\alpha = \pi/2,\ c = -1,\ z = -1,\ r = 1$ and $\alpha = \pi,\ c = -1,\ z = -1,\ r = 1/2$) it only does so by a small amount. Of course these results do not form a definitive test that the eigenfunction representation is better since ways to optimise the integration have not been investigated or the different costs in evaluating the integrands have not been taken into account. However, these results, especially because the cost of evaluating the Struve function which Kim's representation requires has not been considered, do indicate that the eigenfunction representation will perform well numerically in comparison to Kim's representation.

4.5 Numerical aspects of the Green's function in a fixed coordinate system

In this section special aspects regarding the numerical computation of the eigenfunction expansion of the Green's function which allows the representation of the potential in the

coordinates of the body as opposed to the coordinates centred at the undisturbed water surface above the source point will be considered. This representation is given by equation (4.13). Because the vertical dependence does not cause special difficulties, it suffices to investigate the case where $z = c = 0$ given by equation (4.14).

When using the Green's function for a single diffraction calculation, a choice has to be made whether all the terms depending on ν are summed up first and then the sum is integrated (as implied in equation (4.14)) or, making use of the identity

$$\int_0^\infty \frac{\eta^2}{\eta^2+\alpha^2}\left[\sum_{\nu=-\infty}^{\infty} K_\nu(\eta r)I_\nu(\eta s)\mathrm{e}^{\mathrm{i}\nu(\theta-\varphi)}\right]\mathrm{d}\eta$$
$$= \sum_{\nu=-\infty}^{\infty}\left[\int_0^\infty \frac{\eta^2}{\eta^2+\alpha^2}K_\nu(\eta r)I_\nu(\eta s)\,\mathrm{d}\eta\right]\mathrm{e}^{\mathrm{i}\nu(\theta-\varphi)},$$

the summands may each be integrated first and summed up after. Under the assumption that the expansion of the potential in cylindrical eigenfunctions is in a basis, the sum converges uniformly so that integration and summation may be interchanged. Furthermore, in numerical calculations the sum will always be truncated so that only the linearity of the integral is required. However, since the integration is numerically expensive, the number of integrations should be kept at a minimum. Therefore, the first option is used.

Properties of the Bessel functions also reduce the numerical expense. Since

$$H_{-\nu}^{(1)}(x) = (-1)^\nu H_\nu^{(1)}(x), \quad J_{-\nu}(x) = (-1)^\nu J_\nu(x), \quad K_{-\nu}(x) = K_\nu(x), \quad I_{-\nu}(x) = I_\nu(x),$$

for real x and integer values of ν (Abramowitz & Stegun, 1964), it is sufficient to sum up for non-negative values of ν. This results in the simplified Green's function

$$G(r,\theta;s,\varphi) = \frac{\mathrm{i}\alpha}{2}\left(H_0^{(1)}(\alpha r)J_0(\alpha s) + \sum_{\nu=1}^{\infty} H_\nu^{(1)}(\alpha r)J_\nu(\alpha s)\left(\mathrm{e}^{\mathrm{i}\nu(\theta-\varphi)} + \mathrm{e}^{-\mathrm{i}\nu(\theta-\varphi)}\right)\right)$$
$$+ \frac{1}{\pi^2}\int_0^\infty \frac{\eta^2}{\eta^2+\alpha^2}\left(K_0(\eta r)I_0(\eta s) + \sum_{\nu=1}^{\infty} K_\nu(\eta r)I_\nu(\eta s)\left(\mathrm{e}^{\mathrm{i}\nu(\theta-\varphi)} + \mathrm{e}^{-\mathrm{i}\nu(\theta-\varphi)}\right)\right)\mathrm{d}\eta.$$

The eigenfunction expansion of the Green's function contains infinite sums and integrals. For numerical evaluation these have to be truncated. Due to the fact that the modified Bessel function of the second kind, $K_\nu(x)$, decays rapidly and r is always greater than s, the integral only needs to be evaluated up to a relatively small positive number as was shown in the previous section. The summations also only need to be performed up to a small number since the product of the Hankel function of the first kind with the Bessel function of the first kind becomes small with increasing absolute value of the order and

the same applies for the product of the modified Bessel function of the second kind with the one of the first kind. Figure 4.5 illustrates this.

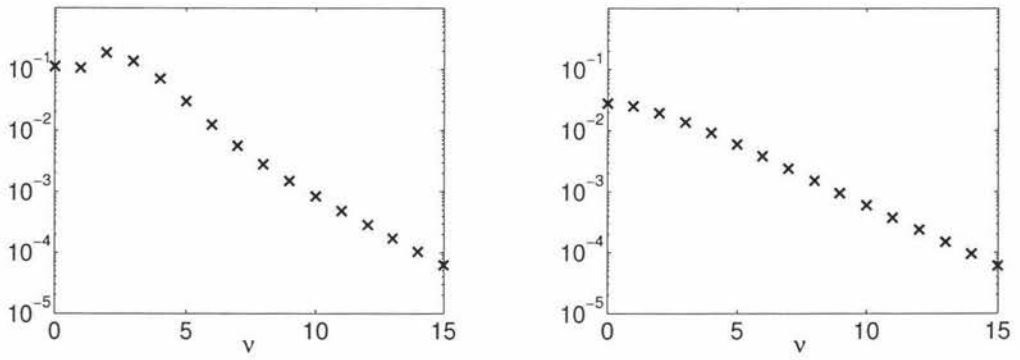

Figure 4.5: The graphs of $|H_\nu^{(1)}(3\pi/2)J_\nu(\pi)|$ and $K_\nu(3\pi/2)I_\nu(\pi)$ for integer values of ν

The Green's function can therefore be implemented as

$$\begin{aligned} G(r,\theta;s,\varphi) = {} & \frac{\mathrm{i}\alpha}{2}\left(H_0^{(1)}(\alpha r)J_0(\alpha s) + \sum_{\nu=1}^{T_H} H_\nu^{(1)}(\alpha r)J_\nu(\alpha s)\left(\mathrm{e}^{\mathrm{i}\nu(\theta-\varphi)} + \mathrm{e}^{-\mathrm{i}\nu(\theta-\varphi)}\right)\right) \\ & + \frac{1}{\pi^2}\int_0^{T_\eta} \frac{\eta^2}{\eta^2+\alpha^2}\left(K_0(\eta r)I_0(\eta s) + \sum_{\nu=1}^{T_K} K_\nu(\eta r)I_\nu(\eta s)\left(\mathrm{e}^{\mathrm{i}\nu(\theta-\varphi)} + \mathrm{e}^{-\mathrm{i}\nu(\theta-\varphi)}\right)\right)\mathrm{d}\eta. \end{aligned} \tag{4.17}$$

for sufficiently large truncation parameters T_H, T_K and T_η. If the eigenfunction expansion does not need to be retained (i.e. if the result does not need to be obtained in the eigenfunction expansion) the Green's function to be implemented can be further simplified by combining the exponential terms in (4.17) to $2\cos\nu(\theta-\varphi)$.

To ensure that these truncations do not lead to inaccurate results, the scattered wavefield of a single ice floe is calculated with the Green's function from equation (2.20), which cannot be used for the interaction theory, and compared to the one in eigenfunction representation.

4.5.1 Numerical results for one single ice floe

The results of the implementation for one ice floe will be illustrated. As defined in the first chapters normalised variables are used such that the ice floe occupies the area $]-1,1[\times]-1,1[$. The properties of the ice floe are chosen to be stiffness $\beta = 0.02$, mass $\gamma = 0.02$ and Poisson's ratio $\nu = 0.3333$. The ambient wavefield is travelling in positive x-direction with amplitude 1. These are the same conditions as discussed in chapter 2.

Figures 4.6 and 4.8 show the surface displacement of the ice floes with incident wavelength 2 and 1 respectively, figures 4.7 and 4.9 show their scattered wavefields only. Each figure consists of three plots, one close view, one far view and one view from above (plan view). While the close view plot contains the discretisation mesh, in the other two plots this has been removed and the greyscale has been interpolated for visibility. Again, animated version can be found on the attached CD-ROM (see appendix B for details).

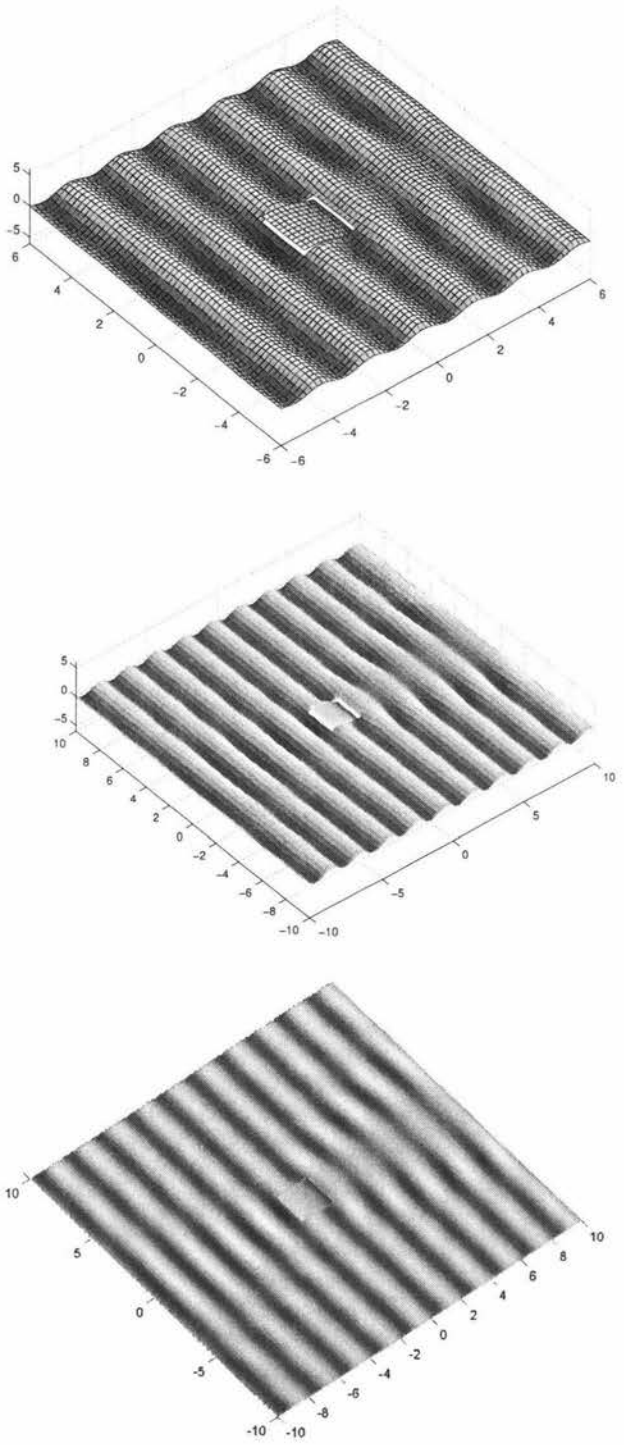

Figure 4.6: Surface displacement in the vicinity of the ice floe under ambient incident wave of wavelength 2

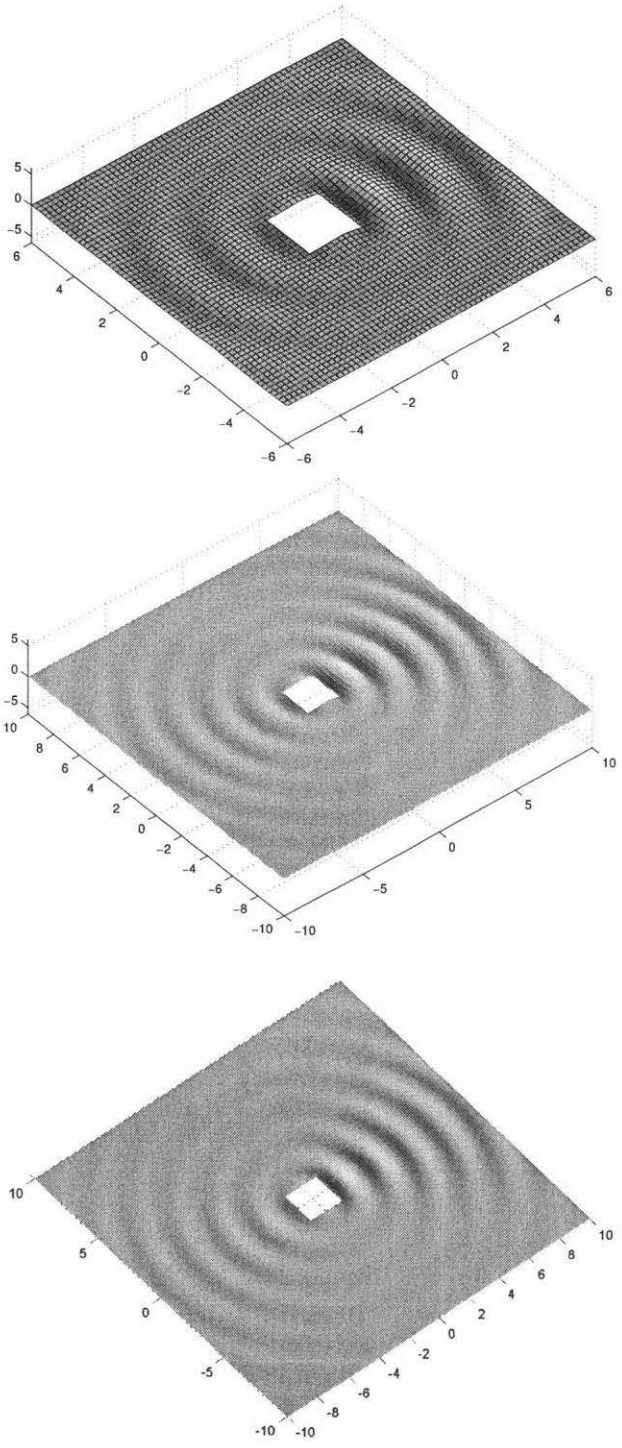

Figure 4.7: Scattered wavefield in the vicinity of the ice floe under ambient incident wave of wavelength 2

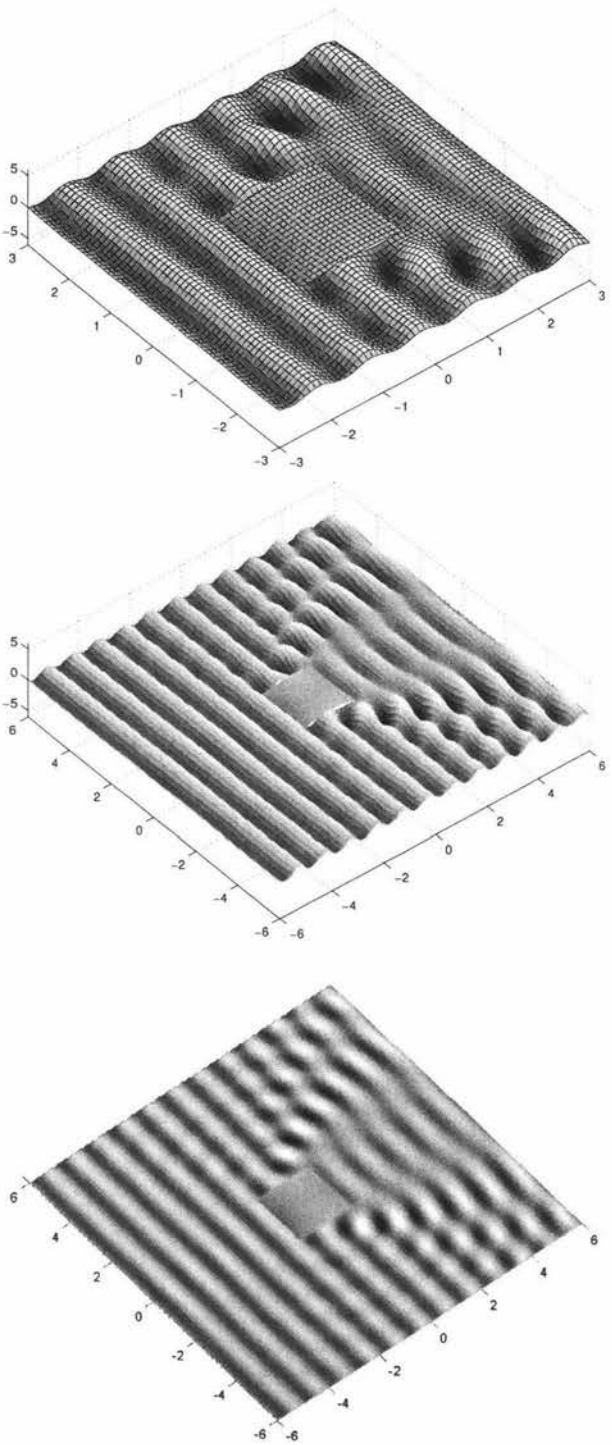

Figure 4.8: Surface displacement in the vicinity of the ice floe under ambient incident wave of wavelength 1

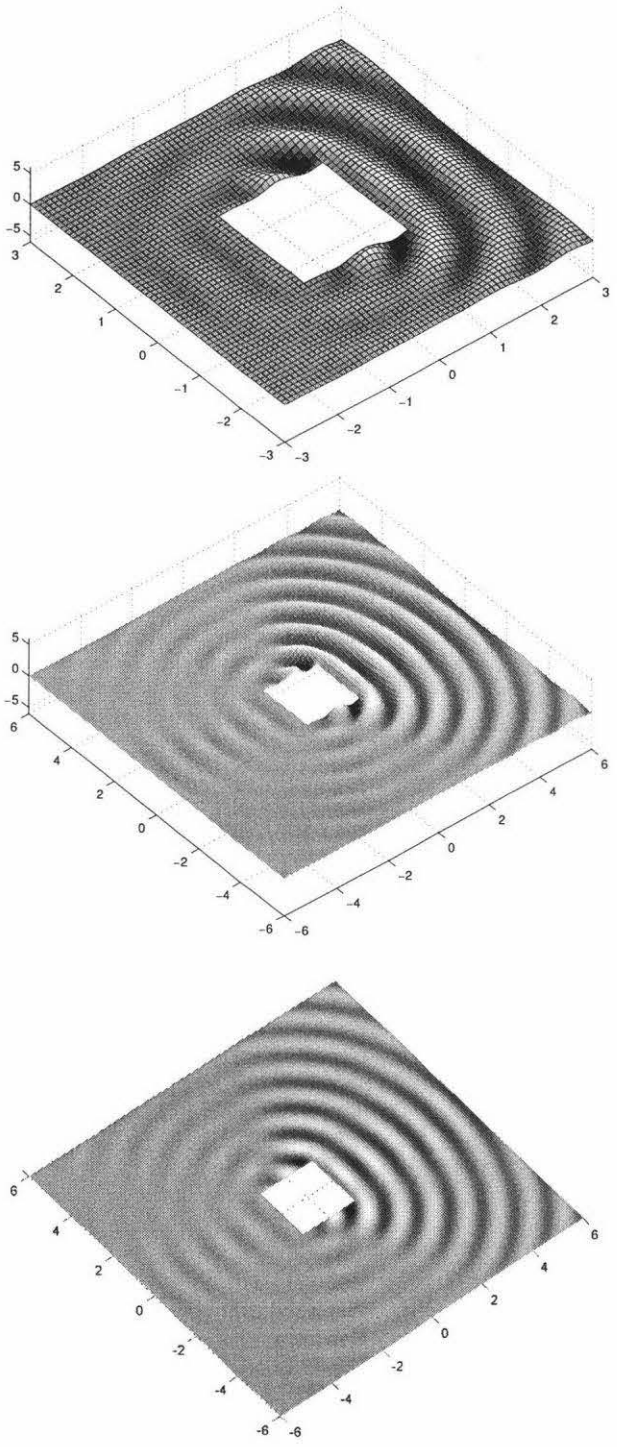

Figure 4.9: Scattered wavefield in the vicinity of the ice floe under ambient incident wave of wavelength 1

Chapter 5

The interaction of multiple bodies

In this chapter, the previous results will be used to develop a solution for the interaction of multiple floating or (fully or partially) submerged, vertically non-overlapping bodies of arbitrary geometry. It was discussed in chapter 2 how the scattered potential of a single body can be calculated from the incident potential upon that body. If more than one body is present, each body scatters the incident waves and therefore alters the total incident potential upon all other bodies. Thus, it is necessary to solve for the scattered potentials (or the total incident potentials) of all bodies simultaneously.

Following the ideas of Kagemoto & Yue (1986), an interaction theory for water of finite depth will be introduced. In this theory, the eigenfunction expansions of the water velocity potential will be used such that the potentials are defined by a set of coefficients only. The derivation will focus on the important ideas and work with already truncated vectors of coefficients. The ideas of the finite depth interaction theory will then be used to derive an analogous theory for infinitely deep water. This derivation will be carried out with a greater emphasis on the full analytic result so the truncation will be performed last.

The interaction theories still require the solutions from single diffraction calculations. Particularly, they require the coefficients of the scattered wavefield in the eigenfunction expansion due to unit incident modes. The coefficients due to the different incident modes are then assembled as columns of a matrix, the diffraction transfer matrix. As discussed in chapter 2, the scattered potential of a body of arbitrary shape can be represented with a Green's function. Using the eigenfunction expansions of the Green's functions from the last chapter, this representation of the scattered potential is in the eigenfunction expansion of an outgoing wave and therefore allows the calculation of the diffraction transfer matrices for bodies of arbitrary geometry.

After the interaction theories have been developed, some steps will be considered in more detail for both finitely and infinitely deep water. Especially the calculation of the diffraction transfer matrices will be discussed thoroughly. At first however, it will be shown how the eigenfunction expansion of the Green's functions developed in the last chapter can be used to represent the scattered potential of a body in the eigenfunction expansion.

5.1 Eigenfunction expansion of the scattered potential

In order to be able to calculate the diffraction transfer matrices, it is required to represent the scattered potentials of the bodies in the eigenfunction representation developed in chapter 3. In the local cylindrical coordinates of the jth body, Δ_j, the scattered potential can be expanded into its cylindrical eigenfunctions as in equation (3.12),

$$\begin{aligned}\phi_j^{\mathrm{S}}(r_j,\theta_j,z) = {} & \frac{\cosh k(z+d)}{\cosh kd} \sum_{\nu=-\infty}^{\infty} A_{0\nu}^j H_\nu^{(1)}(kr_j)\mathrm{e}^{\mathrm{i}\nu\theta_j} \\ & + \sum_{m=1}^{\infty} \frac{\cos k_m(z+d)}{\cos k_m d} \sum_{\nu=-\infty}^{\infty} A_{m\nu}^j K_\nu(k_m r_j)\mathrm{e}^{\mathrm{i}\nu\theta_j},\end{aligned} \tag{5.1}$$

in the finite depth case and, as in equation (3.17),

$$\begin{aligned}\phi_j^{\mathrm{S}}(r_j,\theta_j,z) = {} & \mathrm{e}^{\alpha z} \sum_{\nu=-\infty}^{\infty} A_\nu^j(\mathrm{i}\alpha) H_\nu^{(1)}(\alpha r_j)\mathrm{e}^{\mathrm{i}\nu\theta_j} \\ & + \int_0^{\infty} \psi(z,\eta) \sum_{\nu=-\infty}^{\infty} A_\nu^j(\eta) K_\nu(\eta r_j)\mathrm{e}^{\mathrm{i}\nu\theta_j}\,\mathrm{d}\eta,\end{aligned} \tag{5.2}$$

for infinitely deep water. The scattered potential of body Δ_j is given by equation (2.13),

$$\phi_j^{\mathrm{S}}(r_j,\theta_j,z) = \int_{\Gamma_j} G(r_j,\theta_j,z;s,\varphi,c)\,\varsigma(s,\varphi,c)\,\mathrm{d}\sigma_{(s,\varphi,c)}, \quad (r_j,\theta_j,z) \in D, \tag{5.3}$$

where the source strength distribution function ς is given as the solution of equation (2.14) which depends on the incident wavefield. In the case of an ice floe, the scattered potential can be expressed as in equation (2.17),

$$\phi_j^{\mathrm{S}}(r_j,\theta_j) = \int_{\tilde{\Delta}_j} G(r_j,\theta_j;s,\varphi)\big(\alpha\,\phi(s,\varphi) + \mathrm{i}\sqrt{\alpha}\,w(s,\varphi)\big)\,\mathrm{d}\sigma_{(s,\varphi)}, \quad (r_j,\theta_j,0) \in S, \tag{5.4}$$

where the potential and surface displacement of the ice floe have been calculated as described in chapter 2.

Making use of the Green's functions developed in the previous chapter, the scattered potentials can be represented in the eigenfunction expansions. For the case of an ice floe, this is shown in the following two subsections for finite and infinite depth.

Finite depth

For finite depth the Green's function is given by equation (4.6). The substitution of the Green's function into the representation of the potential (5.4) yields

$$\phi_j^{\mathrm{S}}(r_j,\theta_j) = \sum_{\nu=-\infty}^{\infty} \left[\frac{\mathrm{i}}{2} \frac{\alpha^2-k^2}{d(\alpha^2-k^2)-\alpha} \cosh^2 kd \int_{\tilde{\Delta}_j} J_\nu(ks) \mathrm{e}^{-\mathrm{i}\nu\varphi} \big(\alpha\,\phi_j(s,\varphi) + \mathrm{i}\sqrt{\alpha}\, w_j(s,\varphi)\big)\,\mathrm{d}\sigma_{(s,\varphi)} \right] H_\nu^{(1)}(kr_j)\mathrm{e}^{\mathrm{i}\nu\theta_j} + \sum_{m=1}^{\infty}\sum_{\nu=-\infty}^{\infty} \left[\frac{1}{\pi} \frac{k_m^2+\alpha^2}{d(k_m^2+\alpha^2)-\alpha} \cos^2 k_m d \int_{\tilde{\Delta}_j} I_\nu(k_m s)\mathrm{e}^{-\mathrm{i}\nu\varphi} \big(\alpha\,\phi_j(s,\varphi) + \mathrm{i}\sqrt{\alpha}\, w_j(s,\varphi)\big)\,\mathrm{d}\sigma_{(s,\varphi)} \right] K_\nu(k_m r_j)\mathrm{e}^{\mathrm{i}\nu\theta_j},$$

where the potential and the surface displacement of the ice floe have been calculated depending on the incident wave. Therefore the coefficients $A_{m\nu}^j$ of the eigenfunction expansion of the scattered wavefield (5.1) are given by

$$A_{0\nu}^j = \frac{\mathrm{i}}{2} \frac{(\alpha^2-k^2)\cosh^2 kd}{d(\alpha^2-k^2)-\alpha} \int_{\tilde{\Delta}_j} J_\nu(ks)\mathrm{e}^{-\mathrm{i}\nu\varphi} \big(\alpha\,\phi_j(s,\varphi) + \mathrm{i}\sqrt{\alpha}\, w(s,\varphi)\big)\,\mathrm{d}\sigma_{(s,\varphi)}, \tag{5.5a}$$

$$A_{m\nu}^j = \frac{1}{\pi} \frac{(k_m^2+\alpha^2)\cos^2 k_m d}{d(k_m^2+\alpha^2)-\alpha} \int_{\tilde{\Delta}_j} I_\nu(k_m s)\mathrm{e}^{-\mathrm{i}\nu\varphi} \big(\alpha\,\phi_j(s,\varphi) + \mathrm{i}\sqrt{\alpha}\, w(s,\varphi)\big)\,\mathrm{d}\sigma_{(s,\varphi)}. \tag{5.5b}$$

Infinite depth

For water of infinite depth the Green's function is given by equation (4.14). Substituting the Green's function into the eigenfunction representation of the potential (5.4) yields

$$\phi_j^{\mathrm{S}}(r_j,\theta_j) = \sum_{\nu=-\infty}^{\infty} \left[\frac{\mathrm{i}\alpha}{2} \int_{\tilde{\Delta}_j} J_\nu(\alpha s)\mathrm{e}^{-\mathrm{i}\nu\varphi} \big(\alpha\phi_j(s,\varphi) + \mathrm{i}\sqrt{\alpha} w_j(s,\varphi)\big)\,\mathrm{d}\sigma_{(s,\varphi)} \right] H_\nu^{(1)}(\alpha r_j)\mathrm{e}^{\mathrm{i}\nu\theta_j} + \int_0^{\infty} \sum_{\nu=-\infty}^{\infty} \left[\frac{1}{\pi^2} \frac{\eta^2}{\eta^2+\alpha^2} \int_{\tilde{\Delta}_j} I_\nu(\eta s)\mathrm{e}^{-\mathrm{i}\nu\varphi} \big(\alpha\phi_j(s,\varphi) + \mathrm{i}\sqrt{\alpha} w_j(s,\varphi)\big)\,\mathrm{d}\sigma_{(s,\varphi)} \right] K_\nu(\eta r_j)\mathrm{e}^{\mathrm{i}\nu\theta_j}\,\mathrm{d}\eta,$$

where the potential and the surface displacement of the ice floe have been calculated depending on the incident wave. The coefficients A_ν^j of the eigenfunction expansion of the

scattered wavefield (5.2) are therefore given by

$$A_\nu^j(\mathrm{i}\alpha) = \frac{\mathrm{i}\alpha}{2} \int_{\tilde{\Delta}_j} J_\nu(\alpha s)\mathrm{e}^{-\mathrm{i}\nu\varphi}\big(\alpha\,\phi_j(s,\varphi) + \mathrm{i}\sqrt{\alpha}\,w_j(s,\varphi)\big)\,\mathrm{d}\sigma_{(s,\varphi)}, \tag{5.6a}$$

$$A_\nu^j(\eta) = \frac{1}{\pi^2}\,\frac{\eta^2}{\eta^2+\alpha^2} \int_{\tilde{\Delta}_j} I_\nu(\eta s)\mathrm{e}^{-\mathrm{i}\nu\varphi}\big(\alpha\,\phi_j(s,\varphi) + \mathrm{i}\sqrt{\alpha}\,w_j(s,\varphi)\big)\,\mathrm{d}\sigma_{(s,\varphi)}. \tag{5.6b}$$

5.2 The interaction in water of finite depth

As discussed above, the presence of more than one body necessitates the simultaneous calculation of the scattered potentials of all bodies due to their interaction. Following the ideas of Kagemoto & Yue (1986), a system of equations for the unknown coefficients $A_{m\nu}^j$ in the eigenfunction expansion of the scattered potentials will be developed for water of constant finite depth d. The scattered potential of Δ_j will be represented as an incident wave upon Δ_l $(j \neq l)$ and, doing this for all bodies simultaneously as well as relating the incident and scattered potential of a body through its diffraction transfer matrix, a system of equations for the unknown coefficients is developed.

Implying a suitable truncation, the eigenfunction representation of the potential (5.1) can be written as an inner product for the scattered potential in the vicinity of the jth body, Δ_j,

$$\phi_j^{\mathrm{S}}(r_j,\theta_j,z) = {}^{\mathrm{t}}\mathbf{a}_j\boldsymbol{\Psi}_j^{\mathbf{S}}(r_j,\theta_j,z), \tag{5.7}$$

where $\mathbf{a}_j$ and $\boldsymbol{\Psi}_j$ are, respectively, the vector with the coefficients $A_{m\nu}^j$ and the scattered cylindrical partial waves of the form $\frac{\cosh k(z+d)}{\cosh kd}H_\nu^{(1)}(kr_j)\mathrm{e}^{\mathrm{i}\nu\theta_j}$ for the propagating and $\frac{\cos k_m(z+d)}{\cos k_m d}\,K_\nu(k_m r_j)\mathrm{e}^{\mathrm{i}\nu\theta_j}$ for the decaying modes. Here, and in the sequel of this chapter, $\boldsymbol{\Psi}$ will always denote such unit vectors for the potential.

Now, the scattered potential ϕ_j^{S} of body Δ_j will be represented in terms of the incident potential ϕ_l^{I} upon Δ_l, $j \neq l$. This can be accomplished by utilising Graf's addition theorem for Bessel functions, equations (4.2), as it was illustrated in section 4.1.

A comparison of the triangle illustrating the relation between the variables in the addition theorem, figure 4.1, to the relation of the ice floes in figure 4.2 yields

$$H_\nu^{(1)}(kr_j)\mathrm{e}^{\mathrm{i}\nu(\theta_j-\vartheta_{jl})} = \sum_{\mu=-\infty}^{\infty} H_{\nu+\mu}^{(1)}(kR_{jl})\,J_\mu(kr_l)\mathrm{e}^{\mathrm{i}\mu(\pi-\theta_l+\vartheta_{jl})}, \quad j \neq l, \tag{5.8a}$$

$$K_\nu(k_m r_j)\mathrm{e}^{\mathrm{i}\nu(\theta_j-\vartheta_{jl})} = \sum_{\mu=-\infty}^{\infty} K_{\nu+\mu}(k_m R_{jl})\,I_\mu(k_m r_l)\mathrm{e}^{\mathrm{i}\mu(\pi-\theta_l+\vartheta_{jl})}, \quad j \neq l, \tag{5.8b}$$

as long as $r_l < R_{jl}$. However, this limitation only requires the escribed cylinder of each body Δ_l not to enclose any other origin O_j $(j \neq l)$.

Equations (5.8) can be regarded as defining a coordinate transformation $\mathbf{T}_{jl}$ from Δ_j to Δ_l for the set of partial waves. Implying a suitable truncation, this can be written as

$$\mathbf{\Psi}_j^{\mathrm{S}} = \mathbf{T}_{jl}\, \mathbf{\Psi}_l^{\mathrm{I}}, \tag{5.9}$$

where $\mathbf{\Psi}_l^{\mathrm{I}}$ is the vector of incident partial cylindrical waves upon Δ_l of the propagating form, $\frac{\cosh(k(z+d))}{\cosh kd} J_\mu(kr_l)\mathrm{e}^{\mathrm{i}\mu\theta_l}$, or the decaying form, $\frac{\cos(k_m(z+d))}{\cos k_m d} I_\mu(k_m r_l)\mathrm{e}^{\mathrm{i}\mu\theta_l}$. Making use of the identities

$$\sum_{\mu=-\infty}^{\infty} H_{\nu+\mu}^{(1)}(kR_{jl}) J_\mu(kr_l)\mathrm{e}^{\mathrm{i}(\mu(\pi-\theta_l)+(\nu+\mu)\vartheta_{jl})}$$

$$= \sum_{\mu=-\infty}^{\infty} J_\mu(kr_l)\mathrm{e}^{\mathrm{i}\mu\theta_l}\, H_{\nu-\mu}^{(1)}(kR_{jl})\, \mathrm{e}^{\mathrm{i}(\nu-\mu)\vartheta_{jl}},$$

$$\sum_{\mu=-\infty}^{\infty} K_{\nu+\mu}(k_m R_{jl}) I_\mu(k_m r_l)\mathrm{e}^{\mathrm{i}(\mu(\pi-\theta_l)+(\nu+\mu)\vartheta_{jl})}$$

$$= \sum_{\mu=-\infty}^{\infty} I_\mu(k_m r_l)\mathrm{e}^{\mathrm{i}\mu\theta_l} K_{\nu-\mu}(k_m R_{jl})\mathrm{e}^{-\mathrm{i}\mu\pi}\mathrm{e}^{\mathrm{i}(\nu-\mu)\vartheta_{jl}},$$

which are obtained by inverting the summation, the elements of $\mathbf{T}_{jl}$ are of the form

$$(\mathbf{T}_{jl})_{pq} = H_{p-q}^{(1)}(kR_{jl})\, \mathrm{e}^{\mathrm{i}(p-q)\vartheta_{jl}}, \tag{5.10a}$$

$$(\mathbf{T}_{jl})_{pq} = (-1)^q\, K_{p-q}(k_m R_{jl})\, \mathrm{e}^{\mathrm{i}(p-q)\vartheta_{jl}}, \tag{5.10b}$$

for the propagating and the decaying modes respectively. Substituting equation (5.9) into equation (5.7), the potential ϕ_j^{S} in terms of the wavefield upon body Δ_l is given by

$$\phi_j^{\mathrm{S}}(r_l, \theta_l, z) = {}^{\mathrm{t}}\mathbf{a}_j\, \mathbf{T}_{jl}\, \mathbf{\Psi}_l^{\mathrm{I}}(r_l, \theta_l, z).$$

Also taking the ambient incident wavefield ϕ^{In}, given by equation (2.6), into account and expressing it in terms of the incident field upon Δ_l,

$$\phi^{\mathrm{In}}(r_l, \theta_l, z) = {}^{\mathrm{t}}\mathbf{d}_l^{\mathrm{In}}\, \mathbf{\Psi}_l^{\mathrm{I}}(r_l, \theta_l, z),$$

the total incident potential in the vicinity of Δ_l is thus

$$\phi_l^{\mathrm{I}}(r_l, \theta_l, z) = \Big({}^{\mathrm{t}}\mathbf{d}_l^{\mathrm{In}} + \sum_{\substack{j=1 \\ j\neq l}}^{N} {}^{\mathrm{t}}\mathbf{a}_j\, \mathbf{T}_{jl}\Big)\, \mathbf{\Psi}_l^{\mathrm{I}}(r_l, \theta_l, z), \quad l = 1 \ldots N. \tag{5.11}$$

It must be noted that the elements of $\mathbf{d}_l^{\mathrm{In}}$ are zero except those corresponding to the propagating modes.

In general, it is possible to relate the total incident and scattered partial waves for any body through the diffraction characteristics of that body in isolation. There exist diffraction transfer matrices $\mathbf{B}_l$ that relate the coefficients of the incident and scattered partial waves, such that

$$\mathbf{a}_l = \mathbf{B}_l\, \mathbf{d}_l, \quad l = 1 \ldots N, \tag{5.12}$$

where $\mathbf{d}_l$ is the vector of total incident partial waves upon body Δ_l. The elements $(\mathbf{B}_l)_{pq}$ are the coefficients of the pth partial wave of the scattered potentials due to a single unit-amplitude incident wave of mode q upon Δ_l. They are given from experiments or single body diffraction calculations and will be discussed in detail later. From (5.11) and (5.12) a system of equations for the unknown coefficients is obtained,

$$\mathbf{a}_l = \mathbf{B}_l \left(\mathbf{d}_l^{\mathrm{In}} + \sum_{\substack{j=1 \\ j\neq l}}^{N} {}^{\mathrm{t}}\mathbf{T}_{jl}\, \mathbf{a}_j\right), \quad l = 1 \ldots N. \tag{5.13}$$

5.3 The interaction in water of infinite depth

Now, these ideas will be applied to the case of infinitely deep water. The derivation is similar but this time the analytic result will be emphasised so the coefficients of the scattered potential will be truncated last. Since in the infinite depth case there are no discrete roots of a dispersion relation but a continuous variable, the finite depth diffraction transfer matrices have to be generalised.

The scattered water velocity potential in water of infinite depth can be expanded into its cylindrical eigenfunctions as in equation (5.2),

$$\phi_j^{\mathrm{S}}(r_j, \theta_j, z) = \mathrm{e}^{\alpha z} \sum_{\nu=-\infty}^{\infty} A_\nu^j(\mathrm{i}\alpha) H_\nu^{(1)}(\alpha r_j) \mathrm{e}^{\mathrm{i}\nu\theta_j} + \int_0^\infty \psi(z,\eta) \sum_{\nu=-\infty}^{\infty} A_\nu^j(\eta) K_\nu(\eta r_j) \mathrm{e}^{\mathrm{i}\nu\theta_j}\, \mathrm{d}\eta.$$

Using Graf's addition theorem, the scattered potentials ϕ_j^{S} can once again be represented in terms of the incident potential upon body Δ_l, $j \neq l$,

$$\begin{aligned}\phi_j^{\mathrm{S}}(r_l, \theta_l, z) = \mathrm{e}^{\alpha z} &\sum_{\nu=-\infty}^{\infty} A_\nu^j(\mathrm{i}\alpha) \mathrm{e}^{\mathrm{i}\nu\vartheta_{lj}} \sum_{\mu=-\infty}^{\infty} H_{\nu+\mu}^{(1)}(\alpha R_{jl}) J_\mu(\alpha r_l) \mathrm{e}^{\mathrm{i}\mu(\pi-\theta_l+\vartheta_{jl})} \\ &+ \int_0^\infty \psi(z,\eta) \sum_{\nu=-\infty}^{\infty} A_\nu^j(\eta) \mathrm{e}^{\mathrm{i}\nu\vartheta_{lj}} \sum_{\mu=-\infty}^{\infty} K_{\nu+\mu}(\eta R_{jl}) I_\mu(\eta r_l) \mathrm{e}^{\mathrm{i}\mu(\pi-\theta_l+\vartheta_{jl})}\, \mathrm{d}\eta\end{aligned}$$

$$
\begin{aligned}
&= \mathrm{e}^{\alpha z} \sum_{\nu=-\infty}^{\infty} A_\nu^j(\mathrm{i}\alpha) \sum_{\mu=-\infty}^{\infty} H_{\nu-\mu}^{(1)}(\alpha R_{jl}) J_\mu(\alpha r_l) \mathrm{e}^{\mathrm{i}\mu\theta_l} \mathrm{e}^{\mathrm{i}(\nu-\mu)\vartheta_{jl}} \\
&\quad + \int_0^\infty \psi(z,\eta) \sum_{\nu=-\infty}^{\infty} A_\nu^j(\eta) \sum_{\mu=-\infty}^{\infty} (-1)^\mu K_{\nu-\mu}(\eta R_{jl}) I_\mu(\eta r_l) \mathrm{e}^{\mathrm{i}\mu\theta_l} \mathrm{e}^{\mathrm{i}(\nu-\mu)\vartheta_{jl}} \,\mathrm{d}\eta \\
&= \mathrm{e}^{\alpha z} \sum_{\mu=-\infty}^{\infty} \Big[\sum_{\nu=-\infty}^{\infty} A_\nu^j(\mathrm{i}\alpha) H_{\nu-\mu}^{(1)}(\alpha R_{jl}) \mathrm{e}^{\mathrm{i}(\nu-\mu)\vartheta_{jl}} \Big] J_\mu(\alpha r_l) \mathrm{e}^{\mathrm{i}\mu\theta_l} \\
&\quad + \int_0^\infty \psi(z,\eta) \sum_{\mu=-\infty}^{\infty} \Big[\sum_{\nu=-\infty}^{\infty} A_\nu^j(\eta) (-1)^\mu K_{\nu-\mu}(\eta R_{jl}) \mathrm{e}^{\mathrm{i}(\nu-\mu)\vartheta_{jl}} \Big] I_\mu(\eta r_l) \mathrm{e}^{\mathrm{i}\mu\theta_l} \,\mathrm{d}\eta.
\end{aligned}
$$

The ambient incident wavefield ϕ^{In}, given by equation (2.4), can be represented in these modes,

$$
\phi^{\mathrm{In}}(r_l, \theta_l, z) = \mathrm{e}^{\alpha z} \sum_{\mu=-\infty}^{\infty} D_{l\mu}^{\mathrm{In}}(\mathrm{i}\alpha) J_\mu(\alpha r_l) \mathrm{e}^{\mathrm{i}\mu\theta_l} + \int_0^\infty \psi(z,\eta) \sum_{\mu=-\infty}^{\infty} D_{l\mu}^{\mathrm{In}}(\eta) I_\mu(\eta r_l) \mathrm{e}^{\mathrm{i}\mu\theta_l} \,\mathrm{d}\eta,
$$

with coefficients $D_{l\mu}^{\mathrm{In}}(\cdot)$, which are zero for real argument because of the propagating form of the ambient wave. The coefficients of the total incident potential upon Δ_l are therefore given by

$$
D_{0\mu}^l = D_{l0\mu}^{\mathrm{In}} + \sum_{\substack{j=1 \\ j\neq l}}^{N} \sum_{\nu=-\infty}^{\infty} A_{0\nu}^j H_{\nu-\mu}^{(1)}(\alpha R_{jl}) \mathrm{e}^{\mathrm{i}(\nu-\mu)\vartheta_{jl}}, \tag{5.14a}
$$

$$
D_\mu^l(\eta) = D_{l\mu}^{\mathrm{In}}(\eta) + \sum_{\substack{j=1 \\ j\neq l}}^{N} \sum_{\nu=-\infty}^{\infty} A_\nu^j(\eta) (-1)^\mu K_{\nu-\mu}(\eta R_{jl}) \mathrm{e}^{\mathrm{i}(\nu-\mu)\vartheta_{jl}}. \tag{5.14b}
$$

Again, the coefficients of the total incident and the scattered wavefield at body Δ_l can be related by diffraction transfer operators B_l that relate the coefficients of the incident and scattered partial waves, such that

$$
A_l = B_l(D_l), \quad l = 1 \ldots N,
$$

where A_l are the scattered modes due to the incident modes D_l. In the case of a countable amount of modes, e.g. in finite depth or relating propagating incident modes to propagating outgoing modes in infinite depth, B_l is an infinitely dimensional matrix. Relating coefficient functions, B_l is the kernel of an integral operator. For the propagating and the decaying modes respectively, the scattered potential can be related by diffraction transfer

operators acting in the following ways,

$$A^l_{0\nu} = \sum_{\mu=-\infty}^{\infty} B^{\mathrm{pp}}_{l\nu\mu} D^l_{0\mu} + \int_0^{\infty} \sum_{\mu=-\infty}^{\infty} B^{\mathrm{pd}}_{l\nu\mu}(\xi) D^l_{\mu}(\xi)\,\mathrm{d}\xi, \tag{5.15a}$$

$$A^l_{\nu}(\eta) = \sum_{\mu=-\infty}^{\infty} B^{\mathrm{dp}}_{l\nu\mu}(\eta) D^l_{0\mu} + \int_0^{\infty} \sum_{\mu=-\infty}^{\infty} B^{\mathrm{dd}}_{l\nu\mu}(\eta;\xi) D^l_{\mu}(\xi)\,\mathrm{d}\xi. \tag{5.15b}$$

The superscripts p and d are used to distinguish between propagating and decaying modes, the first superscript denotes the kind of scattered mode, the second one the kind of incident mode. If the diffraction transfer operators are known (their calculation will be discussed later), the substitution of equations (5.14) into equations (5.15) give the required equations to determine the coefficients and coefficient functions of the scattered wavefields of all bodies,

$$\begin{aligned} A^l_{0n} = {} & \sum_{\mu=-\infty}^{\infty} B^{\mathrm{pp}}_{ln\mu}\Big[D^{\mathrm{In}}_{l0\mu} + \sum_{\substack{j=1\\ j\neq l}}^{N} \sum_{\nu=-\infty}^{\infty} A^j_{0\nu} H^{(1)}_{\nu-\mu}(\alpha R_{jl}) \mathrm{e}^{\mathrm{i}(\nu-\mu)\vartheta_{jl}}\Big] \\ & + \int_0^{\infty} \sum_{\mu=-\infty}^{\infty} B^{\mathrm{pd}}_{ln\mu}(\xi)\Big[D^{\mathrm{In}}_{l\mu}(\eta) + \sum_{\substack{j=1\\ j\neq l}}^{N} \sum_{\nu=-\infty}^{\infty} A^j_{\nu}(\eta)(-1)^{\mu} K_{\nu-\mu}(\eta R_{jl}) \mathrm{e}^{\mathrm{i}(\nu-\mu)\vartheta_{jl}}\Big]\,\mathrm{d}\xi, \end{aligned} \tag{5.16a}$$

$$\begin{aligned} A^l_{n}(\eta) = {} & \sum_{\mu=-\infty}^{\infty} B^{\mathrm{dp}}_{ln\mu}(\eta)\Big[D^{\mathrm{In}}_{l0\mu} + \sum_{\substack{j=1\\ j\neq l}}^{N} \sum_{\nu=-\infty}^{\infty} A^j_{0\nu} H^{(1)}_{\nu-\mu}(\alpha R_{jl}) \mathrm{e}^{\mathrm{i}(\nu-\mu)\vartheta_{jl}}\Big] \\ & + \int_0^{\infty} \sum_{\mu=-\infty}^{\infty} B^{\mathrm{dd}}_{ln\mu}(\eta;\xi)\Big[D^{\mathrm{In}}_{l\mu}(\eta) + \sum_{\substack{j=1\\ j\neq l}}^{N} \sum_{\nu=-\infty}^{\infty} A^j_{\nu}(\eta)(-1)^{\mu} K_{\nu-\mu}(\eta R_{jl}) \mathrm{e}^{\mathrm{i}(\nu-\mu)\vartheta_{jl}}\Big]\,\mathrm{d}\xi, \end{aligned} \tag{5.16b}$$

$n \in \mathbb{Z}$, $l = 1 \ldots N$. It has to be noted that all equations are coupled so that it is necessary to solve for all scattered coefficients and coefficient functions simultaneously.

For numerical calculations, the infinite sums have to be truncated and the integrals must be discretised. Implying a suitable truncation, the four different diffraction transfer operators can be represented by matrices which can be assembled in a big matrix $\mathbf{B}_l$,

$$\mathbf{B}_l = \begin{bmatrix} \mathbf{B}^{\mathrm{pp}}_l & \mathbf{B}^{\mathrm{pd}}_l \\ \mathbf{B}^{\mathrm{dp}}_l & \mathbf{B}^{\mathrm{dd}}_l \end{bmatrix},$$

the infinite depth diffraction transfer matrix. Truncating the coefficients accordingly, defining $\mathbf{a}^l$ to be the vector of the coefficients of the scattered potential of body Δ_l, $\mathbf{d}^{\mathrm{In}}_l$ to be the vector of coefficients of the ambient wavefield, and making use of a coordinate transformation matrix $\mathbf{T}_{jl}$ given by

$$(\mathbf{T}_{jl})_{pq} = H^{(1)}_{p-q}(\alpha R_{jl})\, \mathrm{e}^{\mathrm{i}(p-q)\vartheta_{jl}} \tag{5.17a}$$

for the propagating modes, and

$$(\mathbf{T}_{jl})_{pq} = (-1)^q \, K_{p-q}(\eta R_{jl}) \, \mathrm{e}^{\mathrm{i}(p-q)\vartheta_{jl}} \tag{5.17b}$$

for the decaying modes, a linear system of equations for the unknown coefficients follows from equations (5.16),

$$\mathbf{a}_l = \hat{\mathbf{B}}_l \Big(\mathbf{d}_l^{\mathrm{In}} + \sum_{\substack{j=1 \\ j \neq l}}^{N} {}^{\mathrm{t}}\mathbf{T}_{jl} \, \mathbf{a}_j \Big), \quad l = 1 \ldots N. \tag{5.18}$$

The matrix $\hat{\mathbf{B}}_l$ denotes the infinite depth diffraction transfer matrix $\mathbf{B}_l$ in which the elements associated with decaying scattered modes have been multiplied with the appropriate integration weights depending on the discretisation of the continuous variable.

5.4 Explicit details

In this section some steps from the derivation of the interaction theories are performed in more detail. This includes the representation of the ambient wavefield in the eigenfunction expansion and the explicit system of equations that needs to be solved. The calculation of the diffraction transfer matrix and the surface displacement in case of the ice floes will be examined.

5.4.1 Calculation of the diffraction transfer matrix

For the interaction theory the diffraction transfer matrices $\mathbf{B}_j$ are required which relate the total incident and the scattered partial waves for a body through the diffraction characteristics of that body in isolation. Generally, the elements $(\mathbf{B}_j)_{pq}$ are the coefficients of the pth partial wave of the scattered potential due to a single unit-amplitude incident wave of mode q upon Δ_j. For the ice floes this will be described for finite and infinite depth. The general case can be obtained in the same way.

As described in section 5.1, using (5.3) with the eigenfunction expansion of the Green's function yields the coefficients of the scattered wavefield of a body. Solving the integral equation for the source strength distribution function (2.14) for the different incident modes yields the corresponding source distributions. For the ice floes, the solutions of the single diffraction calculations due to the different modes of unit amplitude have to be calculated as described in chapter 2. These solutions are then used to yield the elements of $\mathbf{B}_j$ by making use of equations (5.5) or (5.6) as follows.

Finite Depth

In finite depth, the single diffraction solutions for an ice floe $\tilde{\Delta}_j$ can be expressed in the eigenfunction expansion with the coefficients given by equations (5.5). The elements of $\mathbf{B}_j$ therefore have the form

$$(\mathbf{B}_j)_{pq} = \frac{\mathrm{i}}{2} \frac{(\alpha^2 - k^2)\cosh^2 kd}{d(\alpha^2 - k^2) - \alpha} \int_{\tilde{\Delta}_j} J_p(ks)\mathrm{e}^{-\mathrm{i}p\varphi}\left(\alpha\,\phi_j^q(s,\varphi) + \mathrm{i}\sqrt{\alpha}\,w_j^q(s,\varphi)\right)\mathrm{d}\sigma_{(s,\varphi)},$$

$$(\mathbf{B}_j)_{pq} = \frac{1}{\pi} \frac{(k_m^2 + \alpha^2)\cos^2 k_m d}{d(k_m^2 + \alpha^2) - \alpha} \int_{\tilde{\Delta}_j} I_p(k_m s)\mathrm{e}^{-\mathrm{i}p\varphi}\left(\alpha\,\phi_j^q(s,\varphi) + \mathrm{i}\sqrt{\alpha}\,w_j^q(s,\varphi)\right)\mathrm{d}\sigma_{(s,\varphi)}.$$

for the propagating and the decaying modes, respectively, where $\phi_j^q(s,\varphi)$ and $w_j^q(s,\varphi)$ are, respectively, the potential and surface displacement of the ice floe due to an incident potential of mode q of the form

$$\phi_q^{\mathrm{I}}(s,\varphi) = H_q^{(1)}(ks)\mathrm{e}^{\mathrm{i}q\varphi} \tag{5.19a}$$

for the propagating modes, and

$$\phi_q^{\mathrm{I}}(s,\varphi) = K_q(k_m s)\mathrm{e}^{\mathrm{i}q\varphi} \tag{5.19b}$$

for the decaying modes.

Infinite Depth

In infinite depth, the single diffraction solution for an ice floe $\tilde{\Delta}_j$ can be expressed in the eigenfunction expansion with the coefficients given by (5.6). The elements of $\mathbf{B}_j$ therefore have the form

$$(\mathbf{B}_j)_{pq} = \frac{\mathrm{i}\alpha}{2} \int_{\tilde{\Delta}_j} J_p(\alpha s)\mathrm{e}^{-\mathrm{i}p\varphi}\left(\alpha\,\phi_j^q(s,\varphi) + \mathrm{i}\sqrt{\alpha}\,w_j^q(s,\varphi)\right)\mathrm{d}\sigma_{(s,\varphi)},$$

$$(\mathbf{B}_j)_{pq} = \frac{1}{\pi^2} \frac{\eta^2}{\eta^2 + \alpha^2} \int_{\tilde{\Delta}_j} I_p(\eta s)\mathrm{e}^{-\mathrm{i}p\varphi}\left(\alpha\,\phi_j^q(s,\varphi) + \mathrm{i}\sqrt{\alpha}\,w_j^q(s,\varphi)\right)\mathrm{d}\sigma_{(s,\varphi)},$$

for the propagating and the decaying modes respectively, where $\phi_j^q(s,\varphi)$ and $w_j^q(s,\varphi)$ are, respectively, the potential and surface displacement of the ice floe due to an incident potential of mode q of the form

$$\phi_q^{\mathrm{I}}(s,\varphi) = H_q^{(1)}(\alpha s)\mathrm{e}^{\mathrm{i}q\varphi} \tag{5.20a}$$

for the propagating modes, and

$$\phi_q^{\mathrm{I}}(s,\varphi) = K_q(\eta s)\mathrm{e}^{\mathrm{i}q\varphi} \tag{5.20b}$$

for the decaying modes.

5.4.2 The diffraction transfer matrix of rotated bodies

If the body is not axisymmetric a rotation of the body results in a different diffraction transfer matrix due to the angular dependence of the incident modes and the integral over the immersed surface of the body appearing in the elements of $\mathbf{B}$. For rotations about the mean centre position of the body in the (x,y)-plane, the diffraction transfer matrix of the rotated body can be easily computed from the diffraction transfer matrix of the body which has not been rotated. This will first be illustrated for ice floes and then for the case of a three-dimensional rigid body.

An investigation of the the integral equation for the potential and the surface displacement of the ice floe (2.18) as well as the integral over the ice floes appearing in the elements of $\mathbf{B}$ shows that the additional angular dependence caused by the rotation of the ice floe can be factored out of the elements of the diffraction transfer matrix. The elements of the diffraction transfer matrix corresponding to the ice floe rotated by the angle δ, $\mathbf{B}^\delta$, are given by

$$(\mathbf{B}^\delta)_{pq} = (\mathbf{B})_{pq}\,\mathrm{e}^{\mathrm{i}(q-p)\delta}. \tag{5.21}$$

This applies to propagating and decaying modes in finite and infinite depth likewise.

In the case of a three-dimensional rigid body, equation (5.21) is also valid. The additional angular dependence of the integral over the immersed surface of the body can be factored out analogously to the case of ice floes while it can be factored out of the source strength distribution function as follows. The right-hand-side of the integral equation for the source strength distribution function ς, equation (2.14), is given by the negative normal derivative of the incident potential. The additional angular dependence caused by the rotation of the body can be factored out of the normal derivative of the incident potential and since the integral equation for the source strength distribution function is linear, the additional angular dependence can even be factored out of the source strength distribution function such that

$$\varsigma_{q\delta} = \varsigma_q\,\mathrm{e}^{\mathrm{i}q\delta},$$

where $\varsigma_{q\delta}$ is the source strength distribution function of the rotated body. Therefore, the dependence on the angle of rotation can be factored out of the elements of the diffraction transfer matrix in the same way as for ice floes.

5.4.3 Eigenfunction expansion of the ambient wavefield

For the interaction theory, the ambient wavefield, which is incident upon all bodies, has to be represented in the eigenfunction expansion of an incoming wave. This will be performed for finite and infinite water depth.

Finite depth

In the case of constant finite depth d, the ambient wavefield has to be expanded into the eigenfunctions of cylindrical incoming waves centred at Δ_l,

$$\phi^{\mathrm{In}}(r_l,\theta_l,z) = \frac{\cosh k(z+d)}{\cosh kd} \sum_{\mu=-\infty}^{\infty} D^{\mathrm{In}}_{l0\mu} J_\mu(kr_l)\mathrm{e}^{\mathrm{i}\mu\theta_l} + \sum_{m=1}^{\infty} \frac{\cos k_m(z+d)}{\cos k_m d} \sum_{\mu=-\infty}^{\infty} D^{\mathrm{In}}_{lm\mu} I_\mu(k_m r_l)\mathrm{e}^{\mathrm{i}\mu\theta_l},$$

where $D^{\mathrm{In}}_{lm\mu}$ is zero for $m > 0$. In Cartesian coordinates centred at the origin, the ambient wavefield is given by equation (2.6),

$$\phi^{\mathrm{In}}(x,y,z) = \frac{A}{\sqrt{\alpha}} \frac{\cosh k(z+d)}{\cosh kd} \mathrm{e}^{\mathrm{i}k(x\cos\chi + y\sin\chi)},$$

with the non-dimensional amplitude A and χ representing the angle between the x-axis and the direction in which the wavefield travels. This can be represented in terms of the incoming wave (Linton & McIver, 2001),

$$\mathrm{e}^{\mathrm{i}k(x\cos\chi + y\sin\chi)} = \sum_{\mu=-\infty}^{\infty} \mathrm{e}^{\mathrm{i}\mu(\pi/2-\theta+\chi)} J_\mu(kr),$$

where the polar coordinates (r,θ) are centred at the origin. Since the local coordinates of the bodies are centred at their mean centre positions, a phase factor has to be defined which accounts for the position from the origin,

$$I_l := \mathrm{e}^{\mathrm{i}k(O^l_x\cos\chi + O^l_y\sin\chi)}.$$

Inverting the summation and using the fact that $J_{-\mu}(x) = (-1)^\mu J_\mu(x)$, the coefficients of the ambient wavefield at the lth body are given by

$$D^{\mathrm{In}}_{lm\mu} = \begin{cases} \frac{A}{\sqrt{\alpha}} I_l \mathrm{e}^{\mathrm{i}\mu(\pi/2-\chi)}, & m = 0, \\ 0, & m > 0. \end{cases}$$

Infinite depth

In the case of infinite depth, the ambient potential has to be represented as

$$\phi^{\mathrm{In}}(r_l,\theta_l,z) = \mathrm{e}^{\alpha z}\sum_{\mu=-\infty}^{\infty} D_{l\mu}^{\mathrm{In}}(\mathrm{i}\alpha)J_\mu(\alpha r_l)\mathrm{e}^{\mathrm{i}\mu\theta_l} + \int_0^\infty \psi(z,\eta)\sum_{\mu=-\infty}^{\infty} D_{l\mu}^{\mathrm{In}}(\eta)I_\mu(\eta r_l)\mathrm{e}^{\mathrm{i}\mu\theta_l}\,\mathrm{d}\eta,$$

where $D_l^{\mathrm{In}}(\cdot)$ is zero for real argument. In Cartesian coordinates centred at the origin, the ambient wavefield is given by equation (2.4),

$$\phi^{\mathrm{In}}(x,y,z) = \frac{A}{\sqrt{\alpha}}\,\mathrm{e}^{\mathrm{i}\alpha(x\cos\chi+y\sin\chi)+\alpha z},$$

with the non-dimensional amplitude A and χ representing the angle between the x-axis and the direction in which the wavefield travels. This can be represented in terms of the incoming wave (Linton & McIver, 2001),

$$\mathrm{e}^{\mathrm{i}\alpha(x\cos\chi+y\sin\chi)} = \sum_{\mu=-\infty}^{\infty}\mathrm{e}^{\mathrm{i}\mu(\pi/2-\theta+\chi)}J_\mu(\alpha r),$$

where the polar coordinates (r,θ) are centred at the origin. Since the local coordinates of the bodies are centred at their mean centre positions, a phase factor has to be defined which accounts for the position from the origin,

$$I_l := \mathrm{e}^{\mathrm{i}\alpha(O_x^l\cos\chi+O_y^l\sin\chi)}.$$

Inverting the summation and using the fact that $J_{-\mu}(x) = (-1)^\mu J_\mu(x)$, the coefficients of the ambient wavefield at the lth body are given by

$$D_{l\mu}^{\mathrm{In}}(\xi) = \begin{cases} \frac{A}{\sqrt{\alpha}} I_l\,\mathrm{e}^{\mathrm{i}\mu(\pi/2-\chi)}, & \xi = \mathrm{i}\alpha, \\ 0, & \xi \neq \mathrm{i}\alpha. \end{cases}$$

5.4.4 Solving the resulting system of equations

After all vectors and matrices have been calculated, the system of equations (5.13) in the finite depth case or (5.18) in the infinite depth case have to be solved. For simplification, only the finite depth case is considered, to account for infinite depth, $\mathbf{B}$ has to be replaced by $\hat{\mathbf{B}}$ in the following. The system of equations to be solved is

$$\mathbf{a}_l = \mathbf{B}_l\Big(\mathbf{d}_l^{\mathrm{In}} + \sum_{\substack{j=1\\ j\neq l}}^{N} {}^{\mathrm{t}}\mathbf{T}_{jl}\,\mathbf{a}_j\Big), \quad l = 1\ldots N. \tag{5.22}$$

This can be rewritten as one matrix equation,

$$\begin{bmatrix} \mathbf{a}_1 \\ \mathbf{a}_2 \\ \vdots \\ \mathbf{a}_N \end{bmatrix} = \begin{bmatrix} \mathbf{B}_1\mathbf{d}_1^{\mathrm{In}} \\ \mathbf{B}_2\mathbf{d}_2^{\mathrm{In}} \\ \vdots \\ \mathbf{B}_N\mathbf{d}_N^{\mathrm{In}} \end{bmatrix} + \begin{bmatrix} \mathbf{0} & \mathbf{B}_1{}^{t}\mathbf{T}_{21} & \mathbf{B}_1{}^{t}\mathbf{T}_{31} & \dots & \mathbf{B}_1{}^{t}\mathbf{T}_{N1} \\ \mathbf{B}_2{}^{t}\mathbf{T}_{12} & \mathbf{0} & \mathbf{B}_2{}^{t}\mathbf{T}_{32} & \dots & \mathbf{B}_2{}^{t}\mathbf{T}_{N2} \\ & & \mathbf{0} & & \\ \vdots & & & \ddots & \vdots \\ \mathbf{B}_N{}^{t}\mathbf{T}_{1N} & & \dots & & \mathbf{0} \end{bmatrix} \begin{bmatrix} \mathbf{a}_1 \\ \mathbf{a}_2 \\ \vdots \\ \mathbf{a}_N \end{bmatrix},$$

where $\mathbf{0}$ denotes the zero-matrix of the dimension of $\mathbf{B}_j$, say $n \times n$. This matrix equation can now be transformed into a classical $(Nn \times Nn)$-dimensional linear system of equations,

$$\begin{bmatrix} \mathbf{Id} & -\mathbf{B}_1{}^{t}\mathbf{T}_{21} & -\mathbf{B}_1{}^{t}\mathbf{T}_{31} & \dots & -\mathbf{B}_1{}^{t}\mathbf{T}_{N1} \\ -\mathbf{B}_2{}^{t}\mathbf{T}_{12} & \mathbf{Id} & -\mathbf{B}_2{}^{t}\mathbf{T}_{32} & \dots & -\mathbf{B}_2{}^{t}\mathbf{T}_{N2} \\ & & \mathbf{Id} & & \\ \vdots & & & \ddots & \vdots \\ -\mathbf{B}_N{}^{t}\mathbf{T}_{1N} & & \dots & & \mathbf{Id} \end{bmatrix} \begin{bmatrix} \mathbf{a}_1 \\ \mathbf{a}_2 \\ \vdots \\ \mathbf{a}_N \end{bmatrix} = \begin{bmatrix} \mathbf{B}_1\mathbf{d}_1^{\mathrm{In}} \\ \mathbf{B}_2\mathbf{d}_2^{\mathrm{In}} \\ \vdots \\ \mathbf{B}_N\mathbf{d}_N^{\mathrm{In}} \end{bmatrix},$$

where $\mathbf{Id}$ denotes the $(n \times n)$-dimensional identity matrix.

5.4.5 Calculation of the surface displacement of the ice floes

Additionally, the surface displacement of the ice floes has to be calculated. This can be accomplished easily since the displacement due to the different modes of unit amplitude, $w_j^q(s, \varphi)$, is already known from the calculation of the diffraction transfer matrix. The vector of the coefficients of the incoming wave, $\mathbf{d}_j$, can be easily calculated from the coefficients of the scattered wave,

$$\mathbf{d}_j = \mathbf{d}_j^{\mathrm{In}} + \sum_{\substack{l=1 \\ l \neq j}}^{N} {}^{t}\mathbf{T}_{lj}\,\mathbf{a}_l, \quad j = 1 \dots N.$$

The displacement of the ice floe is now calculated by multiplying each element of $\mathbf{d}_j$ with the corresponding $w_j^q(s, \varphi)$ and summing up all the resulting displacements.

Chapter 6

Numerical results and convergence

In this chapter numerical results for ice floes of different shapes and in different arrangements will be presented and convergence tests will be conducted in the case of two square interacting ice floes. The results from full diffraction calculations will be used as references. These can be implemented straightforwardly as an extension of the single diffraction calculation described in chapter 2.

The dependence on the different truncation parameters, namely the number of propagating modes, the number of decaying angular components and the number of roots of the dispersion relation in finite depth or the discretisation of the continuous variable in infinite depth, will be examined. The dependence on the ice floe positions will be investigated in water of infinite depth. In water of finite depth, if the depth is always chosen deeper than the minimum value for which the water is still considered deep, the water depth can also be considered a free parameter. However, the finite depth Green's function in eigenfunction representation derived in chapter 4 which was also used by Goo & Yoshida (1990) and Chakrabarti (2000) in their calculations only allows the finite depth interaction method for bodies of arbitrary shape to converge up to a certain depth due to a numerical problem. Fortunately, rewriting a factor in the term for the propagating modes by making use of the dispersion relation, this numerical problem can be circumvented.

As discussed in chapter 2, for the single diffraction calculations (implemented by Michael H. Meylan) in infinitely deep water the Green's function (2.20),

$$G(\mathbf{x};\xi) = \frac{1}{2\pi\|\mathbf{x}-\xi\|} - \frac{\alpha}{4}\big(\mathbf{H}_0(\alpha\|\mathbf{x}-\xi\|) + Y_0(\alpha\|\mathbf{x}-\xi\|) - 2\mathrm{i}J_0(\alpha\|\mathbf{x}-\xi\|)\big),$$

is employed since it does not require the evaluation of an integral. In water of finite depth,

the Green's function

$$G(\mathbf{x};\xi) = -\sum_{m=0}^{\infty} \frac{(\cos k_m d)^2}{2\pi N_m} K_0(k_m \|\mathbf{x} - \xi\|),$$

given by Linton (1999), is used where $N_m := \frac{d}{2}(1 + \frac{\sin 2k_m d}{2k_m d})$.

6.1 Numerical results

In the following, several plots for ice floes of different geometries and in different arrangements on water of infinite depth are shown. In all plots, the wavelength λ has been chosen to be 2 and the stiffness β and the mass γ of the ice floes to be 0.02. The ambient wavefield of amplitude 1 propagates in the positive direction of the x-axis, thus it travels from left to right in the plots.

Figures 6.1 and 6.2 show the displacements of multiple interacting ice floes of different shapes and in different arrangements. Since square elements have been used to represent the floes, non-rectangular geometries are approximated, i.e. the circular ice floes in the first two plots in figure 6.1 and the parallelogram-shaped ones in the third plot as well as the triangular ice floes in the first two plots of figure 6.2. All ice floes have an area of 4 so that in the normalisation of variables the elastic properties of the differently shaped ice floes are the same.

As can be seen, the ice floes located in front of all others are not much influenced by the ice floes located behind. This is due to the fact that the scattered wavefield of an ice floe has a large amplitude behind and small amplitude in front (compare section 4.5.1). The displacement of ice floes located behind others is quite different from what it would be in the absence of these other floes.

6.2 Convergence

In this section the convergence of the interaction method will be discussed in the cases of finite and infinite depth. There are a number of parameters that have to be chosen, namely the number of propagating modes and decaying angular components as well as the number of roots of the dispersion relation in finite depth or the discretisation of the continuous variable in infinite depth. Since water is considered deep if the depth is greater than half the wavelength (Sarpkaya & Isaacson, 1981), the depth in the finite depth interaction method (assuming deep water) is also a free parameter (with a lower boundary) which influences the convergence.

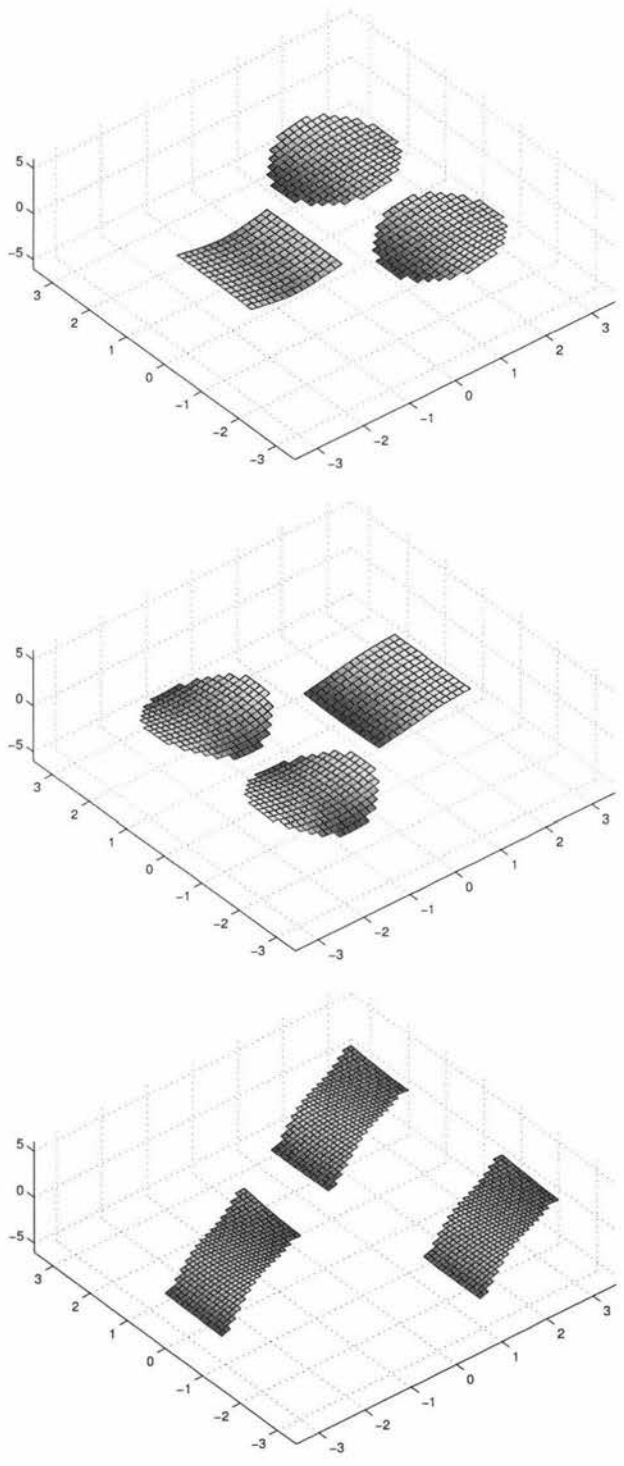

Figure 6.1: Surface displacement of interacting ice floes

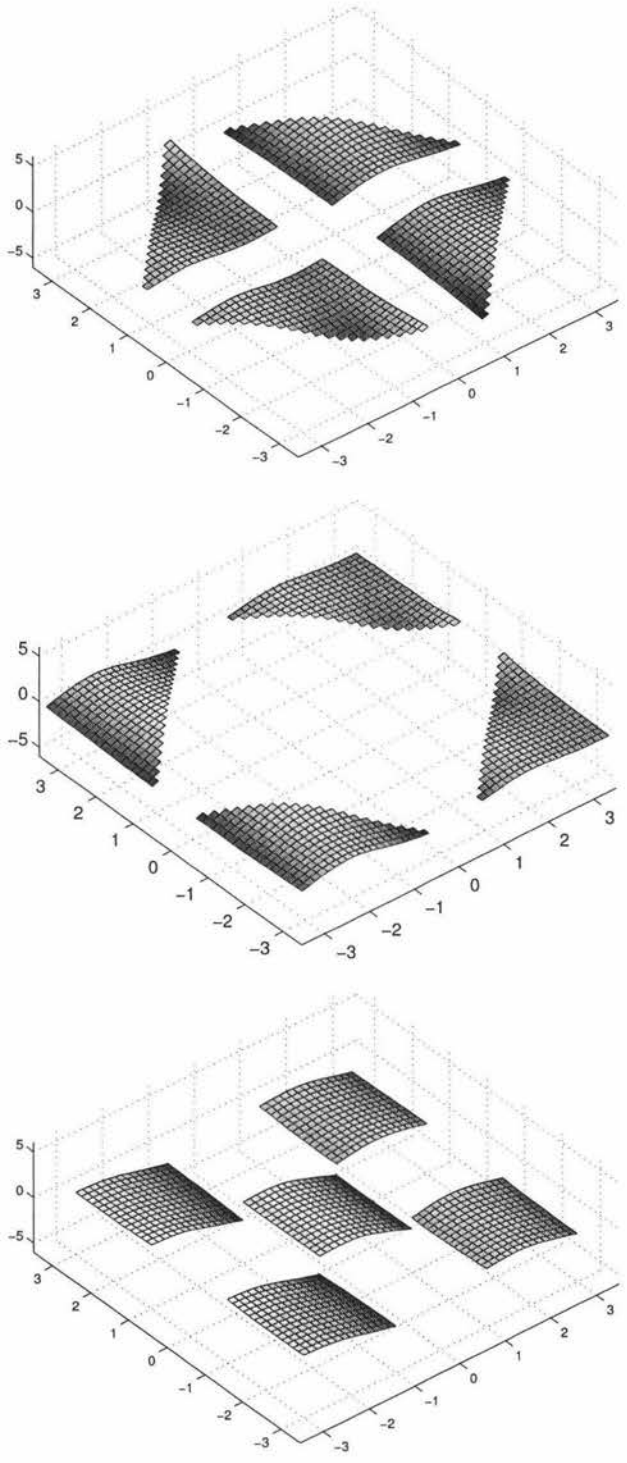

Figure 6.2: Surface displacement of interacting ice floes

All tests are conducted with two square ice floes. The results from full diffraction calculations (implemented by Michael H. Meylan) are used as references. The resolution of the ice floes is such that each square ice floe consists of $24 \times 24 = 576$ elements. For the full diffraction calculation the dimension of the resulting linear system of equations to be solved is therefore 1152. As will be seen, once the diffraction transfer matrix has been calculated (and saved), the dimension of the linear system of equations to be solved in the interaction method is considerably smaller. It is given by twice the dimension of the diffraction transfer matrix.

The greatest deviations from the full diffraction results occur if the two ice floes are either located next to each other or such that one is right behind the other. Since the latter arrangement results in two completely different motions of the ice floes, this one will used when the dependence on the different parameters is examined. To see how the arrangement alters the convergence, tests will also be illustrated for a fixed set of parameters but with differently arranged floes in water of infinite depth.

Two different errors will be used to compare the results: a measure of the overall deviation from the full diffraction solution,

$$E_2 := \left(\int_{\tilde{\Delta}} \left| w_i(\mathbf{x}) - w_f(\mathbf{x}) \right|^2 \mathrm{d}\mathbf{x} \right)^{1/2},$$

and the maximum difference between the two solutions,

$$E_\infty := \sup_{\mathbf{x} \in \tilde{\Delta}} \left| w_i(\mathbf{x}) - w_f(\mathbf{x}) \right|,$$

where w_i and w_f are the solutions of the interaction method and the full diffraction calculation respectively.

Both ice floes will be chosen to have stiffness $\beta = 0.02$ and mass $\gamma = 0.02$. The wavelength is $\lambda = 2$. Unless stated otherwise, one square ice floe, $\tilde{\Delta}_1$, is centred at $(-1.4, 0)$ and the second one is centred at $(1.4, 0)$. Due to the normalisation of the variables, the side of an ice floe has length 2. The ambient wavefield of amplitude 1 propagates along the x-axis. Figure 6.7 shows the solution in the case of water of infinite depth.

6.2.1 Water of finite depth

In water of finite depth the parameters that can be altered are the number of propagating modes, the number of decaying angular components and the number of roots of the dispersion relation. The convergence is also dependent on the water depth.

It is interesting to note that the finite depth interaction method for bodies of arbitrary shape only converges up to a certain depth. This is due to the eigenfunction expansion of the finite depth Green's function, equation (4.6),

$$\begin{aligned} G(r,\theta;s,\varphi) = {} & \frac{\mathrm{i}}{2}\frac{\alpha^2-k^2}{d(\alpha^2-k^2)-\alpha}\cosh^2 kd \sum_{\nu=-\infty}^{\infty} H_\nu^{(1)}(kr)J_\nu(ks)\mathrm{e}^{\mathrm{i}\nu(\theta-\varphi)} \\ & + \frac{1}{\pi}\sum_{m=1}^{\infty}\frac{k_m^2+\alpha^2}{d(k_m^2+\alpha^2)-\alpha}\cos^2 k_m d \sum_{\nu=-\infty}^{\infty} K_\nu(k_m r)I_\nu(k_m s)\mathrm{e}^{\mathrm{i}\nu(\theta-\varphi)}, \quad r>s. \end{aligned} \tag{6.1}$$

It was shown in chapter 3 that as the depth becomes deep, the absolute value of the root of the dispersion relation (3.5), k, tends towards α. Due to the factor $\alpha^2 - k^2$ in the term of propagating modes of the Green's function, for great depths, the summand for the propagating modes contains a factor which is numerically zero. As will be seen, even for moderate depths this subtraction of two almost equal numbers causes bad convergence and it will be shown how the factor can be rewritten to circumvent this problem.

The representation of the water velocity potential is given by equation (3.12). Truncating the infinite sums with truncation parameters T_H, T_K and T_R, the potential can be approximated by

$$\begin{aligned} \phi(r,\theta,z) = {} & \frac{\cosh k(z+d)}{\cosh kd}\sum_{\nu=-T_H}^{T_H} A_{0\nu}H_\nu^{(1)}(kr)\mathrm{e}^{\mathrm{i}\nu\theta} \\ & + \sum_{m=1}^{T_R}\frac{\cos k_m(z+d)}{\cos k_m d}\sum_{\nu=-T_K}^{T_K} A_{m\nu}K_\nu(k_m r)\mathrm{e}^{\mathrm{i}\nu\theta}. \end{aligned} \tag{6.2}$$

The dimension of the diffraction transfer matrix, $\mathbf{B}$, is given by $2T_H + 1 + T_R(2T_K + 1)$. In the following, the dependence on the different truncation parameters will be examined.

Number of propagating modes

The number of propagating modes is determined by the choice of T_H. In the setting described above with depth 3 and 6, the errors develop as displayed in figure 6.3. The number of decaying angular components, T_K, and the number of roots of the dispersion relation, T_R, are fixed to be 5.

Number of decaying angular components

The number of decaying angular components is determined by the choice of T_K. In the setting described above with depth 3 and 6, the errors develop as displayed in figure 6.4.

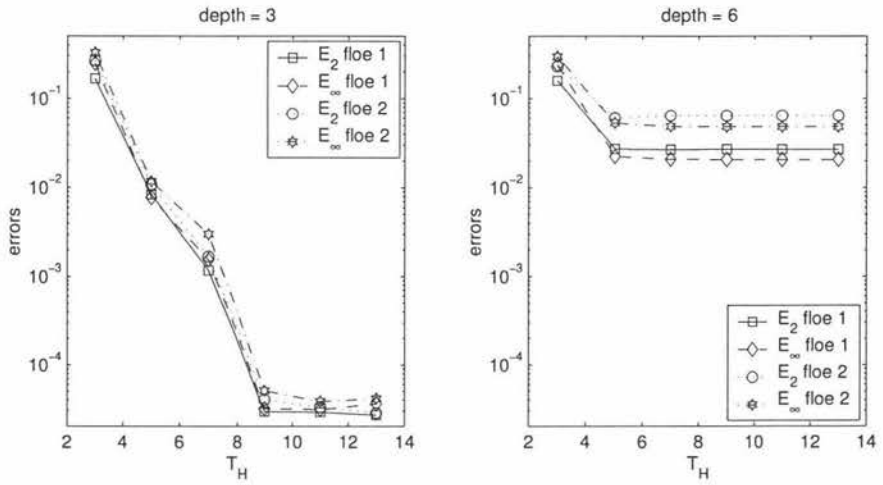

Figure 6.3: Development of the errors as the number of propagating modes is increased

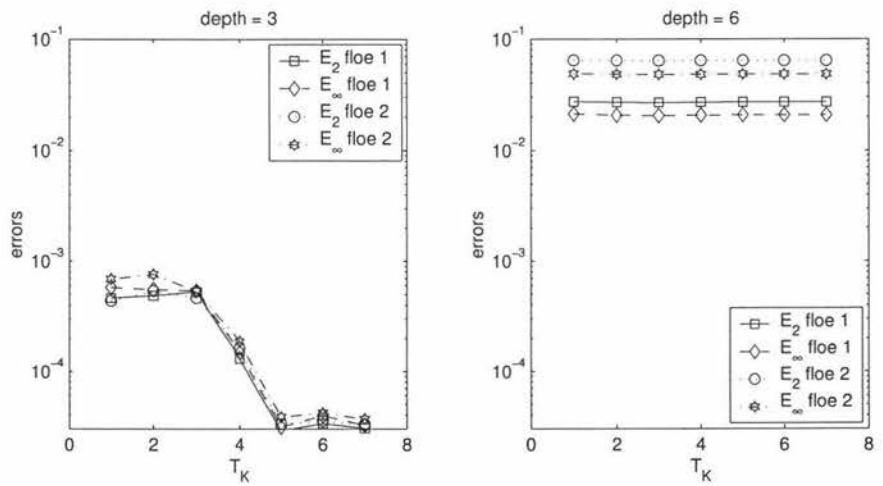

Figure 6.4: Development of the errors as the number of decaying angular components is increased

The number of propagating modes, T_H, is fixed to be 11, the number of roots of the dispersion relation, T_R, is fixed to be 5.

Number of roots of the dispersion relation

The number of roots of the dispersion relation is determined by the choice of T_R. In the setting described above with depth 3 and 6, the errors develop as displayed in figure 6.5. The number of propagating modes, T_H, is fixed to be 11, the number decaying angular components, T_K, is fixed to be 5.

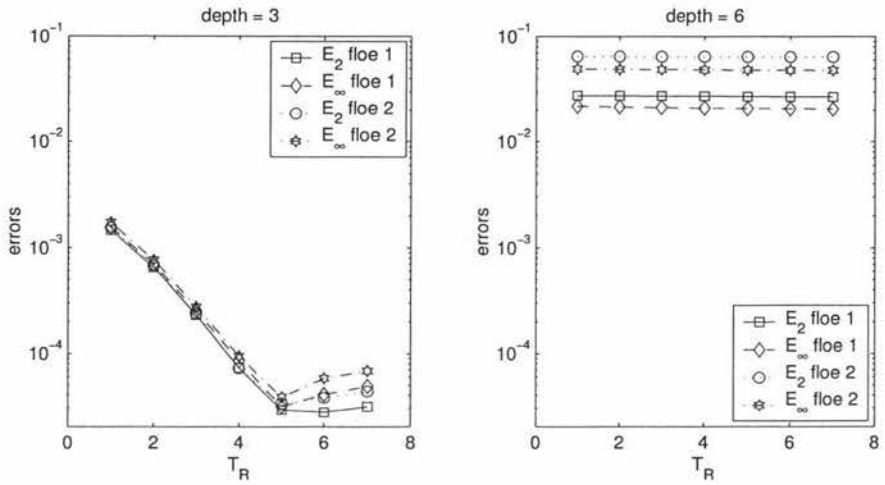

Figure 6.5: Development of the errors as the number of roots of the dispersion relation is increased

Dependence on the water depth

As could be seen in the previous tests, the convergence of the finite depth interaction method strongly depends on the water depth. Further tests with other wavelengths show that the convergence depends on the factor $\alpha^2 - k^2$ that appears in the eigenfunction expansion of the Green's function. As discussed earlier, this factor tends to zero as the depth is increased. Figure 6.6 shows the behaviour of the value of $|\alpha^2 - k^2|$ versus the wavelength and the depth. Values smaller than 10^{-12} have been plotted as $< 10^{-12}$ to avoid numerical disturbances and since this is approximately the value below which the convergence of the finite depth interaction method is strongly affected.

As mentioned earlier, water is considered deep if the depth is greater than half of the wavelength so that for the wavelength of the ambient incident wavefield this criterion

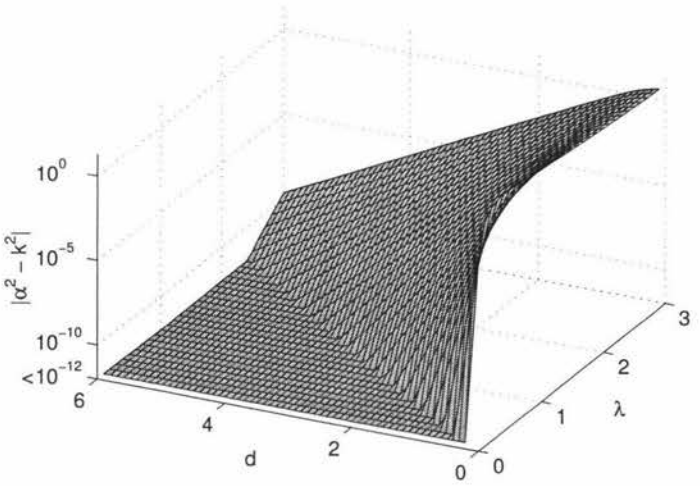

Figure 6.6: $|\alpha^2 - k^2|$ plotted versus the wavelength and the depth

can always be met. However, bodies in the water can change the wavelength as will be discussed in the next chapter.

The problem can be circumvented because the factor $\alpha^2 - k^2$ can be eliminated from the term for the propagating modes in the Green's function. This can be achieved by the calculation

$$\frac{d(\alpha^2 - k^2) - \alpha}{\alpha^2 - k^2} = d + \frac{1}{k}\frac{\alpha/k}{1 - \alpha^2/k^2} = d + \frac{1}{2k}\frac{2\tanh kd}{1 - \tanh^2 kd} = d + \frac{\sinh 2kd}{2k},$$

where the dispersion relation (3.5) and the relation $\sinh 2x = \tanh x \,/\, (1 - \tanh^2 x)$ (Abramowitz & Stegun, 1964) have been used. The eigenfunction expansion of the Green's function can therefore be written as

$$\begin{aligned} G(r,\theta;s,\varphi) = {} & \frac{\mathrm{i}k\cosh^2 kd}{2kd + \sinh 2kd} \sum_{\nu=-\infty}^{\infty} H_\nu^{(1)}(kr) J_\nu(ks) \mathrm{e}^{\mathrm{i}\nu(\theta-\varphi)} \\ & + \frac{1}{\pi} \sum_{m=1}^{\infty} \frac{(k_m^2 + \alpha^2)\cos^2 k_m d}{d(k_m^2 + \alpha^2) - \alpha} \sum_{\nu=-\infty}^{\infty} K_\nu(k_m r) I_\nu(k_m s) \mathrm{e}^{\mathrm{i}\nu(\theta-\varphi)}, \quad r > s. \end{aligned} \tag{6.3}$$

With this representation of the Green's function the depth restriction of the finite depth interaction method for bodies of arbitrary geometry can be circumvented.

In the particular case examined here, water can be considered deep if the depth is greater than approximately 1.5. The finite depth interaction method with the Green's function given by equation (6.1) can therefore be used with depths between 1.5 and approximately 5 while the use of the Green's function given by equation (6.3) does not impose

this upper boundary. Depending on the particular depth however, the convergence differs. Table 6.1 shows the errors for different depths where the number of propagating modes, T_H, is fixed to be 11, the number of decaying angular components, T_K, is 5 and the number of roots of the dispersion relation, T_R, is 4. For illustration, the values of $|\alpha^2 - k^2|$ and both errors, produced with the use of the Green's function in equation (6.1) and that in equation (6.3), are included.

depth	$\lvert\alpha^2 - k^2\rvert$	E_2 floe 1	E_∞ floe 1	E_2 floe 2	E_∞ floe 2
2	$1.37674 \cdot 10^{-4}$	0.00002842	0.00004334	0.00003953	0.00006146
		0.00003572	0.00004060	0.00008701	0.00008846
3	$2.57010 \cdot 10^{-7}$	0.00007341	0.00008591	0.00007260	0.00009493
		0.00007348	0.00008599	0.00007279	0.00009513
4	$4.80117 \cdot 10^{-10}$	0.00025194	0.00027436	0.00025788	0.00029851
		0.00025272	0.00027517	0.00026023	0.00030071
5	$8.98837 \cdot 10^{-13}$	0.00137900	0.00123818	0.00293643	0.00242055
		0.00049115	0.00052718	0.00050971	0.00057767
6	$1.77636 \cdot 10^{-15}$	0.02724111	0.02099747	0.06445855	0.04853413
		0.00072983	0.00077998	0.00075958	0.00085773

Table 6.1: Errors for different depths; the upper values have always been obtained with Green's function (6.1), the lower ones with (6.3)

6.2.2 Water of infinite depth

As in the case of finitely deep water, the number of propagating modes and decaying angular components to be included are free parameters. In infinite depth however, there are no discrete roots of a dispersion relation but a continuous variable that has to be discretised. This allows the freedom of choice of the number of points as well as the points themselves.

Again, two square ice floes are considered, arranged one behind the other. Figure 6.7 shows the standard arrangement. To illustrate the effect on the water in the vicinity, its displacement is also shown. As in chapter 4, a close view, a far view and a view from above (plan view) are available. Different arrangements will also be considered to examine the dependence of the convergence speed on the positions of the ice floes.

The representation of the water velocity potential is given by equation (3.17). Truncating the infinite sums with truncation parameters T_H and T_K and discretising the inte-

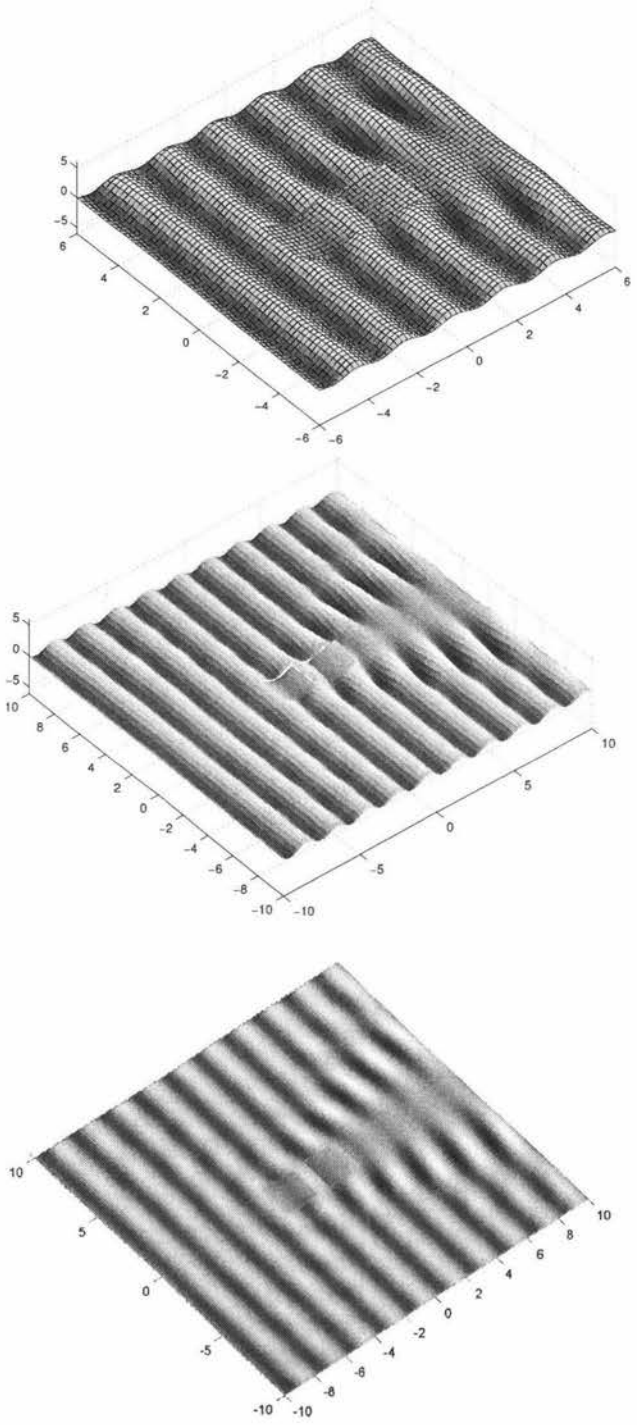

Figure 6.7: Surface displacement of the ice floes and the water in their vicinity, $O_1 = (-1.4, 0)$, $O_2 = (1.4, 0)$

gration by defining a set of nodes, $0 \leq \eta_1 < \ldots < \eta_m < \ldots < \eta_{T_R}$, with weights h_m, the potential can be approximated by

$$\begin{aligned}\phi(r,\theta,z) = \mathrm{e}^{\alpha z} \sum_{\nu=-T_H}^{T_H} A_{0\nu} H_\nu^{(1)}(\alpha r)\mathrm{e}^{\mathrm{i}\nu\theta} \\ + \sum_{m=1}^{T_R} h_m \psi(z,\eta_m) \sum_{\nu=-T_K}^{T_K} A_\nu(\eta_m) K_\nu(\eta_m r)\mathrm{e}^{\mathrm{i}\nu\theta}\,\mathrm{d}\eta.\end{aligned} \tag{6.4}$$

The dimension of the diffraction transfer matrix, $\mathbf{B}$, is given by $2T_H + 1 + T_R(2T_K + 1)$. In the following, the integration weights are chosen to be $h_m = 1/2\,(\eta_{m+1} - \eta_{m-1})$, $m = 2 \ldots T_R - 2$ and $h_1 = \eta_2 - \eta_1$ as well as $h_{T_R} = \eta_{T_R} - \eta_{T_R-1}$ unless stated otherwise. Again, the dependence on the different parameters will be examined.

Number of propagating modes

The number of propagating modes is determined by the choice of T_H. In the setting described above, the error develops as displayed in figure 6.8. The number of decaying angular components, T_K, is fixed to be 5 and η is discretised to be $(0.1, 1.175, 2.25, 3.325, 4.4)$.

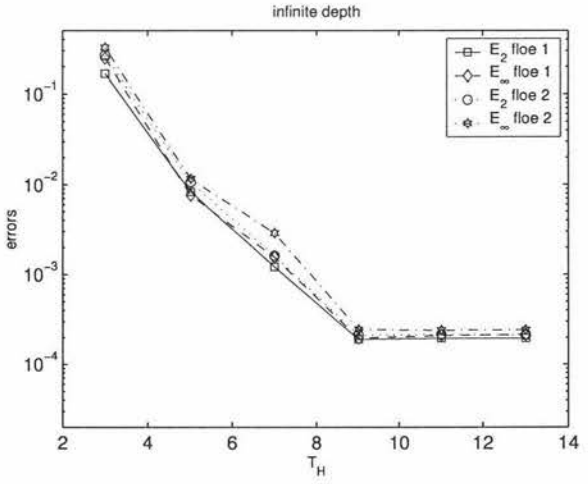

Figure 6.8: Development of the errors as the number of propagating modes is increased

Number of decaying angular components

The number of decaying angular components is determined by the choice of T_K. In the setting described above, the errors develop as displayed in figure 6.9. The number of propagating modes, T_H, is fixed to be 11 and η is discretised to be $(0.1, 1.175, 2.25, 3.325, 4.4)$.

This is a good choice of nodes and therefore minimises possible effects caused by a bad discretisation of η.

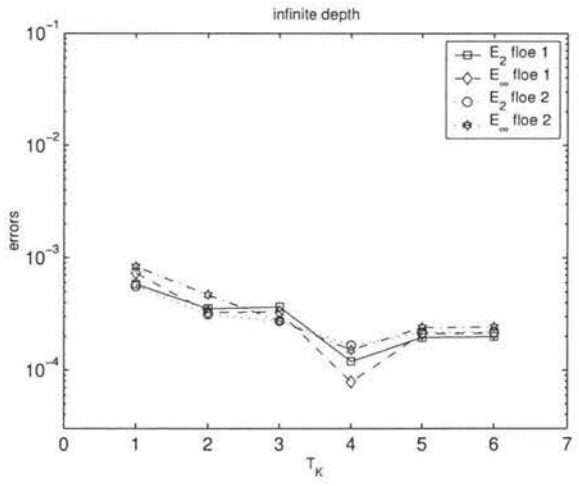

Figure 6.9: Development of the errors as the number of decaying angular components is increased

Discretisation of the integration path

To illustrate the convergence when more points are used to discretise the integration path, the continuous variable is chosen to be discretised with $\eta_m = 0.1 + 4.3\,(m-1)/(T_R - 1)$, $m = 1 \ldots T_R$, such that the number of points in the interval $[0.1, 4.4]$ is increased. In the setting described above, the errors develop as displayed in figure 6.10. The number of propagating modes, T_H, is fixed to be 11 and the number of decaying angular components, T_K, is fixed to be 5.

Of course, other discretisations are possible, especially non-equally spaced ones. Table 6.2 shows the convergence with different discretisations.

Since the function to be integrated always roughly looks like plot (d) in figure 4.4, it is possible to make a clever choice of the discretisation points. Of course, different quadrature rules can also be considered. Using Gaussian quadrature, for instance, the discretisation of the integration variable and the integration weights are determined by the Legendre polynomials, only the integration boundaries and the number of discretisation points are free parameters. Although for general functions this leads to much better results than the mid-point rule used above, the mid-point rule allows a clever choice of the discretisation points such that the convergence with Gaussian quadrature is no better.

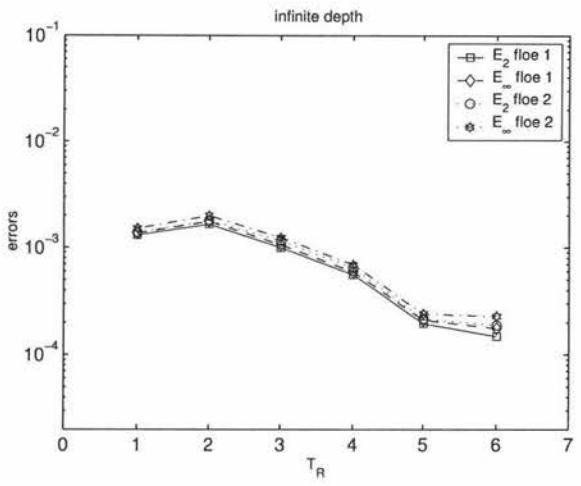

Figure 6.10: Development of the errors as the number of points in the discretisation of the continuous variable is increased

discretisation of η	E_2 floe 1	E_∞ floe 1	E_2 floe 2	E_∞ floe 2
(0.1, 0.4, 0.7, 1.0)	0.00083311	0.00067681	0.00089981	0.00074413
(0.1, 1.067, 2.033, 3.0)	0.00021145	0.00023035	0.00021096	0.000245556
(0.1, 1.733, 3.367, 5.0)	0.00069601	0.00073751	0.00080789	0.000863854
(0.1, 0.8, 1.5, 3.0)	0.00020795	0.00021225	0.00023503	0.00024126
(0.4, 1.4, 2.2, 3.2)	0.00009310	0.00008483	0.00010941	0.00007116
(0.8, 1.8, 3.0)	0.00025377	0.00028810	0.00026844	0.00032156

Table 6.2: Errors with different discretisations

Arrangement of the ice floes

The convergence of the interaction method also depends on the positions of the ice floes. To illustrate this, the errors are computed for different arrangements of the two ice floes. At first, the situation where the two ice floes are located one behind the other is considered. Figure 6.11 shows the errors over the distances between the ice floes. Since R_{12} denotes the distance between them, the mean centre positions of the ice floes are $(-R_{12}/2, 0)$ and $(R_{12}/2, 0)$. The number of propagating modes, T_H, is fixed to be 11, the number of decaying angular components, T_K, is 5 and η is discretised to be $(0.1, 1.533, 2.967, 4.4)$.

It has to be noted that the eigenfunction expansion of the Green's function where the coordinate system is centred above the mean centre position of the body, equation (4.13), is only valid outside the escribed circle of the ice floe. Thus, for the distances smaller than

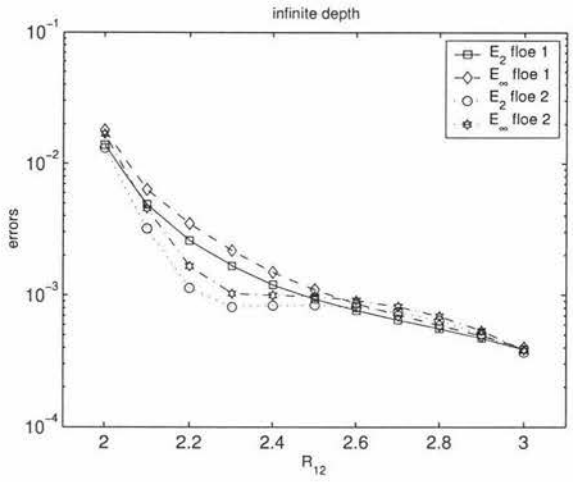

Figure 6.11: Development of the errors as the distance between the ice floes increased

2.5 the theory is not valid which is why the error decreases much faster in the left half of the graph. This especially applies to the second ice floe which is much influenced by the presence of the ice floe in front.

For even more different arrangements, table 6.3 shows the errors depending on the mean centre positions of the ice floes, O_1 and O_2. For reference, the first arrangement is the standard one, shown in figure 6.7, the fourth and the last one are illustrated in figures 6.12 and 6.13 respectively.

O_1	O_2	E_2 floe 1	E_∞ floe 1	E_2 floe 2	E_∞ floe 2
$(-1.4, 0)$	$(1.4, 0)$	0.00056007	0.00059559	0.00064542	0.00069452
$(-2, 0)$	$(2, 0)$	0.00010795	0.00009893	0.0001041	0.00009725
$(-2.5, 0)$	$(2.5, 0)$	0.0000433	0.00003816	0.00004477	0.00003976
$(0, -1.4)$	$(0, 1.4)$	0.00016400	0.00021014	0.00016400	0.00021014
$(-0.6, -1.4)$	$(0.6, 1.4)$	0.00019310	0.00028358	0.00010891	0.00017593
$(-1.4, -0.6)$	$(1.4, 0.6)$	0.00050231	0.00072830	0.00040678	0.00060087

Table 6.3: Errors in different arrangements

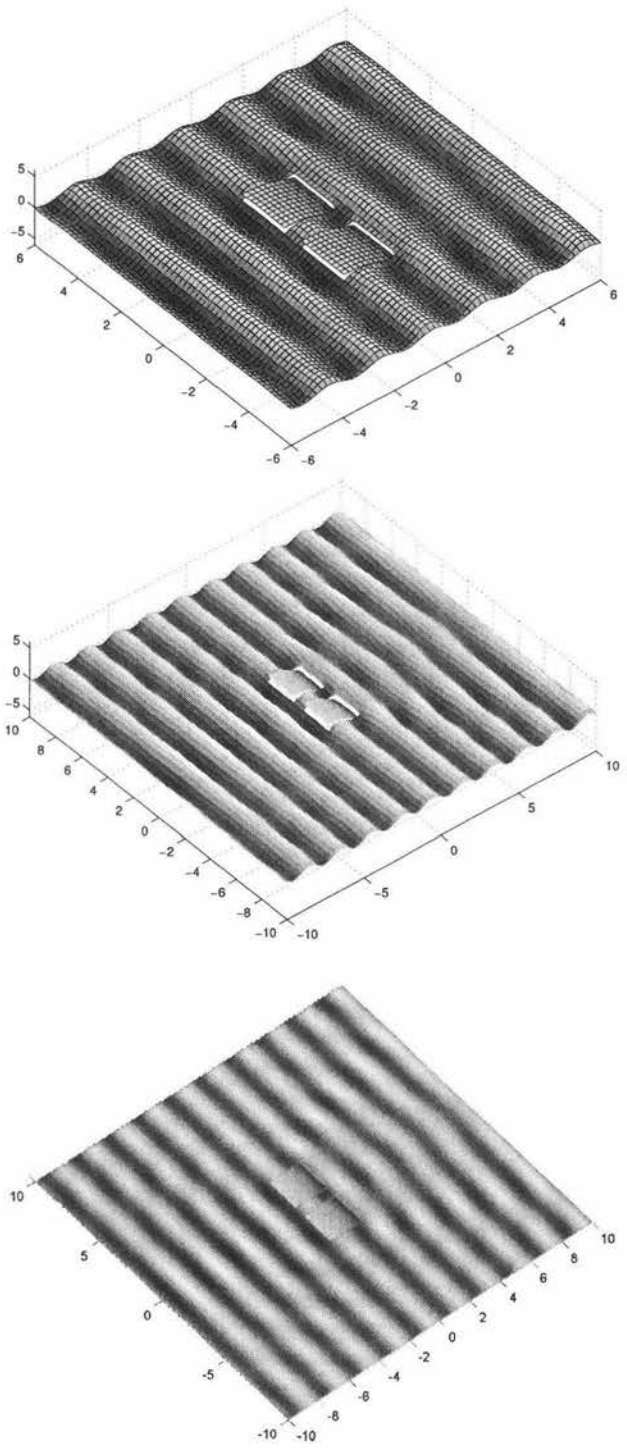

Figure 6.12: Surface displacement of the ice floes and the water in their vicinity, $O_1 = (0, -1.4)$, $O_2 = (0, 1.4)$

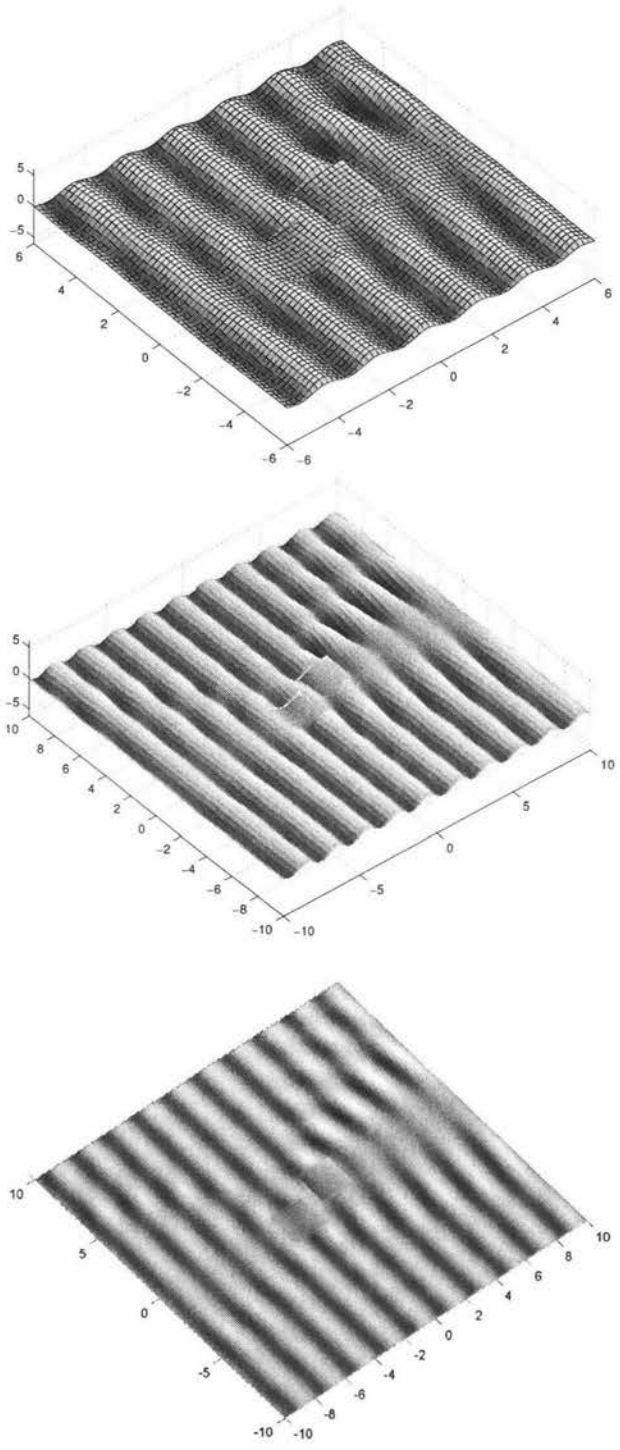

Figure 6.13: Surface displacement of the ice floes and the water in their vicinity, $O_1 = (-1.4, -0.6)$, $O_2 = (1.4, 0.6)$

Chapter 7

Summary and Discussion

The ideas of the finite depth interaction theory developed by Kagemoto & Yue (1986) have been applied to water of infinite depth to present an equivalent infinite depth interaction method. The eigenfunction expansion of the infinite depth free surface Green's function where the coordinate system is centred at the water surface above the mean centre position of the body allows the calculation of the diffraction transfer matrices for bodies of arbitrary geometry in water of infinite depth analogously to the finite depth Green's function given by Black (1975) and Fenton (1978). The depth restriction of the finite depth interaction method which was encountered in the convergence tests in deep water has been removed by rewriting a factor in the finite depth Green's function.

Both interaction theories yield fast methods for the calculation of the scattered wavefields of many interacting floating or (fully or partially) submerged, vertically non-overlapping bodies. They have a number of general advantages over the full diffraction calculation but especially the differences between the infinite depth and the finite depth method in deep water will be pointed out. It will also be discussed why it is important to have removed the depth restriction of the finite depth method.

The eigenfunction expansion of the infinite depth free surface Green's function which emerged in the search for a Green's function that could be used for the infinite depth interaction theory is numerically much easier to evaluate than existing representations in many cases. The results of the comparison with the other representations will be summarised.

7.1 The eigenfunction expansion of the free surface Green's function

The eigenfunction expansion of the free surface Green's function for water of infinite depth which emerged in the derivation of an appropriate Green's function for the interaction theory appears to be much easier to evaluate numerically than existing representations in many cases. It does not require the computation of an uncommon special function and less function evaluations are required in the calculation of the integral. Kim's representation is slightly better when used with long wavelengths but the difference is not significant while in the cases where the calculation with the eigenfunction expansion is numerically less expensive the difference in the amount of required function evaluations is often quite remarkable. However, the comparison performed in chapter 4 does not form a definitive test that the eigenfunction expansion is better than Kim's representation although it indicates that it will perform well in more thorough tests where ways to optimise the integration and the expense of the evaluation of the integrand are included. If no vertical dependence is required however (as in the single diffraction calculations for the ice floes for example), Kim's representations has the advantage that the integral is always zero and therefore does not need to be computed.

7.2 Advantages of the interaction methods over the full diffraction calculation

Compared to a full diffraction calculation (no interaction theory) the interaction methods have a number of advantages. The dimension of the linear system of equations that accounts for the interaction of the bodies is considerably smaller than the one to be solved in the full diffraction calculation. Furthermore, the dimension of the linear system of equations does not depend on the resolution of the bodies.

The main computational work lies in the calculation of the diffraction transfer matrices. However, these only need to be calculated once for each kind of body and can be saved and re-used in further calculations. The eigenfunction expansions of the Green's functions where the coordinate system is centred above the mean centre position of the body make it possible to calculate the diffraction transfer matrices for bodies of arbitrary geometry. While the interaction method itself only requires the escribed cylinder of each body not to contain the origin of any other body, the eigenfunction expansions of the Green's functions imply the stricter restriction that the escribed cylinder of each body may not contain any

other body. This restriction of the interaction methods is due to the general approach of the problem however. The expansion of the scattered potential into cylindrical outgoing waves is only valid outside the escribed cylinder of the body. Still, the interaction methods give good to very good approximations for arrangements which only violate this requirement a little.

Since the diffraction transfer matrices contain the information of the diffraction characteristics of the body, they may also be re-used if the result of a single diffraction calculation is required. Their small dimension allows an efficient way of storing diffraction characteristics of single bodies.

7.3 Comparison of the finite and the infinite depth methods

The finite depth and infinite depth interaction methods share many similarities. However, there are a number of differences in the numerical expense of their computation which will be summarised. It will also be discussed why it is important to remove the depth restriction of the finite depth method that is present when used with the standard form of the eigenfunction representation of the finite depth Green's function.

A very significant advantage of the infinite depth interaction method is the fact that it requires the results of infinite depth single diffraction calculations instead of the finite depth solutions. This is a great advantage because the infinite depth Green's functions, equations (4.15c) and (4.15d), are numerically much easier to evaluate than any available finite depth one. The cost of performing single diffraction calculations in infinite depth is significantly lower than the equivalent finite depth computations.

As was shown in the previous chapter, the finite depth interaction method only converges up to a certain depth depending on the wavelength of the ambient incident wave if used with the standard form of the eigenfunction representation of the Green's function. Water is considered deep if the depth d is greater than half of the wavelength λ. A comparison with figure 6.6 shows that the depth can always be chosen deep enough to meet this criterion for the ambient incident wavefield without encountering the limits of the finite depth interaction method. However, bodies in the water can change the wavelength and lead to longer waves which require deeper water.

In the case of a flexible shallow draft for example, the wavenumber under the body is governed by a more complex dispersion relation given by Fox & Squire (1994). In

non-dimensional form it states

$$\kappa^* \tan \kappa^* d = -\frac{\alpha}{\beta\kappa^{*4} - \gamma\alpha + 1},$$

where κ^* is the wavenumber under the body. The purely imaginary roots of this dispersion relation correspond to the propagating modes and their absolute value is given as the positive root of

$$\kappa \tanh \kappa d = \frac{\alpha}{\beta\kappa^4 - \gamma\alpha + 1}.$$

For given ambient incident wavenumber and water depth, α is determined by the open water dispersion relation. Therefore, there always exist values of stiffness β and mass γ such that the wavenumber under the plate, κ, requires the water to be deeper in order to meet the deep water criterion. Thus, for plates with certain properties the water has to be chosen deeper than the finite depth interaction method allows if used with the standard form of the eigenfunction representation of the Green's function. Although these properties might not be realistic for ice floes, there certainly are cases of bodies in deep water for which the finite depth interaction method with the standard form of the Green's function cannot meet the deep water criterion.

As was shown in chapter 6, however, this problem can be circumvented by rewriting the numerically problematic factor in the term of the Green's function corresponding to the propagating modes. The use of the rewritten Green's function then allows the use of the finite depth interaction method for arbitrary depths.

The problem of choosing the water depth great enough to approximate deep water in the finite depth method also leads to issues regarding the convergence of the interaction methods. Generally, the convergence of the infinite depth interaction method is similar to that of the finite depth method. However, it can be said that the greater the water depth in the finite depth method the poorer its performance. Choosing the water depth very great in order to prevent problems with the infinite depth approximation therefore strongly decreases the numerical performance.

The advantage of the finite depth interaction method is the applicability to water of finite depth which is not deep. However, if the application will always require the water to be deep, ice floes in the Marginal Ice Zone for example, the infinite depth method should be used in order to reduce the numerical expense of the single diffraction calculations as well as of the interaction method itself. If the finite depth method is chosen, however, the rewritten factor for the propagating modes should be used in the Green's function in eigenfunction representation to prevent problems with the deep water criterion.

Appendix A

Nomenclature

Δ	a floating or submerged body, $\Delta \subset \mathbb{R}^3$
$\tilde{\Delta}$	a shallow draft, $\tilde{\Delta} \subset \mathbb{R}^2 \times \{0\}$
Γ	the immersed surface of Δ
D	volume occupied by the water of infinite depth, $D = \{(x, y, z) \in \mathbb{R}^3 \backslash \bar{\Delta} \mid z < 0\}$
D_d	volume occupied by the water of finite depth, $D_d = \{(x, y, z) \in \mathbb{R}^3 \backslash \bar{\Delta} \mid z \in]0, -d[\}$
S	the undisturbed free water surface
T	a closed time interval, $T \subset \mathbb{R}$
$\mathbb{R}^3_-$	the lower three-dimensional half-space
$\mathbf{y} = (x, y, z)$	Cartesian coordinates of a point of the water
$\mathbf{x} = (x, y, 0)$	Cartesian coordinates of a point of the water surface
(r, θ, z)	cylindrical coordinates of $\mathbf{y}$
$\zeta = (a, b, c)$	Cartesian coordinates of a source point
$\xi = (a, b, 0)$	Cartesian coordinates of a source point at the water surface
(s, φ, c)	cylindrical coordinates of ζ
O_j	mean centre position of Δ_j
(R_{jl}, ϑ_{jl})	polar coordinates of mean centre position of Δ_l in coordinates of Δ_j

Φ	the water velocity potential, $\Phi : D \times T \to \mathbb{R}$
W	the surface displacement from the undisturbed position, $W : S \times T \to \mathbb{R}$
p	the pressure in the water relative to the atmospheric pressure, $p : D \times T \to \mathbb{R}$

ϕ	the time-independent water velocity potential, $\Phi(x,y,z,t) = \mathbb{R}e\,\{\phi(x,y,z)\mathrm{e}^{-\mathrm{i}\omega t}\}$
w	the time-independent surface displacement, $W(x,y,t) = \mathbb{R}e\,\{w(x,y)\mathrm{e}^{-\mathrm{i}\omega t}\}$
ϕ^{In}	the time-independent ambient wavefield, $\phi^{\mathrm{In}} : D \to \mathbb{C}$
ς	the source strength distribution function $\varsigma\colon \Gamma \to \mathbb{C}$
g	potential due to a single source point
G	a Green's function
ψ	$\psi(z,\eta) = \cos(\eta z) + \alpha/\eta\,\sin(\eta z),\ (z,\eta) \in \mathbb{R}_{\leq 0} \times \mathbb{R}_{>0}$
J_ν	Bessel function of the first kind and of integer order ν
Y_ν	Bessel function of the second kind and of integer order ν
I_ν	modified Bessel function of the first kind and of integer order ν
K_ν	modified Bessel function of the second kind and of integer order ν
$H_\nu^{(1)}$	Hankel function of the first kind and of integer order ν
$\mathbf{H}_0$	Struve function of order zero
i	the imaginary unit, $\mathrm{i} = \sqrt{-1}$
g	the acceleration due to gravity
d	the water depth
ω	the radian frequency
λ	the wavelength
α	$\alpha = \omega^2/g$
k	the wavenumber, $k = 2\pi/\lambda$
k_m	roots of the dispersion relation (3.4)
κ	wavenumber under a flexible floating thin plate
χ	angle of the x-axis with the direction of propagation of the ambient wavefield
$A_\nu^j(\cdot)$	coefficients of outgoing water velocity potential (infinite depth)
$D_\nu^j(\cdot)$	coefficients of incident water velocity potential (infinite depth)
$A_{m\nu}^j$	coefficients of outgoing water velocity potential (finite depth)
$D_{m\nu}^j$	coefficients of incident water velocity potential (finite depth)

$\mathbf{a}_j$	truncated vector of coefficients of the scattered wavefield of Δ_j
$\mathbf{d}_j$	truncated vector of coefficients of the incident wavefield upon Δ_j
$\mathbf{d}_j^{\mathrm{In}}$	truncated vector of coefficients of the ambient incident wavefield upon Δ_j
$\mathbf{\Psi}_l^{\mathbf{S}}$	truncated vector of scattered partial waves of Δ_j
$\mathbf{\Psi}_l^{\mathbf{I}}$	truncated vector of incident partial waves upon Δ_j
$\mathbf{T}_{jl}$	coordinate transformation matrix from Δ_j to Δ_l, $j \neq l$
$\mathbf{B}_j$	diffraction transfer matrix
$\hat{\mathbf{B}}_j$	diffraction transfer matrix with integration weights (infinite depth only)

ρ	the density of the water
ρ_Δ	the density of the ice floe
h	the thickness of the ice floe
D	the modulus of rigidity of the ice floe
β	the non-dimensionalised stiffness of the ice floe
γ	the non-dimensionalised mass of the ice floe
ν	Poisson's ratio for the ice floe

Appendix B

Contents of the CD-ROM

The attached CD-ROM contains animated versions of the plots of the ice floes appearing in this thesis. The animations always show one wave period and are best viewed repeatedly to obtain a continuing motion.

The filenames of the animations were given according to the figure they belong to. The addition of `cls` to the filename denotes the close view, `far` denotes the far view and `abv` is added to the view from above (the plan view). This applies to all figures except figures 2.1 and 2.2 which only contain single plots as well as figures 6.1 and 6.2 for which the additions `a`, `b` and `c` refer to the first, second and third configuration.

The animations were produced with MATLAB and compressed with the INDEO 3 algorithm. Priority was given to compatibility as opposed to compression quality. Where it makes a great difference, high quality versions, compressed with the INDEO 5 algorithm, are also available. These are marked by the addition of `_hq` to the filename.

The animations should be viewable with WINDOWS MEDIA PLAYER or XMPS if the correct decompression algorithm is installed.

Table B.1 summarises the contents of the CD-ROM.

Filename	Description
`contents.txt`	Plain text version of this appendix
`figure21.avi`	Displacement of the ice floe under incident wave of wavelength 2
`figure22.avi`	Displacement of the ice floe under incident wave of wavelength 1
`figure46*.avi`	Displacement of the ice floe and the water in its vicinity under incident wave of wavelength 2
`figure47*.avi`	Scattered wavefield of the ice floe under incident wave of wavelength 2
`figure48*.avi`	Displacement of the ice floe and the water in its vicinity under incident wave of wavelength 1
`figure49*.avi`	Scattered wavefield of the ice floe under incident wave of wavelength 2
`figure61a.avi`	Surface displacement of interacting ice floes (one square, two circles)
`figure61b.avi`	Surface displacement of interacting ice floes (two circles, one square)
`figure61c.avi`	Surface displacement of interacting ice floes (three parallelograms)
`figure62a.avi`	Surface displacement of interacting ice floes (four triangles)
`figure62b.avi`	Surface displacement of interacting ice floes (four triangles)
`figure62c.avi`	Surface displacement of interacting ice floes (five squares)
`figure68*.avi`	Displacement of two interacting square ice floes behind one another and the water in its vicinity
`figure612*.avi`	Displacement of two interacting square ice floes beside one another and the water in its vicinity
`figure613*.avi`	Displacement of two interacting square ice floes almost behind one another and the water in its vicinity

Table B.1: Contents of the CD-ROM

Bibliography

ABRAMOWITZ, M. & STEGUN, I., ed. 1964 *Handbook of Mathematical Functions*. Dover Publications.

BLACK, J. L. 1975 Wave forces on vertical axisymmetric bodies. *J. Fluid Mech.* **67**, 369–376.

CHAKRABARTI, S. 2000 Hydrodynamic interaction forces on multi-moduled structures. *Ocean Engng* **27**, 1037–1063.

FENTON, J. D. 1978 Wave forces on vertical bodies of revolution. *J. Fluid Mech.* **85** (2), 241–255.

FOX, C. & SQUIRE, V. A. 1994 On the oblique reflexion and transmission of ocean waves at shore fast sea ice. *Phil. Trans. R. Soc. Lond. A* **347**, 185–218.

GOO, J.-S. & YOSHIDA, K. 1990 A numerical method for huge semisubmersible responses in waves. *SNAME Transactions* **98**, 365–387.

HAVELOCK, T. H. 1955 Waves due to a floating sphere making periodic heaving oscillations. *Proc. Roy. Soc. Lond. A* **231**, 1–7.

HEARN, G. E. 1977 Alternative methods of evaluating Green's function in three-dimensional ship wave problems. *J. Ship Res.* **21**, 89–93.

JOHN, F. 1950 On the motion of floating bodies II. *Comm. Pure Appl. Maths* **3**, 45–101.

KAGEMOTO, H. & YUE, D. K. P. 1986 Interactions among multiple three-dimensional bodies in water waves: an exact algebraic method. *J. Fluid Mech.* **166**, 189–209.

KIM, W. D. 1965 On the harmonic oscillations of a rigid body on a free surface. *J. Fluid Mech.* **21**, 427–451.

KUZNETSOV, N., MAZ'YA, V. & VAINBERG, B. 2000 *Linear Water Waves: A Mathematical Approach*. Cambridge University Press.

LINTON, C. & MCIVER, P. 2001 *Handbook of Mathematical Techniques for Wave / Structure Interactions*. Chapman & Hall /CRC.

LINTON, C. M. 1999 Rapidly converging representations for Green's functions for Laplace's equation. *Proc. R. Soc. Lond. A* **455**, 1767–1797.

MEYLAN, M. H. 2002 The wave response of ice floes of arbitrary geometry. *J. Geophys. Res. - Oceans* **107** (C6), doi: 10.1029/2000JC000713.

SARPKAYA, T. & ISAACSON, M. 1981 *Mechanics of Wave Forces on Offshore Structures*. Van Nostrand Reinhold Company.

STOKER, J. J. 1958 *Water Waves: The Mathematical Theory with Applications*. John Wiley & Sons.

WEHAUSEN, J. & LAITONE, E. 1960 Surface waves. In *Handbuch der Physik IX: Fluid Dynamics III* (ed. S. Flügge & C. Truesdell). Springer Verlag.